Final Design Report

for

NASA Ames/University of Arizona

Cooperative Agreement No. NCC2-426

For the period

1 April 1989 - 30 April 1990

by

Daniel Vukobratovich

Ralph M. Richard

Tina M. Valente

Myung K. Cho

of the

Optical Sciences Center

University of Arizona

Tucson, AZ 85721

TABLE OF CONTENTS

1. SCALING LAWS FOR LIGHT-WEIGHT OPTICS

1.1. ABSTRACT

Scaling laws for light-weight optical systems are examined. A cubic relationship between mirror diameter and weight has been suggested and used by many designers of optical systems as the best description for all light-weight mirrors. A survey of existing light-weight systems in the open literature has been made to clarify this issue. Fifty existing optical systems were surveyed with all varieties of light-weight mirrors including glass and beryllium structured mirrors, contoured mirrors, and very thin solid mirrors. These mirrors were then categorized and weight to diameter ratio was plotted to find a best fit curve for each case. A best fitting curve program tests nineteen different equations and ranks a "goodness-to-fit" for each of these equations. The resulting relationship found for each light-weight mirror category helps to quantify light-weight optical systems and methods of fabrication and provides comparisons between mirror types.

1.2. INTRODUCTION

Understanding light-weight optics has become an important issue for many optical systems. Many systems are weight limited including space optics and pointing and tracking systems. In many cases the weight of the optics are the primary influence on the system weight as well as the cost. Although these light-weight mirrors are often more costly to produce, their decreased weight often can produce a savings in the mounting. Various scaling laws for light-weight optics have previously been used. Generally, a cubic relationship has been assumed between weight and diameter.[1] Another proposed generic equation commonly used for all light-weight mirrors is cited by Hamill[2].

$$W = \frac{\frac{k D^{2.6}}{D}}{t} \tag{1.1}$$

Where:

D	=	diameter
k	=	constant
t	=	mirror thickness
W	=	mirror weight

It is suggested that for advanced space optics, this constant k should be reduced by a factor of 2. Many authors have developed other scaling relationships of interest including cost scaling laws developed by Meinel[3] and weight scaling relationships for the total tube moving weight developed by Rule.[4] To continue this interest in scaling and preferred mirror types for systems, a survey of existing light-weight systems was proposed.

Once weight to diameter ratio for these mirror is known it is necessary to quantify these ratios mathematically. It was proposed to use a best fit curve program developed by Myung Cho of the Optical Sciences Center. The nineteen different mathematical equations that were used to fit the data are listed in Table 1.1.

1.3. MIRRORS STUDIED

The literature seach of existing light-weight systems also included a few famous conventinal systems for comparison. In each case, mirror dimensions, material, configuration, and weight were tabulated. Table 1.2 lists the conventional or solid mirror systems studied. It should be noted that for future analysis, a very thin solid mirror with an aspect ratio (thickness/diameter) of less than 0.1 was considered as a light-weight mirror. Listed in Table 1.3 are the light-weight systems studied. These

mirror types include structured mirrors, contoured mirrors, and beryllium mirrors. Mirrors referred to as structured mirrors contain ribbed cells such as openback and sandwich mirrors. Contoured mirrors are mirrors that have been light-weighted by cutting contours in the back of the mirror; i.e. single arch and double arch.

1.4. RESULTS

After data compilation was completed and the mirrors were categorized, both the best fitting function and the power function for weight vs. diameter were found for each category. The power function represents the common weight to diameter relationship used for both solid and light-weight mirrors. Figure 1.1 illustrates the functions found for solid mirrors with conventional aspect ratios (diameter to thickness) as well as very thin solids with small aspect ratios. Although conventional solids are best described with a parabolic function, the power function using a nearly cubic exponent also describes the data well as expected. The very thin solid mirrors are best described by a hoerl function and in the case of the power function, have an exponent slightly smaller than that of conventional solids.

All light-weight mirrors are represented in Figure 1.2. In this case, the power function was the best fitting function with an exponent of approximately 3. This would indicate that in general, a cubic raltionship between weight and diameter is a good rule of thumb for light-weight mirrors. Figure 1.3 illustrates both the solid curves and the light-weight curve for comparison.

Specific light-weight mirror types were next investigated. The weight to diameter relationship for strucutred mirrors, contoured mirrors, and beryllium mirrors are shown in Figures 1.4, 1.5, and 1.6 respectively. Upon examination of the power functions fit to the data, it is apparent that each specific type has a significantly different coefficient and exponent. It is also interesting to note the difficulty in achieving a good data fit for the beryllium mirror category. This category contains a variety of unusual optical designs including innovative space optics.

Finally the mirrors were categorized using the weight relationship cited earlier (equation 1.1):

$$W = \frac{k D^{2.6}}{\frac{D}{t}}$$

The constant k was calculated for each mirror, and optics with roughly equivalent constants were grouped together. The category of traditional mirrors, shown in Figure 1.7, is comprised of solids and heavier light-weights (primarily contoured mirrors) and has an average k of 2560. The light-weight mirror category consisting of commonly configured light-weights has an average k of 802 (see Figure 1.8). The smallest average k value belongs to the ultra-lightweight mirror category. This group, shown in Figure 1.9, includes the very unusual light-weight designs and the majority of the beryllium mirrors. Figure 1.10 illustrates the weight to diameter relationship of all 3 of these categories on a single graph for comparison. It is noteworthy that light-weight mirrors fit the power law the best, and the ultra-lightweights came the closest to satisfying the 2.6 exponent of the light-weight equation (1.1).

1.5. CONCLUSIONS

A sample size of approximately 50 light-weight mirrors was used to examine the relationship between weight and diameter. Table 1.4 summarized the results found for each mirror category and includes both the best fitting function and the commonly used power function.

While 50 samples of approximately 50 light-weight mirrors was used to examine the relaionship between weight and diameter. Table 1.4 summarizes the results found for each mirror category and includes both the best fitting functino and the commonly used power function.

Solid Mirrors:	W	=	$246\ D^{2.92}$
Light-weight Mirrors:	W	=	$82\ D^{2.95}$

For specific mirror types, however, a more precise relationship can be used to scale weight as a function of diameter:

Structured Mirrors	W	=	$68\ D^{2.90}$
Contoured Mirrors	W	=	$106\ D^{2.71}$
Beryllium Mirrors	W	=	$26\ D^{2.31}$

Mirrors may also be described using the light-weight relationship of equation (1.1):

Traditional $k_{avg} = 2560$	W	=	$192\ D^{2.76}$
Light-weight $k_{avg} = 802$	W	=	$120\ D^{2.82}$
Ultra-lightweight $k_{avg} = 387$	W	=	$53\ D^{2.67}$

With a better understanding of the weight to diameter relationship of specific mirror types, more informed choices can be made for candidate light-weight mirrors and more accurate weight estimations can be made for weight sensitive systems.

REFERENCES

1. Vukobrtovich, D., "Introduction to Opto-Mechanical Design," *Opto-Mechanical Course Notes*, Optical Sciences Center, University of Arizona, Tucson, AZ, 85721, pp. 202-203, 1986.

2. Hamill, D., "Fabrication Technology of Advanced Space Optics," *Workshop on Optical Fabrication and Testing, Tucson, Arizona*, Optical Society of America, Washington, DC, 1980.

3. Meinel, A.B., "Cost Scaling Laws Applicable to Very Large Optical Telescopes," *Proc. SPIE 172* pp. 2-7, 1979.

4. Rule, B.H., "Large Telescope Mounts," *Large Telescope Design Proceedings ESO/CERN Conference*, Geneva, March 1-5, 1971, pp. 283-297

5. King, H.C., *The History of the Telescope*, Dover Pub., New York, NY, 1979.

6. Pearson, E.T., "Effects of the Cassegrain Hole on Axial Ring Supports," in *Support and Testing of Large Astronomical Mirrors*, edited by Crawford, D.L., Meinel, A.B., and Stockton, M.W., Kitt Peak National Observatory, Tucson, AZ, July, 1968.

7. Humphries, C.M., "Thin Mirror Telescopes: Experience Gained with the U.K. Infrared Telescope," in *Optical and Infrared Telescopes for the 1990s*, edited by Hewitt, A., Kitt Peak National Observatory, Tucson, AZ, May 1980.

8. Nelson, J.E., Mast, T.S., and Faber, S., *The Design of the Keck Observatory and Telescope*, Keck Observatory Report No. 90, Keck Observatory Science Office, Lawrence Berkley, CA, January, 1985.

9. Scott, R.M., "Optical Engineering," *Appl. Opt.*, Vol. 1, No. 4, pp. 387-397, July 1962.

10. Malvick, A.J., "Theoretical Elastic Deformations of the Steward Observatory 230-cm and the Optical Sciences Center 154-cm Mirrors," *Appl. Opt.*, Vol. II, No. 3, pp. 575-585, March 172.

11. Babbish, R.C., and Rigby, R.R., "Optical Fabrication of a 60-inch mirror," *Proc. SPIE 183*, pp. 105-108, 1979.

12. Jones, L.R., "Control Software for the La Palma Telescopes," *Proc. SPIE 628*, pp. 429-433, 1986.

13. Pavlov, V.N., "Load Relief System of the Primary Mirror of the Large Azimuth Telescope (LAT)," *Sov. J. Opt. Technol.*, Vol. 46, No. 2, pp.104-106, (Feb. 1979).

14. Jackson, B.W., "Structural Design for Large Space Telescopes," *Optical Telescope Technology, MSFC Workshop, April 1969*, NASA Report SP-233, pp. 351-357.

15. Tarenghi, M., "Eurpoean Souther Observatory (ESO), 3.5m New Technology Telescope," *Pric. SPIE 628*, pp.213-220, 1986.

16. Kodaira, K., "Status Report of the JNLT Project," in *Workshop on Japanese National Telescope*, Tokyo Astronomical Observatory, pp. 6-9, June 1987.

17. Young, P. and Schreilbman, M., "Alignment Design for a Cryogenic Telescope," *Proc. SPIE 251*, PP. 171-178, 1980.

18. Kilpatrick, D.H., *Mirror Deformation due to Thermal Cycling*, unpublished report.

19. Tobin, E., Gardopee, G.., Fink, R., Petrie, W., Vernold, C., and Carbone, F., *One Meter Beryllium Mirror Polishing and Characterization Program*, Perkin-Elmer Corp., 100 Wooster Heights Road, Danbury, CT., 16810, May 1989.

20. Altenhof, R.R., "The Design and Manufacutre of Large Beryllium Optics," *Proc. SPIE 65*, pp. 20-32, 1975.

21. Starkus, C.J., "Large scan mirror assembly of the new Thematic Mapper developed for LANDSAT 4 earth resources satellite, "*Proc. SPIE 430*, PP. 85-92, 1983.

22. Paquin, R.A., "Hot Isostatic Pressed Beryllium for Large Optics, " *Proc. SPIE 571*, pp. 259-266, 1985.

23. Paquin, R.A., and Groggin, W.R., "Beryllium Mirror Technology-State-of-the-Art Report,"Perkin-Elmer Optical Group, 100 Wooster Heights Road, Danbury, CT, 16810, 1983.

24. Bowen, I.S., "The 200-Inch Hale Telescopes in *Telescopes*, edited by Kuiper, G.P., and Middlehurst, B.M., The University of Chicago Press, Chicago, IL, 1960.

25. Richard, R.M., and Malvick, A.J., "Elastic Deformations of Lightweight Mirrors," *Appl. Opt.*, Vol. 12, No. 6, pp. 1220-1226, (June 1973).

26. Huss, C.E., *Axisymmetric Shells under Arbitrary Loading*, Ph.D. thesis, University of Arizona, Tucson, AZ, May, 1980.

27. Muffoletto, C.V., "Fabrication of a 92 cm Diameter Light-weight F/2 Paraboloid Ultraviolet Telescope Mirror," *Workshop on Optical Fabrication and Testing, Tucson, Arizona*. Optical Society of America, Washington, DC, 1980.

28. Lewis, W.C., "Space telescope mirror substrates," *Proc., SPIE 183*, pp. 114-117, 1979.

29. Pepi, J.W., and Wollensak, R.J., "Ultra-lightweight Fused Silica Mirrors for a Cryogenic Space Optical Systems," *Proc. SPIE 183*, pp. 131-137, 1979.

30. Yoder, P.R., *Opto-Mechanical Systems Design*, Marcel-Dekker, New York, NY, 1986.

31. Lillie, C.F., and Lawrence, G.M., "A Rocket-Borne Faint Object Spectograph with a Codacon Detector," *Proc. SPIE 172*, pp. 321-321-325, 1979.

32. Goble, L., Angel, J.R.P., and Hill, J.M. "Steps Toward 8m Honeycomb Mirrors VII. Spin Casting and Experimental f/1 1.8m Honeycomb Blank of Borosilicate Glass," *Proc. SPIE 571*, PP. 92-100, 1985.

33. Melugin, R.K., et al, "Development of lightweight, glass mirror segments for the Large Deployable Reflector," *Proc. SPIE 571*, pp. 101-114, 1985.

34. Bulge, J.H., and Mayor, R.A., "Thermal Stability of Lightweight Graphite Glass Sandwich Reflectors for Far infrared Astronomy," *Proc. SPIE 571*, pp. 254-258, 1985.

35. Siegmund, W.A., and Mannery, E.J., "Design of the Apache Point Observatory 3.5 m Telescope II. deformation analysis of the primary mirror," *Proc. SPIE 628*, pp. 377-389, 1986.

36. Eastman Kodak Co., "A Mirror for the World's Most Powerful Telescope," U.S. Apparatus Division, Rochester, NY 14650, 1983.

37. Hill, J.M., and Angel, J.R.P., "Steps Toward 8m Honeycomb Mirror Blanks II, experiments with a waffleplate and honeycomb casting," *Proc. SPIE 380*, pp. 100-109, 1983.

38. Anderson, D., Parks, R.E., Hansen, Q.M., and Melugin, R., "Gravity Deflections of LightweightMirrors," *Proc. SPIE 332*, pp. 424-435, 1982.

39. Lansing, J.C., Jr., Wise, T.D., and Harney, E.D., "Thematic Mapper Design Description and Performance Prediction," *Proc. SPIE 183*, pp. 224-234, 1979.

40. Schlegelmilch, R., et al, *GIRL-German Infrared Laboratory; Final report of the Telescope study, Phase B*. NASA TM-75911, January 1981.

41. Espiard, J., Paseri, J., Cerutti-Maori, G., and Singer, C., "Lightweight Cold Mirrors and Fixation," *Proc. SPIE 589*, 589, pp. 193-197, 1985.

42. Hextek Corp., "Lightweight Gas Fusion Blanks," P.O. Box 42943, Tucson, AZ 85733, 1989.

43. Meinel, A.B., "Design of Reflecting Telescopes," in *Telescopes*, edited by Kuiper, G.P., and Middlehurst, B.M., The University of Chicago Press, Chicago IL, 1960.

44. McCarthy, D.J., and Facey, T.A., "Design and Fabrication of the NASA 2.4 meter space telescope" *Proc. SPIE 330*, PP. 139-143, 1982.

45. DeMottoni, G., "An Italian 54-Inch Reflector of Unusual Design," *Sky and Telescope*, pp. 296-297, May 1972.

46. Hoffman, W.F., Fazio, G.G., and Harper, P.A., "A balloon-borne three-meter telescope for far infrared and submillimeter astronomy," *Proc. SPIE 444*, pp. 53-64, 1983.

47. Robachevskaya, V.I., and Rodevich, G.V., "A Study of the Stiffness of Light-weight mirrors of various constructions," *Sov. J. Opt. Technol. Vol. 44, No. 1*, pp. 6-11, January 1977.

48. Robachevskya, V.I., and Ivantosvskii, P.P., and Petrova, L.A., "Experience in the Fabrication and testing of 370-millimeter light-weight silica mirrors," *Sov. J. Opt. Technol., Vol.44, No. 7*, pp. 423-424, July 1977.

49. Derevenskii, V.D., Dul'kin, L.Z. Karavashkin, A.I., Paimushia, V.N., and Saitov, I.Kh., "Thermal Characteristics and thermal deformations of light-weight mirrors," *Sov. J. Opt. Technol., Vol. 50, No. 4*, April 1983, pp. 221-225.

50. Vitrichenko, E.A., et al, "Investigation of the possibility of building large light-weight metal mirrors for the long-wave IR spectrum," *Sov. J. Opt. Technol., Vol. 52, No. 3*, pp. 140-143, March 1985.

51. Barnes, W.P., "Transverse Deflections of a 45-Inch Diameter Lightweight Mirror Blank: Experiment and Theory," *Optical Telescope Technology, MSFC Workshop, April 1969*, NASA Report SP- 233, pp. 287-290.

52. Vukobratovich, D., "Ultra-lightweight optics for laser communications," *Proc. SPIE 1218*, 1990.

53. Carter, W.E., "Lightweight Center-Mounted 152-cm f/2.5 Cer-Vit Mirror," *Appl. Opt., Vol. 11, p. 467, 1972.*

I.D.	NAME OF CURVE	EQUATION OF CURVE
1)	Linear	Y = a + bX
2)	Recip. Linear	Y = 1/(a + bX)
3)	Linear Hyperbola	Y = a + bX + c/X
4)	Hyperbola	Y = a + b/X
5)	Recip. Hyperbola	Y = X/(aX + b)
6)	2nd Hyperbola	Y = a + b/X + c/X**2
7)	Parabola	Y = a + bX + cX**2
8)	Cauchy Distribution	Y = 1/(a + (X + b)**2 + c)
9)	Logarithmic	Y = a + b lnX
10)	Recip. Logarithmic	Y = 1/(a + b lnX)
11)	Power	Y = a + X**b
12)	Super Geometry	Y = a + X**(bX)
13)	Mod. Geometry	Y = a + X**(b/X)
14)	Hoerl	Y = a b**X X**c
15)	Modified Hoerl	Y = a b**(1/X) X**c
16)	Log Normal	Y = a EXP ((b - lnX)**2/c)
17)	Modified Power	Y = a b**X
18)	Root	Y = a b**(1/X)
19)	Normal Distribution	Y = a EXP ((X - b)**2/c)

Table 1.1 List of Curve Fit Options

MIRROR	REF	YEAR	DIA (M)	THICK (M)	WEIGHT (KG)	MATL	CONFIG	MISC.
Mount Wilson	5	1918	2.5	0.33	4083	glass	solid	Aspect ratio=13
Mayall	6	1973	4.0	0.56	15880	quartz	solid w/.66M hole	Aspect ratio=14
UKIRT	7	1979	3.8	0.24	6500	Cervit	solid w/1.0M hole	Aspect ratio=06
KECK	8	1990	2.0	0.08	763	Zerodur	solid 36 hex segs	Aspect ratio=03
Stratascope II	9	1965	0.91	0.13	181	F silica	solid	Aspect ratio=14
Steward Stellar	10	1972	2.3	0.33	2340	Cervit	solid w/.7M hole	Aspect ratio=14
P-E 60 inch	11	1979	1.52	0.09	380	ULE	solid w/.25M hole	Aspect ratio=06
WHT	12	1988	4.2	0.52	16000	Cervit	solid	Aspect ratio=12
Soviet Crimea	13	1976	6.0	0.65	42000	Pyrex	solid w/.36M hole	Aspect ratio=11
OAO-B	14	1970	0.97	0.04	57	Beryllium	solid meniscus	Aspect ratio=04
ESO NTT	15	1988	3.5	0.24	6000	Zerodur	solid w/.58M hole	Aspect ratio=06
JNLT	16	1983	7.5	0.2	17236	ULE	solid w/hole	Aspect ratio=03
OSC Test mirror	16	1972	1.54	0.25	910	------	solid	Aspect ratio=16

Table 1.2 Solid Mirrors Surveyed

MIRROR	REF	YEAR	DIA. (M)	THICK. (M)	WEIGHT (KG)	MATL	CONFIG	MISC.
RAS	17	1983	0.60	0.09	12.6	Beryllium	Openback	annular ribs
Ball Relay	18	1989	0.60	0.06	9.07	Beryllium	Openback tri. cells	Hip process
P-E 40 inch	19	1989	1.02	0.05	18.14	Beryllium	Sandwich hex cells	2.265 in cells
P-E Scan	20	1975	36x 81	0.08	14.52	Beryllium	Openback sqr. cells	Flat to 20
P-E second.	20	1975	1.65x1.02	0.08	53.5	Beryllium	Openback sqr. cells	f/0.67
Thematic Map.	21	1972	406x.508	0.04	1.36	Beryllium	Sandwich sqr. cells	Brazed
P-E 9.5 inch	22	984	0.24	0.05	0.98	Beryllium	Sandwich hex cells	HIP process
P-E Test	23	----	0.57	0.04	13.25	Beryllium	Double arch	------
P-E Test	23	----	0.51	0.05	5.51	Beryllium	Double arch	1 in circ. cores
Hale	24	1950	5.0	0.60	13158	Pyrex	Openback	------
MMT	25	1979	1.8	0.30	567	F silica	Sandwich sqr. cells	6 mirrors
RCT	26	1965	1.3	0.15	200	Aluminum	Single arch	------
Spacelab UV	27	1979	0.92	0.15	100	Cervit	Double arch	------
Hubble	28	1990	2.48	0.30	773	ULE	Sandwich sqr. cells	------
Teal Ruby	29	1980	0.50	0.08	7.3	F silica	Sandwich hex cells	------
OAO-c	30	1972	0.82	0.13	48	F silica	Sandwich sqr. cells	------
U of Colorado	31	1979	0.41	0.05	9.98	Cervit	Double arch	f/2.5, 1.4λ
Steward Obs.	32	1985	1.8	0.36	703	Boromlicate	Sandwich hex cells	f/1.0
LDR test	33	1985	0.38	0.13	6.24	Boromlicate	Sandwich hex cells	sand-blasing
LDR test	33	1985	0.15	0.05	0.53	Vycor	Sandwich hex cells	air pressure
UTRC	34	1985	0.30	0.06	1.1	Glass TSC	Sandwich	Frit bonded
Ft. Apache	35	1986	3.5	0.46	1893	Boromlicate	Sandwich hex cells	------
Naas	36	1983	2.48	0.30	771	Glass	Sandwich sqr. cells	------
Los Alamos	37	1982	1.1x1.1	0.20	204	Tempax	Openback sqr. cells	------
SIRTF test	38	1983	0.51	0.089	16-25	quartz	Single arch	------
SIRTF test	38	1983	0.51	0.102	19-29	F silica	Double arch	f/4
Landsat-D	39	1979	0.42	0.07	9	ULE	Sandwich sqr. cells	------
GIRL	40	1985	0.50	0.074	25	Zerodur	Double taper	------
ISO	41	1985	0.64	0.075	20	F silica	Sandwich	machined
Hextek	42	1989	1.0	0.15	73	Boromlicate	Sandwich hex cells	f/0.5, meniscus
Hextek	42	1989	0.46	0.086	5.17	Boromlicate	Sandwich hex cells	------
Hextek	42	1989	0.38	0.076	7.71	Boromlicate	Sandwich hex cells	------
Shane 3 M.	43	1959	3.0	0.406	3856	Pyrex	Openback tri. cells	f/5
NASA 2.4 M.	44	1981	2.4	0.305	748	ULE	Sandwich sqr. cells	f/2.35
Milan 54 inch	45	1968	1.37	0.20	907.2	Aluminum	Single arch	------
Steward 68 cm.	46	----	0.68	0.10	25.4	Pyrex	Sandwich hex cells	------
Soviet test	47	1977	0.506	0.076	13.7	quartz	Openback hex cells	54mm cells
Soviet test	47	1977	0.50	0.065	12.5	quartz	Sandwich hex cells	54mm cells
Soviet test	48	1977	0.37	0.052	5.2	F silica	Sandwich hex cells	28mm cells
Soviet test	49	1983	0.52	0.053	12.4	F silica	Sandwich	70mm cells
Soviet test	49	1983	0.57	0.057	13.2	F silica	Sandwich	71mm cells
Soviet test	49	1983	0.42	0.059	11.2	F silica	Sandwich	77mm cells
Soviet test	50	1985	0.70	0.10	20	Al alloy	Openback	annular ribs
Schott test	51	----	1.143	0.159	204.12	F silica	Sandwich	------
OSC 16 in scope	52	1989	0.406	0.076	6.17	SXA	Single arch	------
OSC 12 in scope	52	1988	0.305	0.064	2.04	Aluminum	Double concave	Al foam core
OSC 12 in scope	52	1988	0.305	0.043	1.95	Aluminum	Double concave	Al foam core
AFCRL	53	1972	1.524	0.165	363	Cervit	Single arch	------

Table 1.3. Lightweight Mirrors Surveyed

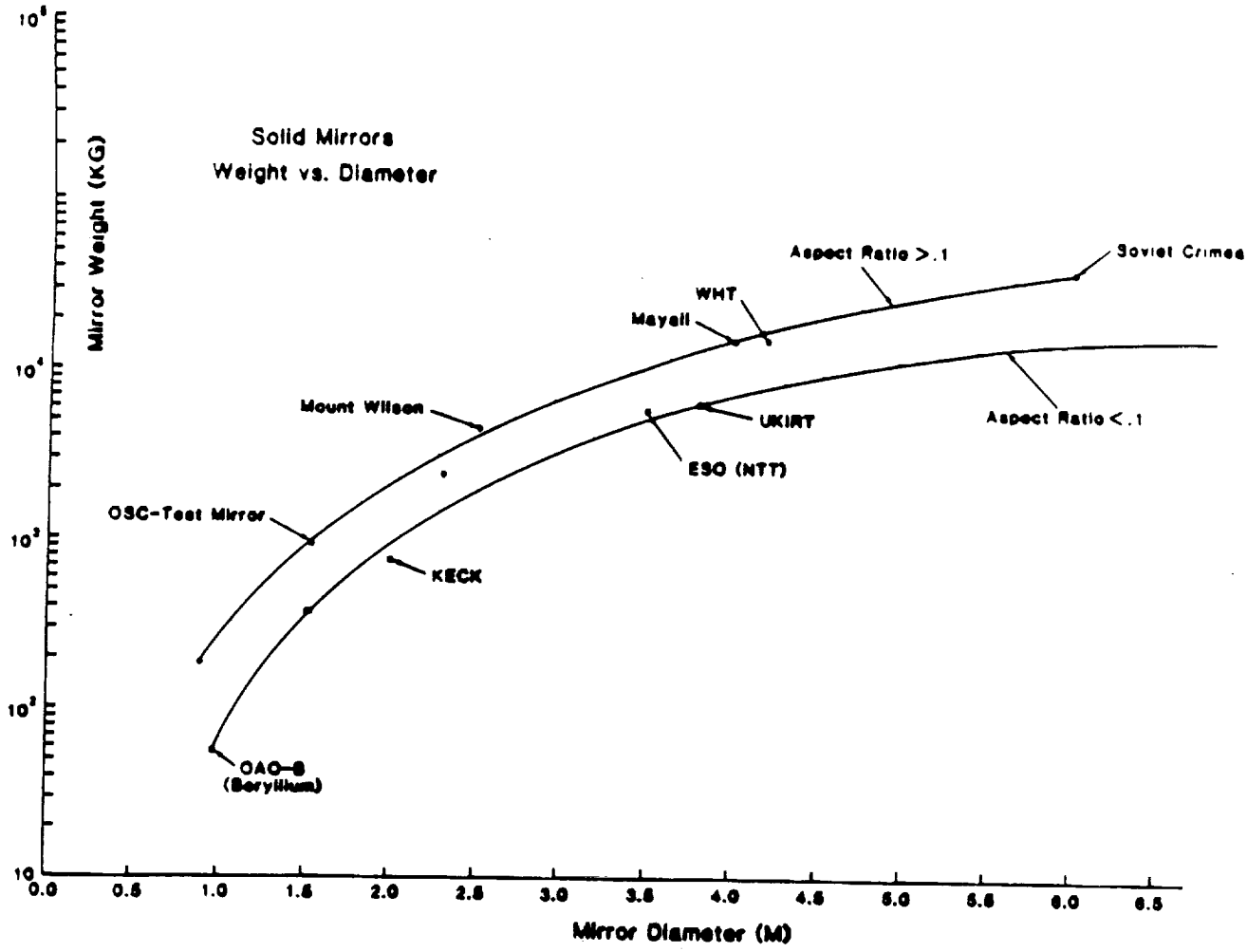

	Aspect Ratio h/D <.1	Aspect Ratio h/D >.1
BEST FIT FUNCTION	HOERL FUNCTION $Y = (117.7).5457^X \, X^{4.738}$	PARABOLA FUNCTION $Y = 2279 - 3721X + 1721X^2$
GOODNESS OF FIT	.9951	.9974
POWER FUNCTION	$Y = 98.78X^{2.867}$	$Y = 246.1X^{2.917}$
GOODNESS OF FIT	.9452	.9957

Figure 1.1. Weight vs. Diameter of Solid Mirrors

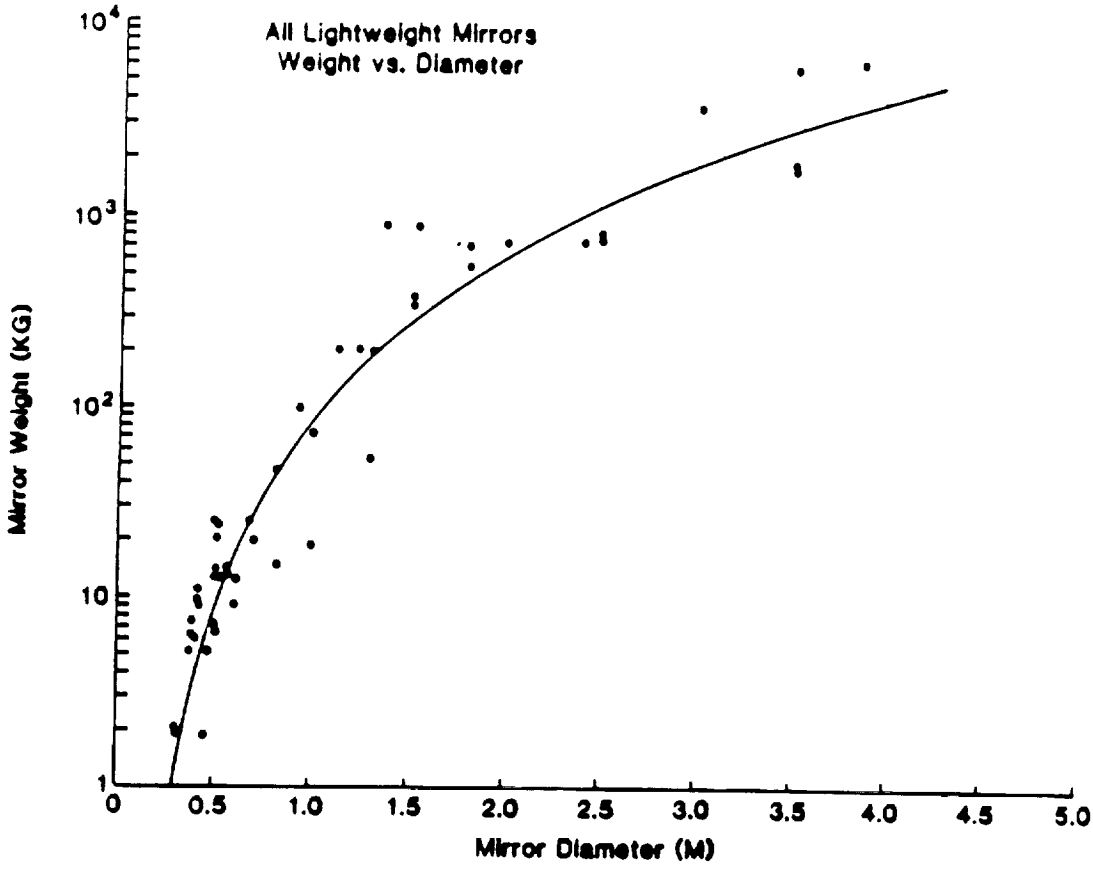

BEST FIT FUNCTION	POWER FUNCTION $Y = 11.89X^{2.949}$	GOODNESS OF FIT .9459

Figure 1.2. Weight vs. Diameter of All Light-Weight Mirrors

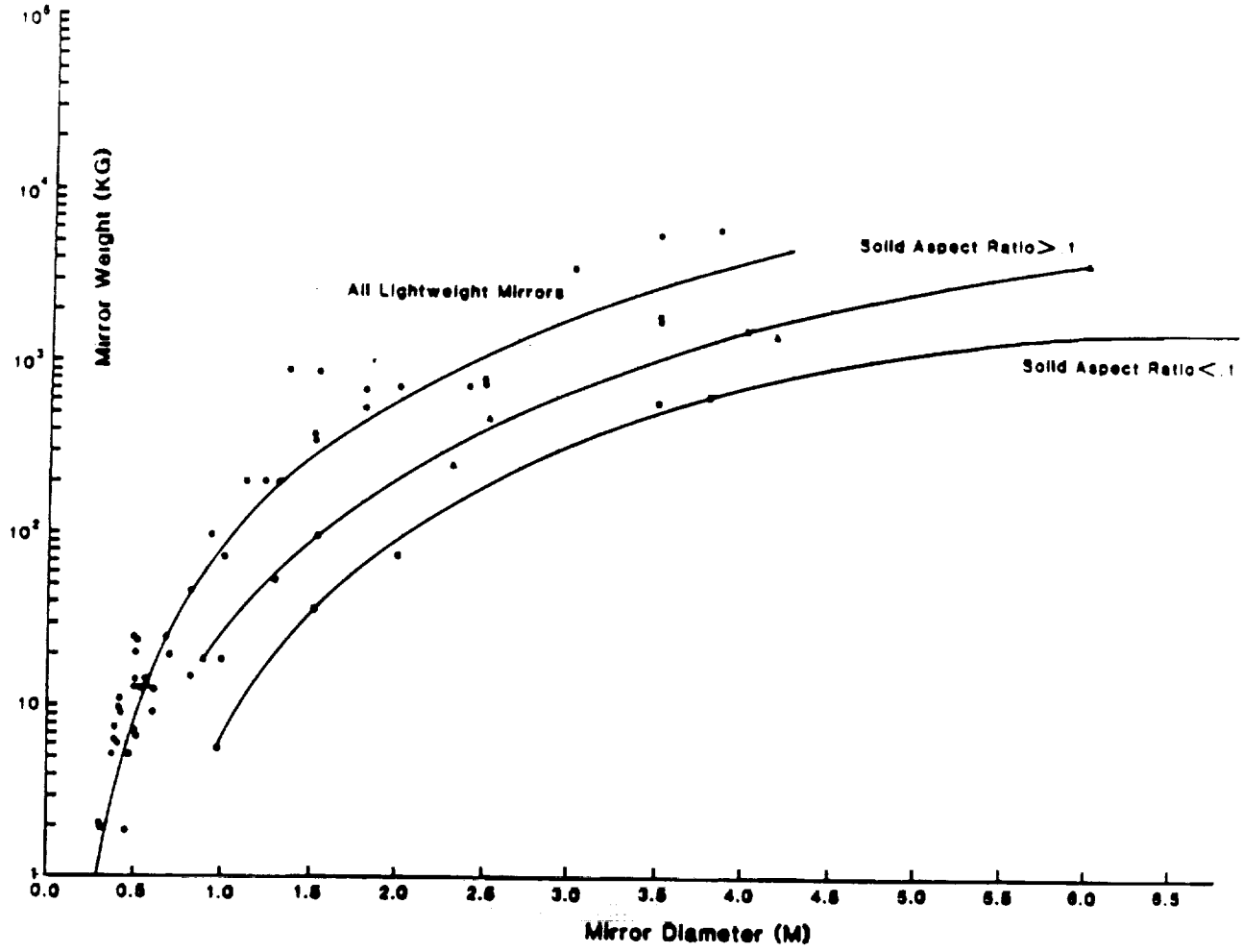

Figure 1.3. Weight vs. Diameter of Solids and Light-Weight Mirrors.

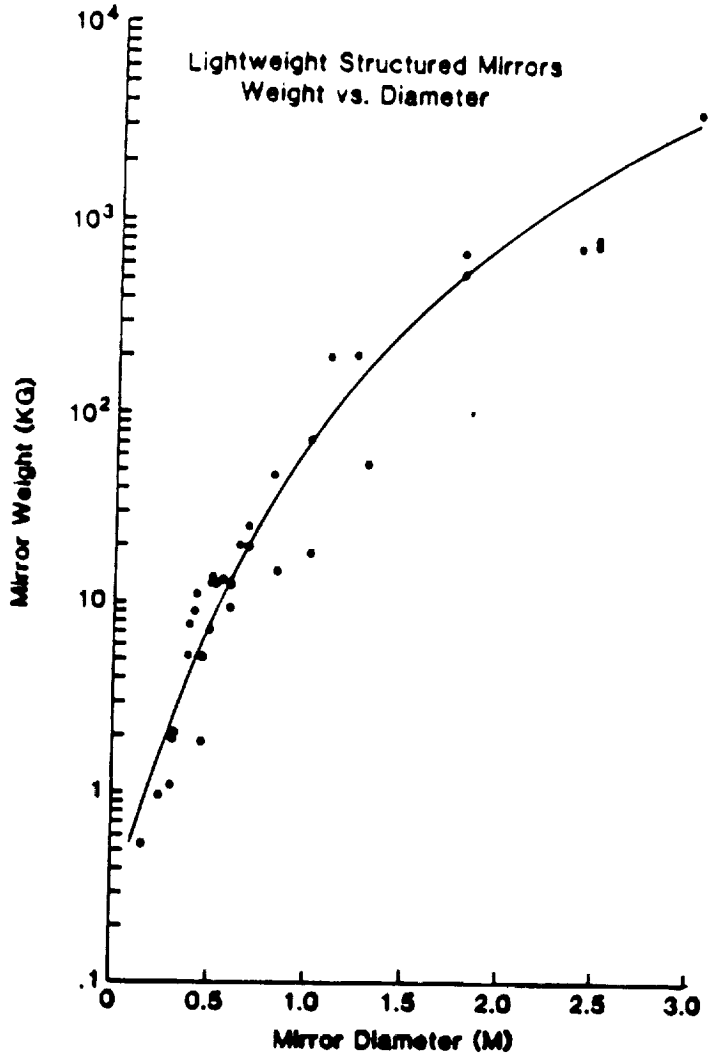

		GOODNESS OF FIT
BEST FIT FUNCTION	LOG NORMAL $Y = .177 \times 10^{-3} \exp\left[(-8.739 - \ln X)^{\frac{2}{5.998}}\right]$	.9512
POWER FUNCTION	$Y = 106X^{2.712}$	.9499

Figure 1.4. Weight vs. Diameter of Structured Mirrors

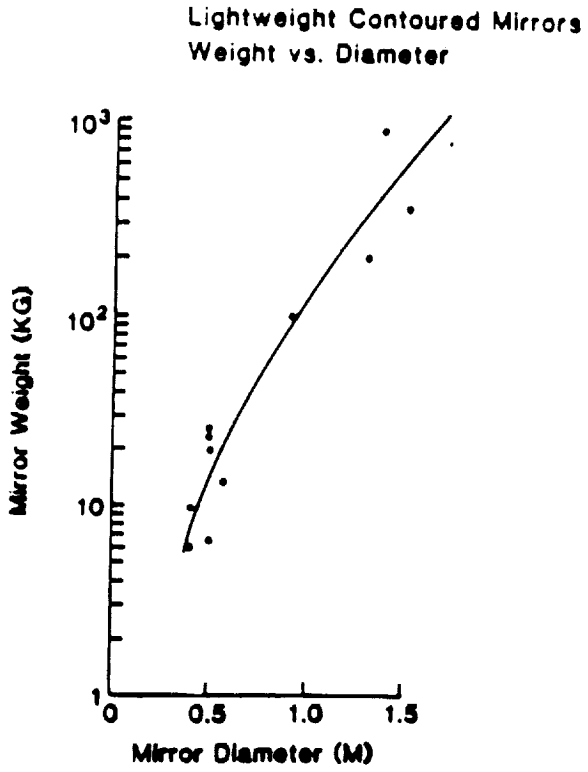

		GOODNESS OF FIT
BEST FIT FUNCTION	LINEAR HYPERBOLA $Y = -4409+2854X+1439/X$	.9967
POWER FUNCTION	$Y = 106X^{2.712}$	.9728

Figure 1.5. Weight vs. Diameter of Contoured Mirrors

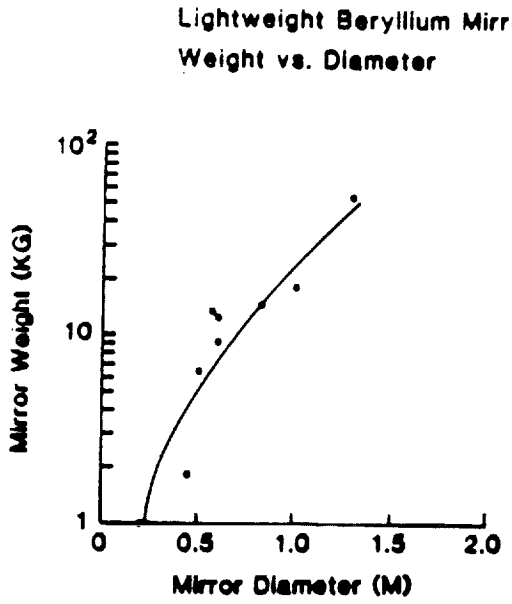

		BEST FIT FUNCTION
BEST FIT FUNCTION	PARABOLA FUNCTION $Y = 7.75-27.12X+45.41X^2$	.8784
POWER FUNCTION	$Y = 26.19X^{2.305}$	.8566

Figure 1.6. Weight vs. Diameter of Beryllium Mirrors

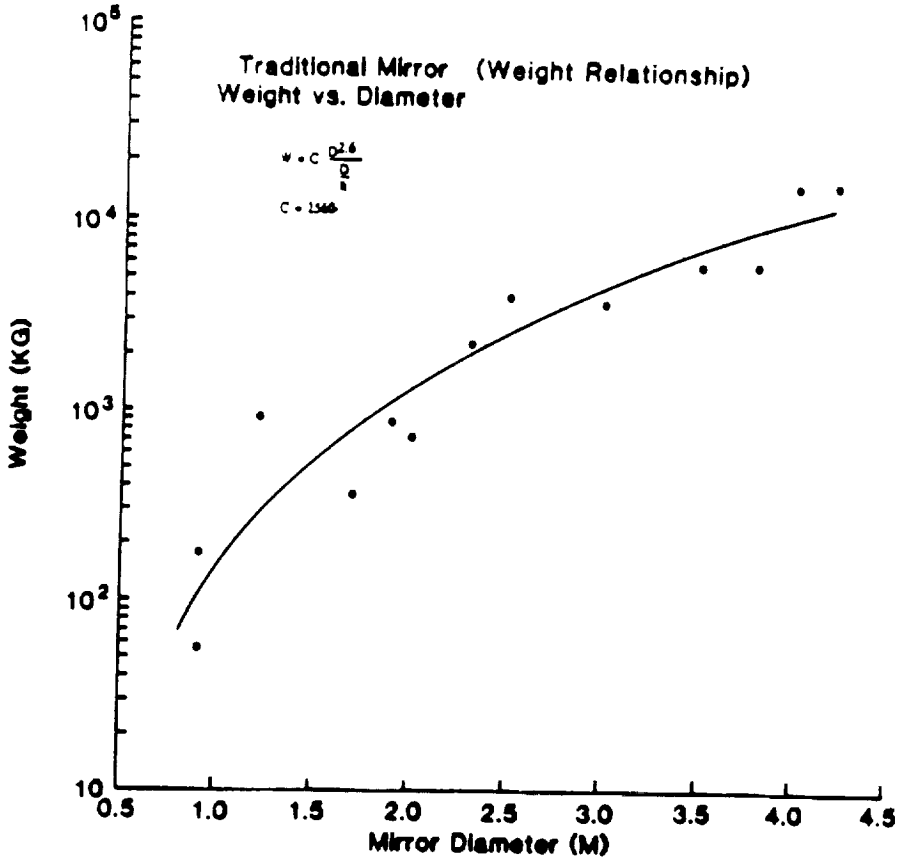

		GOODNESS OF FIT
BEST FIT FUNCTION	HOERL FUNCTION $Y = (232.9).6399^X X^{4.037}$	.9249
POWER FUNCTION	$Y = 191.8X^{2.763}$	.9097

Figure 1.7. Weight vs. Diameter of Traditional Mirrors (weight dependent)

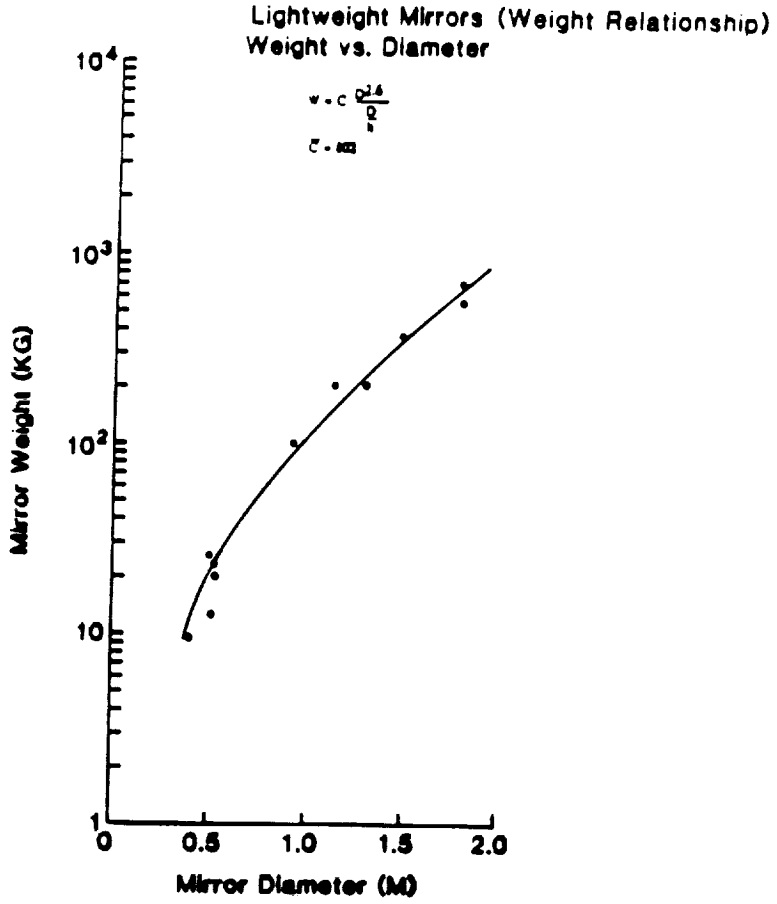

		GOODNESS OF FIT
BEST FIT FUNCTION	PARABOLA FUNCTION $Y = 95.2 - 332.2X + 349.4X^2$	.9707
POWER FUNCTION	$Y = 120.4X^{2.828}$	.9707

Figure 1.8. Weight vs. Diameter of Light-Weight Mirrors (weight dependent)

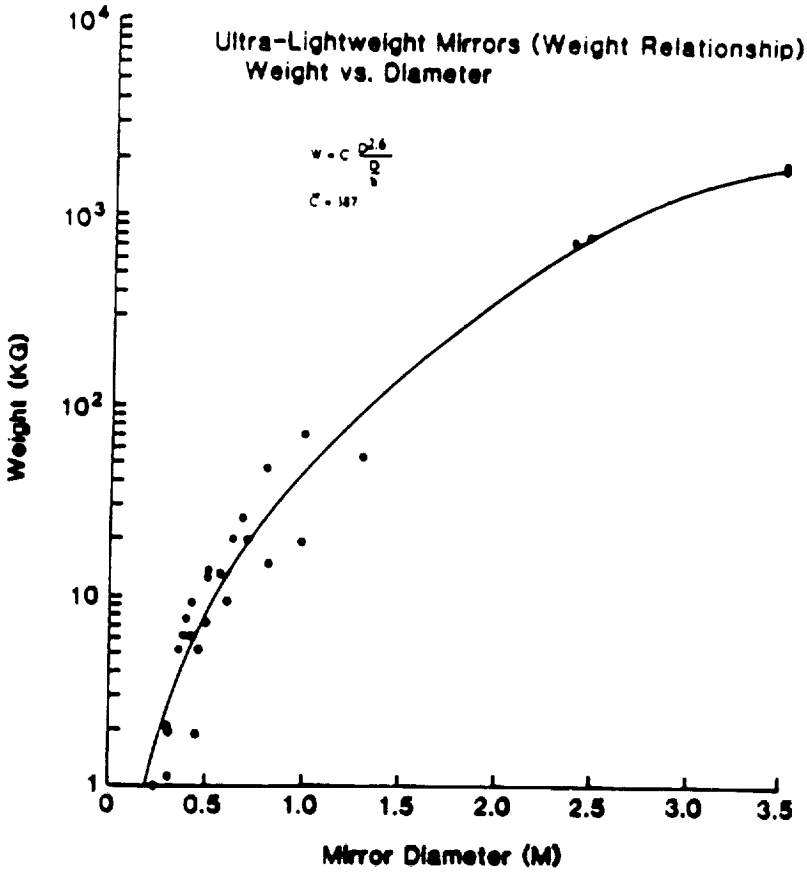

		GOODNESS OF FIT
BEST FIT FUNCTION	PARABOLA FUNCTION $Y = 62.76 - 229.3X + 211.4X^2$	.9977
POWER FUNCTION	$Y = 53.15X^{2.666}$	.9423

Figure 1.9. Weight vs. Diameter of Ultra-Lightweight Mirrors (weight dependent)

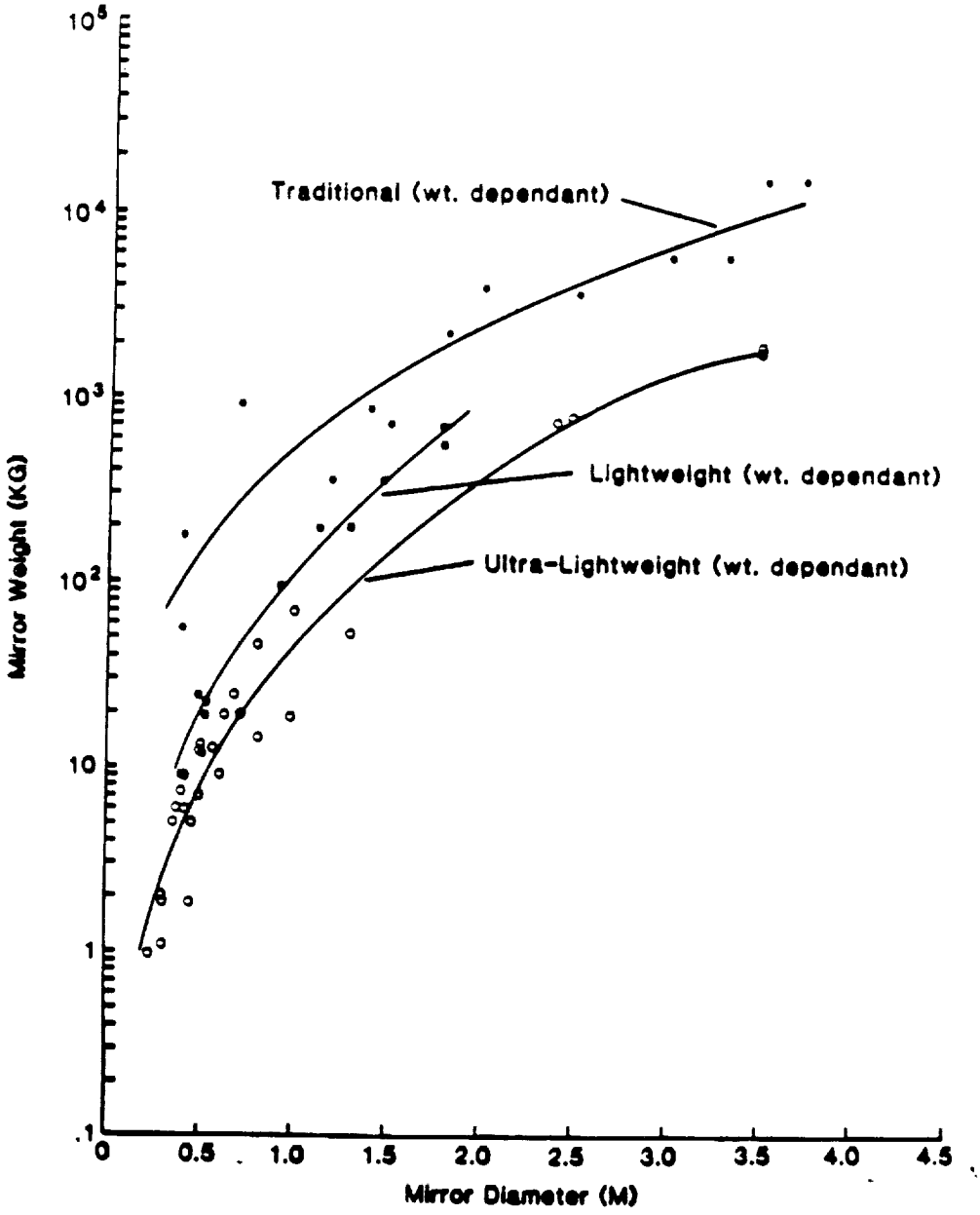

Figure 1.10. Weight vs. Diameter of Traditional, Light-Weight and Ultra-lightweight Mirrors

MIRROR CATEGORY	BEST FIT CURVE	GOODNESS OF FIT	POWER FUNCTION CURVE	GOODNESS OF FIT
Solids with large aspect ratios $\frac{h}{D}$	Parabola Fcn $Y = a + bX + cX^2$ $a = 2279$, $b = -3721$ $c = 1721$	.9974	$Y = aX^b$ $a = 246.1$ $b = 2.917$	.9957
Solids with small aspect ratios $\frac{h}{D}$	Hoerl Fcn $Y = ab^X X^c$ $a = 117.7$, $b = .546$ $c = 4.74$	.9951	$Y = aX^b$ $a = 98.78$ $b = 2.867$	.9452
All lightweight mirrors	Power Fcn $Y = a + X^b$ $a = 81.89$ $b = 2.949$	.9459	$Y = aX^b$ $a = 81.99$ $b = 2.949$	.9459
Structured mirrors	Log Normal Fcn $Y = a\,EXP(b - \ln X)^{\frac{2}{c}}$ $a = .18E-3$, $b = -8.74$ $c = 5.996$	.9512	$Y = aX^b$ $a = 67.97$ $b = 2.898$	.9499
Contoured mirrors	Linear Hyperbola $Y = a + bX + \frac{c}{X}$ $a = -.4409$, $b = 2854$ $c = 1439$	.9967	$Y = aX^b$ $a = 106.0$ $b = 2.712$	.9728
Lightweight beryllium mirrors	Parabola Fcn $Y = a + bX + cX^2$ $a = 7.75$, $b = -27.12$ $c = 45.4$	.8784	$Y = aX^b$ $a = 26.19$ $b = 2.305$	.8566
Traditional mirrors ($C_{avg} = 2560$) $W = \frac{CD^{2.6}}{\frac{D}{h}}$	Hoerl Fcn $Y = ab^X X^c$ $a = 232.9$, $b = .636$ $c = 4.037$	.9249	$Y = aX^b$ $a = 191.8$ $b = 2.763$	.9097
Lightweight mirrors ($C_{avg} = 802$) $W = \frac{CD^{2.6}}{\frac{D}{h}}$	Parabola Fcn $Y = a + bX + cX^2$ $a = 95.2$, $b = -332.2$ $c = 349.4$	.9707	$Y = aX^b$ $a = 120.4$ $b = 2.820$	.9707
Ultra lt.wt. mirrors ($C_{avg} = 387$) $W = \frac{CD^{2.6}}{\frac{D}{h}}$	Parabola Fcn $Y = a + bX + cX^2$ $a = 62.76$, $b = -229.3$ $c = 211.4$	.9977	$Y = aX^b$ $a = 53.15$ $b = 2.666$	.9423

Table 1.4. Curve Fitting Summary

2. STUDIES OF LIGHTWEIGHT MIRROR MOUNTING AND DYNAMIC MIRROR STRESS

2.1. SUMMARY

Mounting concepts for lightweight mirrors were reviewed, analytical methods were developed for determining global stress in mirrors due to dynamic loadings, and parametric studies of local stress for both flat pad and conical mounts were made. Nine different mounting concepts for lightweight mirrors were reviewed; the most suitable designs for the SIRTF primary mirror mount are the conical mount, the bolted mount for glass mirrors, and the bolted mount for beryllium mirrors. Global stress in the primary mirror due to launch loads is an important design parameter. For a given dynamic environment, characterized by a Power Spectral Density Function (PSD), a new material parameter for minimum mirror weight was identified, and is given by:

$$W_{min} \propto (\rho/\sigma_A)^2 (\rho E)^{1/2} \qquad (2.1)$$

where:

W_{min}	is the minimum mirror weight
ρ	is the mirror material density
σ_A	is the maximum allowable stress for the mirror material (fracture stress for glass, micro-yield stress for beryllium)
E	is the elastic modulus of the mirror material

Analytical expressions for both flat pad mounts and conical mounts were used to determine mounting stress as a function of geometry, size, and dynamic response of the mirror mount. Use of closed form expressions dramatically simplify the cost and time required to perform initial design of the primary mirror mount.

2.2. MOUNTING CONCEPT REVIEW

The review of mounting methods concentrated on mirror mounting concepts which were relevant to the SIRTF primary mirror problem. Criteria used to evaluate suitability were the ability of the mount to limit stress in the mirror due to changes in temperature, and the adaptability of the mirror mount to a spacecraft application. Only mount designs which involved some hardware experience were considered. No effort was expended on evaluating mirror mount designs which have only been developed as concepts. This hardware emphasis in the concept review limits the review to a historical perspective. Promising new configurations which are under development were not considered.

Classified programs were not evaluated as part of the mirror mount review. Use of open university facilities precluded examination of classified materials. Since the final report is intended to be an open public document, classified concepts could not be included.

The concept review was carried out in three phases. In the first phase, a literature search for information on mirror mounting was carried out as part of the overall literature search for the program. Abstracts of papers identified from this literature search were then reviewed, and if promising, the supporting documentation obtained. At the same time, extensive use of the personal contacts of members of the Optical Sciences Center was made to find projects in which suitable mirror mount designs might exist. These contacts were followed up by correspondence, telephone calls, and personal visits. In the second phase of the concept review, nine candidate concepts were selected for detailed examination. These concepts were reviewed on the basis of recorded performance; if performance figures were not available, calculations were made to attempt to predict performance. Cost, ease of fabrication, and adaptability to different mirror configurations, were

other factors in the review. In the third phase of the review, three designs were selected as candidates for the SIRTF primary mirror mount. The performance of these three designs was then modeled under another portion of the program.

The following types of mirror mounts were reviewed:

1. Bonded mounts
2. Conical mounts
3. Sphere/cone mounts
4. Sphere/cylinder mounts
5. Cylindrical clamps
6. Ball foot/clamp
7. Bolted mount (glass)
8. Flat pad mount
9. Bolted/pinned mount (beryllium)

Criteria used to evaluate the mirror mount performance included[1]:

1. Ability to support the SIRTF primary mirror, assumed to weigh no more than 150 kg, with a diameter of 1.0 m and a thickness of less than 130 mm. (The thickness limit is set by the availability of fused silica mirror blanks if a single boule is used.)

2. Mount induced distortion due to a 292 K drop in temperature, from 300 K to 8 K, the temperature of the liquid helium dewar, should be less than 89 nm RMS.

3. Maintain optical alignment following insertion into orbit. Allowable despace is 135 microns, allowable decenter is 30 microns, and allowable tilt is 167 micro-radians.

4. The mount must retain the mirror safely in the event of an emergency landing of the Space Shuttle. Anticipated loads are 4.5 g in all axes.

5. The launch load criterion is a PSD function; the PSD is given in fig. 2.1.

Following is the detailed review of the mounting concepts studied:

2.3. BONDED MOUNTS

The descriptive term "bonded mounts" is not quite correct for this type of mounting for the SIRTF application. Due to the large thermal coefficient of expansion difference between most adhesives (silastic has a thermal coefficient of expansion of about 200 x 10^{-6} m/m-K, for example), and optical materials such as fused silica or beryllium, a classic bonded mounting is not feasible. Instead, bonding is used to attach the mirror to a flexure system which isolates the mirror from thermal coefficient of expansion effects. Adhesives are used as a mirror to flexure transition. Flexure mounting principles are discussed in Vukobratovich and Richard[2]. Tangential flexure mounts of the type most often used for mounting of lightweight space mirrors were discussed by Chin[3].

Representative examples of the combination of a bonded mirror mount and tangential flexure are the 0.5 m mirror for the TEAL RUBY[4,5], shown in fig. 2.2 and the 0.65 m Itek fused silica test mirror[6,7,8]. The bonded mount is a semi-kinematic three point design. Three square bosses extend radially from the mid-plane of the mirror circumference. Four "T" shaped flexures are bonded to the

sides of the square boss. The flexures are attached to an outer ring which surrounds the boss. The outer ring is carried on the tip of a tapered cantilever beam flexure which is tangential to the mirror edge. A mounting ring or bezel surrounds, but does not contact the mirror; the three tangential flexures attach to this ring.

The three tangential flexures provided isolation of the mirror from expansion or contraction of the outer bezel with respect to the mirror. The four inner flexures provide additional rotational compliance to allow for assembly errors which might otherwise induce moments in the mirror. Fig. 2.3 shows the metal to glass interface of this flexure configuration. Stress induced in the square boss is unlikely to propagate to the mirror surface.

Performance of the bonded mount designs has been quite good. The TEAL RUBY primary mirror was designed to operate at 70 K, and to survive a launch acceleration of 7 g steady state, with a 10 g RMS random vibration. Fundamental frequency of the mirror and mount assembly was about 45 hz, which substantially exceeded the design specification of 15 hz. Cryogenic deformation of the Itek 0.65 m test mirror was very low, with a cryogenic surface distortion of 0.26 waves RMS (1 wave = 633 nm) at 13 K.

A serious concern with the bonded design is integrity of the glass to metal adhesive joint. In the experimental 0.65 m Itek mirror, fracture and failure of the glass occurred when the flexure assembly temperature was reduced to 77 K. In fig. 2.4, fragments of the fractured glass are seen still attached to the flexure. This design used an aluminum flexure, PR-1660 polyurethane adhesive and an aluminum flexure boss. Changing the flexure material to Invar did not solve the problem; failures continued at 77 K. Etching the fused silica boss in hydrofluoric acid to strengthen the glass, and switching to a PR-1578 polyurethane adhesive specially formulated for cryogenic use prevented failures at 77 K when combined with an invar flexure. Failures continued with the aluminum flexure[9]. More recent analysis of the stress in the adhesive bond area indicates that proper selection of adhesive coupled with a very limited bond area can reduce failure probability[10].

Although the bonded mount represents a traditional and well tested mounting concept, this design is not well suited to the SIRTF primary mirror problem. Performance of the Itek 0.65 m mirror and mount at 13 K is roughly comparable with that of beryllium mirrors and about twice as bad (0.26 waves RMS for this mirror, versus 0.12 waves RMS for the ARC/Arizona double arch or 0.13 waves RMS for the ARC/Arizona single arch, one wave = 633 nm) as other types of glass mirror and mount concepts[11]. Failures in the glass to metal adhesive joint are catastrophic. Recent analysis indicates the need for relatively small adhesive bond areas, limiting bond strength. These failures during test, and the limited strength of the mount for a mirror half the size of the SIRTF primary, suggest a serious concern with the strength of a similar design for the 1 m SIRTF primary.

Additional concerns are a possible lack of long term stability due to creep of the adhesive joint, possible contamination of the optics dues to adhesive outgassing, and poor batch-to-batch repeatability of current adhesives. Use of a bonded mount for SIRTF would require research into adhesive behavior at 13 K.

2.4. CONICAL MOUNTS

Conical mounts utilize conical geometry to athermalize the contact between glass and metal. This a very traditional way of making a glass to metal contact, and is extensively used in applications such as high voltage insulators. Two different conical mounting schemes are used; a cone and a flat bearing surface, and two conical surfaces.

Use of a conical bearing surface combined with a flat surface permits athermalization of the mount if the apex of the conical surface is coincident with the flat surface and if the axis of the conical surface is perpendicular to the flat surface. Expansion or contraction of the mount materials maintains geometry, and the apex of the cone remains coincident with the flat surface. This athermalization scheme does require slip of the bearing surfaces relative to the mirror surface.

An example of an athermalized conical surface and flat surface is the primary mirror mount of the 0.35 m Mars Observer Camera (MOC) developed by Perkin-Elmer[12] and shown in fig. 2.5. The illustrated configuration was not a success, and failed during dynamic testing. Failure occurred due to the limited area available to react axial loads. In addition, when the conical surface was preloaded to the level necessary to maintain contact in the dynamic environment, excessive moments were induced in the mirror, with resultant figure changes. When clamped, the conical surface attempts to spread the mirror surface, with a resulting change in mirror figure.

Use of a flat upper washer to directly oppose the flat bearing surface below the mirror eliminated the need for the conical surface to react axial loads. Allowing the upper flat surface to slide along the mirror hub mount athermalized the mount. The conical surface was lowered, and used primarily to maintain radial centration of the mirror. This mounting scheme was very successful, and is used on the flight hardware.

Other variants of the cone and flat mounting scheme include the University of Arizona/Ames 0.5 m fused silica test mirror[13] and the Zeiss 0.5 m Zerodur mirror developed for the German Infrared Laboratory (GIRL) project[14,15]. Both of these mounts were developed for double arch mirrors, and are employed in a three socket configuration, the sockets being located in the back of the mirror. Although the conical surfaces and flats athermalize the metal to glass contacts, additional flexures are required to athermalize the difference in thermal coefficient of expansion between mirror and mount.

The University of Arizona/Ames 0.5 m mirror mount shown in fig. 2.6 and 2.7 was successful in isolating the mirror from temperature changes. When tested at 6 K. a total figure change of 0.12 waves RMS (1 wave = 633 nm) was observed[16]. Although a promising result, the mount design is not suitable for a dynamic environment, and this result should therefore be viewed with caution.

Performance of the GIRL primary mirror mount shown in fig. 2.8 under dynamic test was quite good. Transverse natural frequency was 108 Hz, and axial natural frequency was 230 Hz. Tests using sinusoidal acceleration with an amplitude of 12 g and maximum frequency of 35 Hz, with a change of 3 octaves per minute did not produce any change in the mirror.

Although widely used in other applications the double cone mount has so far not been used in an optical mount. This mount uses a pair of conical surfaces; athermalization requires coincidence of the conical axes and that the apexes of the two conical surfaces coincide. This configuration offers increased bearing surface. Since opposite and equal moments are produced in the mounted optics, clamping forces cancel. For best performance, the intersection of the two conical apexes should occur at the plane of the center of gravity of the mirror. Since this type of mount has not yet been constructed, it was not evaluated for the SIRTF program.

Conical mounts are relatively simple, and offer good contact area. Fabrication, at least for center hub configurations used to mount single arch mirrors, is straightforward. Athermalization is good, and stability is excellent. Since no adhesives or compliant materials are employed in the mount, outgassing is not an issue.

When multiple socket configurations are used, as in the case of the University of Arizona/Ames and GIRL mirrors, mounting surface area is reduced. Stresses increase dramatically and fabrication becomes difficult. Since the socket is a blind hole, insertion of the clamp becomes a difficult design problem. The complex geometry of the socket makes determination of mounting stress very difficult. Since the apex of the conical mounting surface is located away from the mid-plane or center of gravity plane of the mirror, clamping stress induced in the socket can produce changes in optical surface figure.

The good athermalization performance of the conical mount, combined with the favorable (but limited) test experience make this type of mount a good candidate for the SIRTF program. Use of this type of mount is dependent on a mirror configuration with sufficient material in the area of the mount. A conical clamp could not be developed for a fritted ultra-lightweight mirror.

2. STUDIES OF LIGHTWEIGHT MIRROR MOUNTING AND DYNAMIC MIRROR STRESS

2.1. SUMMARY

Mounting concepts for lightweight mirrors were reviewed, analytical methods were developed for determining global stress in mirrors due to dynamic loadings, and parametric studies of local stress for both flat pad and conical mounts were made. Nine different mounting concepts for lightweight mirrors were reviewed; the most suitable designs for the SIRTF primary mirror mount are the conical mount, the bolted mount for glass mirrors, and the bolted mount for beryllium mirrors. Global stress in the primary mirror due to launch loads is an important design parameter. For a given dynamic environment, characterized by a Power Spectral Density Function (PSD), a new material parameter for minimum mirror weight was identified, and is given by:

$$W_{min} \propto (\rho/\sigma_A)^2 \, (\rho E)^{1/2} \qquad (2.1)$$

where:

W_{min}	is the minimum mirror weight
ρ	is the mirror material density
σ_A	is the maximum allowable stress for the mirror material (fracture stress for glass, micro-yield stress for beryllium)
E	is the elastic modulus of the mirror material

Analytical expressions for both flat pad mounts and conical mounts were used to determine mounting stress as a function of geometry, size, and dynamic response of the mirror mount. Use of closed form expressions dramatically simplify the cost and time required to perform initial design of the primary mirror mount.

2.2. MOUNTING CONCEPT REVIEW

The review of mounting methods concentrated on mirror mounting concepts which were relevant to the SIRTF primary mirror problem. Criteria used to evaluate suitability were the ability of the mount to limit stress in the mirror due to changes in temperature, and the adaptability of the mirror mount to a spacecraft application. Only mount designs which involved some hardware experience were considered. No effort was expended on evaluating mirror mount designs which have only been developed as concepts. This hardware emphasis in the concept review limits the review to a historical perspective. Promising new configurations which are under development were not considered.

Classified programs were not evaluated as part of the mirror mount review. Use of open university facilities precluded examination of classified materials. Since the final report is intended to be an open public document, classified concepts could not be included.

The concept review was carried out in three phases. In the first phase, a literature search for information on mirror mounting was carried out as part of the overall literature search for the program. Abstracts of papers identified from this literature search were then reviewed, and if promising, the supporting documentation obtained. At the same time, extensive use of the personal contacts of members of the Optical Sciences Center was made to find projects in which suitable mirror mount designs might exist. These contacts were followed up by correspondence, telephone calls, and personal visits. In the second phase of the concept review, nine candidate concepts were selected for detailed examination. These concepts were reviewed on the basis of recorded performance; if performance figures were not available, calculations were made to attempt to predict performance. Cost, ease of fabrication, and adaptability to different mirror configurations, were

other factors in the review. In the third phase of the review, three designs were selected as candidates for the SIRTF primary mirror mount. The performance of these three designs was then modeled under another portion of the program.

The following types of mirror mounts were reviewed:

1. Bonded mounts
2. Conical mounts
3. Sphere/cone mounts
4. Sphere/cylinder mounts
5. Cylindrical clamps
6. Ball foot/clamp
7. Bolted mount (glass)
8. Flat pad mount
9. Bolted/pinned mount (beryllium)

Criteria used to evaluate the mirror mount performance included[1]:

1. Ability to support the SIRTF primary mirror, assumed to weigh no more than 150 kg, with a diameter of 1.0 m and a thickness of less than 130 mm. (The thickness limit is set by the availability of fused silica mirror blanks if a single boule is used.)

2. Mount induced distortion due to a 292 K drop in temperature, from 300 K to 8 K, the temperature of the liquid helium dewar, should be less than 89 nm RMS.

3. Maintain optical alignment following insertion into orbit. Allowable despace is 135 microns, allowable decenter is 30 microns, and allowable tilt is 167 micro-radians.

4. The mount must retain the mirror safely in the event of an emergency landing of the Space Shuttle. Anticipated loads are 4.5 g in all axes.

5. The launch load criterion is a PSD function; the PSD is given in fig. 2.1.

Following is the detailed review of the mounting concepts studied:

2.3. BONDED MOUNTS

The descriptive term "bonded mounts" is not quite correct for this type of mounting for the SIRTF application. Due to the large thermal coefficient of expansion difference between most adhesives (silastic has a thermal coefficient of expansion of about 200 x 10^{-6} m/m-K, for example), and optical materials such as fused silica or beryllium, a classic bonded mounting is not feasible. Instead, bonding is used to attach the mirror to a flexure system which isolates the mirror from thermal coefficient of expansion effects. Adhesives are used as a mirror to flexure transition. Flexure mounting principles are discussed in Vukobratovich and Richard[2]. Tangential flexure mounts of the type most often used for mounting of lightweight space mirrors were discussed by Chin[3].

Representative examples of the combination of a bonded mirror mount and tangential flexure are the 0.5 m mirror for the TEAL RUBY[4,5], shown in fig. 2.2 and the 0.65 m Itek fused silica test mirror[6,7,8]. The bonded mount is a semi-kinematic three point design. Three square bosses extend radially from the mid-plane of the mirror circumference. Four "T" shaped flexures are bonded to the

sides of the square boss. The flexures are attached to an outer ring which surrounds the boss. The outer ring is carried on the tip of a tapered cantilever beam flexure which is tangential to the mirror edge. A mounting ring or bezel surrounds, but does not contact the mirror; the three tangential flexures attach to this ring.

The three tangential flexures provided isolation of the mirror from expansion or contraction of the outer bezel with respect to the mirror. The four inner flexures provide additional rotational compliance to allow for assembly errors which might otherwise induce moments in the mirror. Fig. 2.3 shows the metal to glass interface of this flexure configuration. Stress induced in the square boss is unlikely to propagate to the mirror surface.

Performance of the bonded mount designs has been quite good. The TEAL RUBY primary mirror was designed to operate at 70 K, and to survive a launch acceleration of 7 g steady state, with a 10 g RMS random vibration. Fundamental frequency of the mirror and mount assembly was about 45 hz, which substantially exceeded the design specification of 15 hz. Cryogenic deformation of the Itek 0.65 m test mirror was very low, with a cryogenic surface distortion of 0.26 waves RMS (1 wave = 633 nm) at 13 K.

A serious concern with the bonded design is integrity of the glass to metal adhesive joint. In the experimental 0.65 m Itek mirror, fracture and failure of the glass occurred when the flexure assembly temperature was reduced to 77 K. In fig. 2.4, fragments of the fractured glass are seen still attached to the flexure. This design used an aluminum flexure, PR-1660 polyurethane adhesive and an aluminum flexure boss. Changing the flexure material to Invar did not solve the problem; failures continued at 77 K. Etching the fused silica boss in hydrofluoric acid to strengthen the glass, and switching to a PR-1578 polyurethane adhesive specially formulated for cryogenic use prevented failures at 77 K when combined with an invar flexure. Failures continued with the aluminum flexure[9]. More recent analysis of the stress in the adhesive bond area indicates that proper selection of adhesive coupled with a very limited bond area can reduce failure probability[10].

Although the bonded mount represents a traditional and well tested mounting concept, this design is not well suited to the SIRTF primary mirror problem. Performance of the Itek 0.65 m mirror and mount at 13 K is roughly comparable with that of beryllium mirrors and about twice as bad (0.26 waves RMS for this mirror, versus 0.12 waves RMS for the ARC/Arizona double arch or 0.13 waves RMS for the ARC/Arizona single arch, one wave = 633 nm) as other types of glass mirror and mount concepts[11]. Failures in the glass to metal adhesive joint are catastrophic. Recent analysis indicates the need for relatively small adhesive bond areas, limiting bond strength. These failures during test, and the limited strength of the mount for a mirror half the size of the SIRTF primary, suggest a serious concern with the strength of a similar design for the 1 m SIRTF primary.

Additional concerns are a possible lack of long term stability due to creep of the adhesive joint, possible contamination of the optics dues to adhesive outgassing, and poor batch-to-batch repeatability of current adhesives. Use of a bonded mount for SIRTF would require research into adhesive behavior at 13 K.

2.4. CONICAL MOUNTS

Conical mounts utilize conical geometry to athermalize the contact between glass and metal. This a very traditional way of making a glass to metal contact, and is extensively used in applications such as high voltage insulators. Two different conical mounting schemes are used; a cone and a flat bearing surface, and two conical surfaces.

Use of a conical bearing surface combined with a flat surface permits athermalization of the mount if the apex of the conical surface is coincident with the flat surface and if the axis of the conical surface is perpendicular to the flat surface. Expansion or contraction of the mount materials maintains geometry, and the apex of the cone remains coincident with the flat surface. This athermalization scheme does require slip of the bearing surfaces relative to the mirror surface.

An example of an athermalized conical surface and flat surface is the primary mirror mount of the 0.35 m Mars Observer Camera (MOC) developed by Perkin-Elmer[12] and shown in fig. 2.5. The illustrated configuration was not a success, and failed during dynamic testing. Failure occurred due to the limited area available to react axial loads. In addition, when the conical surface was preloaded to the level necessary to maintain contact in the dynamic environment, excessive moments were induced in the mirror, with resultant figure changes. When clamped, the conical surface attempts to spread the mirror surface, with a resulting change in mirror figure.

Use of a flat upper washer to directly oppose the flat bearing surface below the mirror eliminated the need for the conical surface to react axial loads. Allowing the upper flat surface to slide along the mirror hub mount athermalized the mount. The conical surface was lowered, and used primarily to maintain radial centration of the mirror. This mounting scheme was very successful, and is used on the flight hardware.

Other variants of the cone and flat mounting scheme include the University of Arizona/Ames 0.5 m fused silica test mirror[13] and the Zeiss 0.5 m Zerodur mirror developed for the German Infrared Laboratory (GIRL) project[14,15]. Both of these mounts were developed for double arch mirrors, and are employed in a three socket configuration, the sockets being located in the back of the mirror. Although the conical surfaces and flats athermalize the metal to glass contacts, additional flexures are required to athermalize the difference in thermal coefficient of expansion between mirror and mount.

The University of Arizona/Ames 0.5 m mirror mount shown in fig. 2.6 and 2.7 was successful in isolating the mirror from temperature changes. When tested at 6 K. a total figure change of 0.12 waves RMS (1 wave = 633 nm) was observed[16]. Although a promising result, the mount design is not suitable for a dynamic environment, and this result should therefore be viewed with caution.

Performance of the GIRL primary mirror mount shown in fig. 2.8 under dynamic test was quite good. Transverse natural frequency was 108 Hz, and axial natural frequency was 230 Hz. Tests using sinusoidal acceleration with an amplitude of 12 g and maximum frequency of 35 Hz, with a change of 3 octaves per minute did not produce any change in the mirror.

Although widely used in other applications the double cone mount has so far not been used in an optical mount. This mount uses a pair of conical surfaces; athermalization requires coincidence of the conical axes and that the apexes of the two conical surfaces coincide. This configuration offers increased bearing surface. Since opposite and equal moments are produced in the mounted optics, clamping forces cancel. For best performance, the intersection of the two conical apexes should occur at the plane of the center of gravity of the mirror. Since this type of mount has not yet been constructed, it was not evaluated for the SIRTF program.

Conical mounts are relatively simple, and offer good contact area. Fabrication, at least for center hub configurations used to mount single arch mirrors, is straightforward. Athermalization is good, and stability is excellent. Since no adhesives or compliant materials are employed in the mount, outgassing is not an issue.

When multiple socket configurations are used, as in the case of the University of Arizona/Ames and GIRL mirrors, mounting surface area is reduced. Stresses increase dramatically and fabrication becomes difficult. Since the socket is a blind hole, insertion of the clamp becomes a difficult design problem. The complex geometry of the socket makes determination of mounting stress very difficult. Since the apex of the conical mounting surface is located away from the mid-plane or center of gravity plane of the mirror, clamping stress induced in the socket can produce changes in optical surface figure.

The good athermalization performance of the conical mount, combined with the favorable (but limited) test experience make this type of mount a good candidate for the SIRTF program. Use of this type of mount is dependent on a mirror configuration with sufficient material in the area of the mount. A conical clamp could not be developed for a fritted ultra-lightweight mirror.

2.5. SPHERE/CONE MOUNTS

Sphere/cone mounts utilize a pre-loaded semi-kinematic contact between a sphere and conical hole to athermalize the glass to metal contact between mirror and mount. A combination of sphere and cone mounts is used to mount a mirror; additional flexures are needed to athermalize the mirror with respect to expansion or contraction of the outer mount.

Perkin-Elmer has developed a proprietary design of sphere/cone mount for use in the cryogenic optics of the Boeing Infrared Sensor (BIRS) calibration facility. This configuration uses three combinations of sphere/cone mounts equi-spaced around the perimeter of the mirror. Each combination uses a radial constraint with a sphere/cone contact, and two axial restraints, directly opposing each other, with sphere/cone contacts, as shown in fig. 2.9. This combination is not kinematic, and over-constrains the mirror. Over-constraint results in deformation of the mirror when the mirror is mounted; this deformation increases as the mirror is cooled[17]. Although performance of the sphere/cone mirror mount has not been reported in the open literature, a cryogenic distortion at 80 K of over 0.2 waves (1 wave = 633 nm) has been mentioned in discussions with Boeing. The sphere/cone mount is relatively simple, and quite easy to fabricate. Since there is direct metal to glass contact, stability is excellent. No adhesives or compliant materials are used in the mount, eliminating concerns about outgassing.

Space inside the clear aperture of the mirror is required for mounting. Another approach is to provide the mirror with bosses or extensions for the mounts. Line contact occurs between sphere and cone, which results in very high stress. Due to over-constraint, athermalization is poor, and the mirror figure is likely to be affected during mounting. The use of sliding contacts in the preload mechanism for the spheres may induce hysteresis due to friction during mechanical or thermal cycling.

Without more extensive test data, this configuration is not considered a suitable choice for the SIRTF application. High stress, and possible cryogenic distortion of the mirror make the sphere/cone mount unsuitable. Although a modified design might be a candidate for SIRTF, the relatively complex geometry would make analysis of the modified design very difficult.

2.6. SPHERE/CYLINDER MOUNTS

Sphere/cylinder mounts employ a spherical bearing surface sliding in a radial cylinder to athermalize the mount. Thermal coefficient of expansion mis-match between mirror and mount is reduced by employing three sphere/cylinder mounts equi-spaced around the mirror, with the spheres free to slide radially. Use of spherical contact allows three-degree of freedom rotation between sphere and cylinder. Three degrees of freedom in rotation at each of three contacts, plus radial translation, insures that the mount does not over constrain the mirror. Assembly errors such as tilts of the mounting points relative to the back of the mirror can induce moments in the mirror. Moments induced by the mount can cause figure errors in the mirror surface. This type of assembly error is reduced by bending of the mounting flexures.

A patent issued to B. Meseo[18] and shown in fig. 2.10 is the primary source of information on the sphere/cylinder mount. Performance data on the mount is limited; an article by Barnes[19] suggested a "small" change over 20-25 degrees F.

Use of the sphere/cylinder mount does not address the metal to glass contact problem. This type of mount requires attachment of the spherical bearing surfaces to the edge of the mirror. It is suggested in the original patent that the spherical bearings could be bonded to the mirror edge. This infers a relatively large bond area, with resultant concern about strength and possible cryogenic distortion of the mirror. Creep of the adhesive could result in a loss of optical alignment. Outgassing is also a concern with adhesives.

A relatively tight tolerance on the clearance between sphere and cylinder is required. Mesco's patent suggests a clearance of about 250 nm. Such a tolerance is very expensive to achieve, and is unlikely to be maintained over a wide range of temperature. Friction between sphere and cylinder is a source of hysteresis with resultant figure error and loss of alignment.

Some of the above difficulties could be overcome by preloading the contact between cylinder and sphere with a spring. This reduces the mount stiffness, and may present a dynamic problem. A "zero clearance" sliding contact achieved by preloading is a possible source of wear. Use of dissimilar materials, such as a beryllium copper spring and stainless steel sphere reduces the potential for wear. Line contact between the sphere and cylinder produces very high stress.

Until better information on the performance of the sphere/cylinder mount is available, is not a suitable choice for the SIRTF primary mirror mount. If this configuration is selected, a representative mirror and mount should be tested at 10 K to determine performance. Use of the sphere/cylinder mount would require an experimental program to develop a database for application to the SIRTF primary mirror.

2.7. CYLINDRICAL CLAMP

The cylindrical clamp uses a cylindrical mount which is a light force fit over a cylinder at the edge of the mirror. A cylindrical core drill is used to produce an annular cylindrical bore in the edge of the mirror; the metal clamp fits over this bore. As the temperature is lowered, the metal clamp tightens on the cylindrical annulus, placing the glass into compression. Although this type of mount provides a transition from glass to metal, it is necessary to provide additional flexures to allow for mount tolerances and the thermal coefficient of expansion mis-match between mirror and mounting structure.

The cylindrical clamp mount is under development for the Infrared Space observatory (ISO). A 0.6 m fused silica test mirror has been developed for ISO by REOSC and Aerospatiale[20]. A flexure system with radially compliance to minimize thermal coefficient of expansion effects and two degrees of freedom in rotation to reduce the effects of assembly tolerances has been patented by J. Paseri[21]. The ISO mirror mount and flexure assembly is shown in fig. 2.11.

The critical issue in the performance of the cylindrical clamp is stress induced in the glass as the temperature is lowered. La Fiandra[22] has developed equations for the analysis of the maximum allowable radial clearance, stress and maximum frictional force between metal and glass over the design temperature range. A more generic discussion is given by Iraninejad et al[23]. For the SIRTF temperature range (300 K to 10 K), stress in this type of mount appears acceptable. Mounts of this type were used in the heat conductor assemblies of the Zeiss GIRL demonstration mirror, with good results.

Performance data on the REOSC demonstration mirror for ISO is not available. Discussion with ISO personnel indicate that REOSC has had great difficulty with mirror fabrication. The fabrication problem can be understood by considering the standard method for making a blind hole in glass. To make a blind hole in glass, a core drill is used. The core drill produces an annular cut in the glass, leaving a cylindrical piece of glass free-standing in the hole, attached only at its bottom. A sharp rap on the plug will break the plug loose at the bottom. The REOSC mount configuration duplicates this blind hole geometry. To avoid breaking the plug, a large radius is required at the bottom of the annulus. In addition, considerable care, particularly in surface finish, is required during fabrication.

The cylindrical mount offers a large contact area. With direct glass to metal contact, stability is excellent. Outgassing is not a problem, since no adhesives or compliant materials are used. The relatively simple geometry of the mount allows closed form analysis or use of inexpensive axi-symmetric finite element models.

For efficient use of the cylindrical mount concept, the cylinders should act radially on the outside edge of the mirror. This is a strong constraint on the mirror geometry, and rules out the use of this type of mount with contoured back or ultra-lightweight mirrors. If the axis of the cylinder is not located on the plane of the center of gravity of the mirror, possible surface distortion with temperature drop, or with mechanical loads applied to the mirror, is possible. Precise information on the temperature range of the mirror is required to set the assembly force fit of the mirror to the mount.

Until test data becomes available on the performance of the cylindrical mount, this design is not considered suitable for use with the SIRTF primary mirror. However, the cylindrical mount does have considerable promise. Should good data become available on performance in a cryogenic environment, and should the fabrication issue be settled, the cylindrical mount could be a strong candidate for the SIRTF primary mirror.

2.8. BALL FOOT/CLAMP (WITH BIPOD)

The ball foot/clamp mount uses three spherical feet frit bonded to the back of a glass mirror, equi-spaced on a common diameter. A metal clamp is placed around the glass feet and preloaded to insure contact as temperature is reduced. Each clamp and foot assembly is attached to a bipod. The bipod legs have reduced or necked down sections at each end to act as rotationally compliant joints. The centerlines of the two bipod legs of each assembly intersect at the center plane of the mirror.

Athermalization of the ball foot/clamp mount depends on the preload and mechanical fit of the clamp to the spherical surface of the foot. Since the radius of curvature of the sphere changes with temperature, contact in the clamp is at best located on two diameters of the sphere. Although the ball foot/clamp provides athermalization of the glass to metal contact, additional flexures are required to isolate the mirror from thermal coefficient of expansion mis-match effects between mirror and mounting structure. Bipod flexures provide this additional isolation. Use of bipod flexures allows radial and tangential changes in the physical dimension of the mounting structure with respect to the mirror.

The combination of ball foot/clamp mounts and bipod flexures was originally suggested in a limited circulation Kodak document. Mention of the concept in public was made in a paper by Crowe[24]. Discussion with Kodak employees indicates that the mounting concept may have been employed on a number of government space projects. Recently, the performance of this type of mount was discussed[25] for a scan mirror application. An 0.73 m by 0.47 m elliptic fritted sandwich ULE mirror was mounted using this approach, and is shown in fig. 2.12. A first modal frequency of over 200 Hz was achieved with this mirror and mount. No data is available on the temperature performance of this mirror,

The ball foot/clamp mount is a simple design that has very low impact on the mirror design. Using fritting, mounting balls can be attached to virtually any point of the surface of a wide variety of mirror configurations. This is currently the only technology that has been demonstrated for mounting ultra-lightweight glass mirrors. Stability is excellent, since there is direct metal to glass contact. No adhesives or compliant materials are used, so outgassing is not a concern. Athermalization between metal and glass is acceptable.

Use of line contacts in the ball foot/clamp assembly produces relatively high stress in the assembly. This high stress is aggravated by the re-entrant angle between spherical foot and mirror surface. A sharp corner or re-entrant angle dramatically increases stress, and is normally avoided in working with brittle materials such as glass. Unfortunately, a re-entrant angle is necessary in this mounting configuration.

Although the bipod provides athermalization and reduces the effects of assembly error on the mirror surface, the bipod location is not optimum. Mounting to a point behind the rear surface of the mirror will result in moments being induced in the mirror, with resulting surface figure error.

The high stresses, re-entrant angle of the ball foot, and poor location of the bipod flexures indicate that the ball foot/clamp (with bipod) design is not suitable for use with SIRTF. In the absence of performance data, evaluation of the magnitude of these effects is difficult. Should performance data on this type of mirror become available that indicated performance comparable to some of the more promising mirror mount configurations, the ball foot/clamp could be a candidate for the SIRTF primary mirror mount.

2.9. BOLTED MOUNT (GLASS)

The bolted mounted uses contact between large flat washers and the mirror surface to transfer loads to the mirror. Large bolts provide a preload force on the flat washers to insure contact between the washer and mirror. Typically, two washers per bolt are used, with a portion of the mirror between the two washers. This insures contact with the mirror even if the direction of load is reversed. A relatively low preload is used, so that the mirror is just barely in contact with the flat washers when not subjected to loads due to acceleration or vibration. Each bolted connection can be considered as a kinematic defining point. For complete definition of mirror position, six bolted connections are needed.

Athermalization of the bolted mount relies on the use of low thermal coefficient materials which match the thermal coefficient of expansion of the glass. An alternate approach uses a composite bolt, made of both high and low thermal coefficient of expansion materials. Use of dissimilar materials permits tailoring the equivalent thermal coefficient of expansion of the bolted assembly to match that of the glass. Although the bolted mount provides a glass to metal interface, additional flexures are required to reduce the effects of mounting structure to mirror thermal coefficient of expansion mismatch.

The need to pass the bolted mount through the mirror places strong limits on mirror geometry. To react against axial loads, it may be necessary to pass three bolts through the mirror in the axial directions. These bolts will be within the clear aperture of the mirror. This solution was used on the primary mirror mount for the Hubble Space Telescope, as shown in fig. 2.13. Placing three bolts through the optical surface of the mirror is not very desirable. The mirror optical surface figure may be distorted by the contact with the bolts, collecting surface area is reduced, and diffraction effects are increased.

Instead of passing bolts through the mirror surface, the mirror can be designed with mounting blocks around the perimeter of the mirror. Bolts are attached to these circumferential mounting blocks. This approach reduces the effect on mirror optical surface figure, and eliminates the adverse effects on collecting surface and diffraction. Unfortunately, mounting blocks increase the diameter of the mirror, and increase fabrication cost.

If an open back lightweight configuration is used for the mirror, the bolted mounts can be connected to the ribs of the lightweight shear core of the mirror. This approach was successfully employed in the bolted mounts for the Airborne Optical Adjunct (AOA) mirrors, as shown in fig. 2.14[26]. Three cubes are bolted to the ribs of the AOA mirrors; the cubes are attached to a six leg (hexapod) support. The hexapod is kinematic and serves to athermalize the mirror with respect to the mounting structure. Mirror figure was reportedly maintained over a 180 K temperature change.

The bolted mount has the important advantage of providing a relatively large contact area between the mount and mirror, which significantly reduces stress and optical figure distortion. Long term stability is excellent, due to direct metal to glass contact. The design is simple and relatively easy to analyze. An important aspect of the bolted mount is its successful use in other systems. Outgassing problems are reduced by the very limited use of compliant materials or bonding.

A very serious disadvantage of the bolted mount is the strong impact of the mount on the mirror design. If intrusion of the bolted mount into the clear aperture of the mirror is to be avoided, the mirror must either be provided with external mounting blocks, or an open back lightweight

configuration must be used. Athermalization of the bolted mount is poor; the bolted mount is not inherently athermal. Use of low thermal coefficient materials or bi-metallic compensators is mandatory to reduce thermal effects. For the nearly 300 K temperature drop, and high optical surface quality required, in the SIRTF system, the bolted mount may not provide sufficient isolation from thermal coefficient of expansion mis-match.

Despite the strong impact on mirror configuration, and the relatively poor athermalization, the bolted mount is considered a strong possibility for the SIRTF mirror mount. Successful prior application of the bolted mount to large and lightweight systems indicates that this design may be suitable if re-designed for the large temperature change. Changing washer size allows the designer to change the stress level in the mount. The capability to handle a wide range of stress could be very important as the SIRTF program (and hence primary mirror requirement) changes. This early in the program major change in specification is probable.

2.10. FLAT PAD MOUNT

The flat pad mount was developed by George Sarver at NASA Ames, Moffett Field, CA[27], and is a modification of the bolted mount. The flat pad mount uses bolted joints with a large preload to pull spherical or flat contact surfaces against mounting surfaces external to the mirror. Preload is provided by stacks of belleville springs on the bolts. Each flat pad mount is considered as a kinematic mounting point, so a total of six are needed to define the location of the mirror.

Very good contact is required between the contact surfaces and the mirror to reduce stress in the contact area. A tolerance analysis of the flat pad contacts indicates that "optical" tolerances are required for the contact surfaces. The use of flat or spherical surfaces contact surfaces means that traditional optical fabrication methods can be used to obtain the required surface quality.

Like the bolted mount, the flat pad mount has a strong effect on mirror configuration. Mounting blocks external to the mirror are likely to be required. Another approach requires relatively deep machined mounting pockets in the mirror.

The flat pad mount offers relatively low stress. Long term stability is likely to be very good, due to direct metal to glass contact. Outgassing problems are reduced by the lack of compliant materials.

Like the bolted mount, the flat pad mount requires a separate set of mounting flexures to reduce the thermal coefficient of expansion mis-match between mirror and mounting structure. The very high surface quality required in the area of the mount leads to relatively high fabrication costs. A change in stress level could be difficult to accommodate if spherical contacts are used. Good contact between mirror and mount is unlikely to be maintained due to thermal coefficient of expansion mis-match effects. A drop in temperature will turn the area contact between an invar spherical pad and spherical socket into a line contact.

Since there is lack of performance data on the flat pad mount, this type of mount is not considered suitable for SIRTF. Development of the flat pad mount is underway at Nasa Ames, and it is possible that this mount may evolve into a suitable configuration for the SIRTF primary mirror mount.

2.11. BOLTED/PINNED MOUNT (BERYLLIUM)

Beryllium offers the great advantage of bolting mounts directly to the mirror. Beryllium is a metal, and can be drilled, tapped, and pinned like most metals. The thermal coefficient of expansion of beryllium is significantly highly than that of optical glasses. This high thermal coefficient of expansion is actually an advantage, since there are a number of other metals that are a good thermal coefficient of expansion match to beryllium, most notably titanium.

Beryllium mirror mount designs have exploited the characteristics of the material, by bolting to the beryllium. Beryllium is an exotic and difficult to fabricate material with poor fracture toughness. To minimize the possibility of fracture, high stress hardware for mounting, such as flexures and bolts, are normally fabricated from metals other than beryllium. Titanium is often used for this purpose. The thermal coefficient of expansion of titanium (6Al-4V) is about 8.8 x 10^{-6} m/m-K, and the thermal coefficient of expansion for beryllium (I-70A) is about 11.2 x 10^{-6} m/m-K.

Direct bolting and pinning was used for mounting on the 0.6 m Infrared Astronomical Satellite (IRAS) primary mirror[28],[29]. A three point mirror mount was used, with titanium flexures isolating the mirror from contraction of the baseplate relative to the mirror due to thermal coefficient of expansion mis-match. The titanium flexures were single blades with radial compliance. Atop each flexure blade was a cruciform flexure; this flexure provided rotary compliance about an axis parallel to the mirror surface and aligned in the circumferential direction. Since the single blade flexure could rotate as well as translate, the combination of single blade flexure and cruciform flexure provided two degrees of freedom in rotation. Two degrees of freedom in rotation were required to remove any effects of mounting error. The IRAS mirror and mount design are shown in fig. 2.15. At 25 K, the cryogenic surface distortion of the IRAS primary mirror was 0.34 waves RMS (1 wave = 633 nm).

The titanium alloy used in the IRAS flexures was 5Al-2.5Sn ELI (ELI means extra-low interstitial). During the design of the IRAS mirror mounts, this titanium alloy appeared a good selection for cryogenic applications[30]. More recent research into the properties of 5Al-2.5Sn ELI at cryogenic temperatures[31],[32],[33],[34] indicates that the fracture toughness of titanium, a critical parameter for avoidance of cracking at cryogenic temperature is variable, and much lower than the earlier research indicated. (Anomalous low values of fracture toughness of Ti-5Al-2.5Sn were reported as early as 1968[35].) Despite the successful application of Ti-5Al-2.5Sn ELI in the IRAS, the low values of fracture toughness measured in recent research strongly suggest that other materials be considered for beryllium mirror mounts. The performance of Ti-6Al-4V ELI is much better understood[36,37,38] than that of Ti-5Al-2.5Sn ELI, suggesting that the former alloy is a better choice for SIRTF applications.

More complex flexure configurations than the IRAS mirror mount design were described by Altenhof[39]. A 0.81 m by 0.86 m beryllium flat mounted by this complex flexure scheme was tested at 150 K[40]. The flexure and bolting technology applied to this mirror was very similar in concept to that of the IRAS design. Kinematic principles were used to develop the required degrees of freedom, and individual flexures designed for each required degree of freedom.

Bolting and pinning, combined with flexures, appears to be a very mature technology for mounting beryllium lightweight mirrors. Bolting and pinning is relative simple, and low in weight. Use of direct metal to metal contacts provides excellent dimensional stability. No compliant materials are employed, reducing outgassing. Athermalization is achieved through the use of flexures and matching of thermal coefficients of expansion (use of titanium, and is acceptable. Bolting and pinning have minimum impact on the mirror configuration. Mounts can be attached to the back or side of the mirror.

It is very difficult to analyze the behavior of the bolted and pinned connections. The difficulty of analysis complicates the design. Beryllium has a very low microyield strength, requiring a very conservative design for the mirror mount. Since it is very difficult to determine the exact stress condition in the mount, design of a conservative mount to avoid microyield is also very difficult.

Should a beryllium mirror be selected for use in the SIRTF program, bolting and pinning would be an acceptable choice for the mirror mount. Two cautions connected with bolting and pinning are the need for careful selection of mounting materials, and the requirement for better analysis techniques for the stress condition of the mount.

2.12. CONCLUSIONS OF MIRROR MOUNTING CONCEPT STUDY

Due to very high loads induced by the dynamic specifications of the SIRTF system, only low stress mount configurations are suitable for the primary mirror. The extreme range of operating temperature requires excellent athermalization of the mount. A very tight specification on optical figure requires good isolation of the mirror from mounting stress. Finally, since a candidate mirror configuration has not yet been identified, the mirror mount must have minimum impact on the mirror design.

If the selection of a mount is restricted to designs for which there is test data, three strong candidates emerge: the conical mount (suitable for glass or metal), the bolted mount for glass, and the bolted mount for beryllium. The conical mount is a good choice for a center supported single arch type mirror. Use of the conical concept for other mirror configurations is difficult, owing to the limited contact area available. The bolted mount, combined with a large bearing surface near the bolt, is a very mature design that has been very successful in a variety of other space systems. Bolted mounts are the best choice for an open back or structured mirror. Should a beryllium mirror be selected for SIRTF, a bolted mount would be a good choice. There is a considerable body of experience in the design of bolted mounts for beryllium mirrors.

Regardless of what type of mount is selected for SIRTF, a key issue is the design of the transition from the actual mirror to metal mount and the mounting structure. This transition is likely to require some type of flexure to isolate the mirror from thermal coefficient of expansion mis-match effects. The current survey indicates that flexure design, and the issues of clamped versus un-clamped, or caged, are not well understood. It is suggested that future work be considered to better understand the flexure problem.

2.13. MIRROR GLOBAL STRESS

For most terrestrial applications, global stress in optical mirrors is neglected. When a lightweight mirror is subject to the type of dynamic loading characteristic of the SIRTF launch vehicle, significant stresses are induced in the mirror. Two types of mirror stress are significant: global stress induced by vibration of the mirror in its mount, and local stress, in the area of the mount. Both types of stress were studied; global stress will be discussed in this section of the report.

An important simplification in modeling global stress of a mirror subjected to a random vibration environment is the Miles approximation. This approximation is valid for lightly damped, single degree of freedom systems, and is given by[41]:

$$g_{rms} = \left[\frac{\pi}{2} f_n Q\ (PSD)\right]^{1/2} \tag{2.2}$$

where:

g_{rms}	is the root-mean-square (RMS) response of the mirror in its mount
f_n	is the natural frequency of the mirror mount
Q	is the mirror mount transmissibility at the natural frequency f_n
PSD	is the environmental power spectral density at the mirror mount natural frequency f_n

Normally, the maximum response is found by multiplying the above RMS response by a factor of 3. This maximum response is the "3 sigma" response. The basis for the "3-sigma" approach is the assumption that the random vibration can be characterized by a Gaussian distribution. With a Gaussian distribution, events outside of plus or minus 3 sigma will happen about 0.027% of the time.

The power spectral density function is given in units of g^2-Hz^{-1}. Response of the mirror is given by equation 2 in units of "g." Equation 2 can be used to find the maximum dynamic stress in the mirror by multiply the response in g given by equation 2 times the maximum stress in the mirror due to self-weight. If this is done, and the "3-sigma" approximation included, the global maximum mirror stress is given by:

$$\sigma_{max} = 3\ \sigma_{STATIC} \left[\frac{\pi}{2} f_n\ Q\ (PSD) \right]^{1/2} \tag{2.3}$$

where:

σ_{max} is the maximum global dynamic stress in the mirror
σ_{STATIC} is the maximum stress due to mirror self weight

To make use of equation 3, the maximum global stress in the mirror due to self-weight must be known. The maximum global stress is computed using the finite element method, or by using a closed form analytical expression. In the important case of a conventional right circular cylinder mirror, supported on a continuous edge ring, the maximum global stress due to self-weight loading is given by[42]:

$$\sigma_{max} = \frac{3}{8} \frac{\rho r_s^2}{h} \left\{ (1 + 3\upsilon) \left[\left(\frac{r_o}{r_s} \right)^2 - 1 \right] - 4\ (1 + \upsilon) \left(\frac{r_o}{r_s} \right)^2 ln \left(\frac{r_o}{r_s} \right) \right\} \tag{2.4}$$

where:

σ_{max} is the maximum global stress in the mirror
ρ is mirror material density
υ is Poisson's ratio for the mirror material
h is the mirror thickness
r_o is the mirror outer radius
r_s is the mirror support radius

This solution assumes a simple continuous support, no central hole in the mirror, and no significant surface curvature.

As a check for calculations performed elsewhere in the report, equation 4 was used to compute the maximum stresses in conventional right circular cylinder mirrors made of fused silica with the following properties:

1. Material: Fused silica Corning 7940
2. Material density: 0.08 lb/in^3
3. Poisson's ratio: 0.17
4. Elastic modulus: 10 x 10^6 lb/in^2

Stresses for the same mirrors were then computed using the finite element method. A comparison of the results is given in table 2.1, for mirrors 3 to 6 in. thick. The major error is in mirrors supported at intermediate locations. Modeling of the support ring can introduce significant errors in the finite element method, and are the cause of the discrepancy between the closed form and finite element results.

Similar calculations of maximum global stress were made using the finite element method for contoured back mirrors. Both single arch and double arch mirrors were considered, with a range of thickness of 4 to 7 in., and a range of weights of 175 to 253 lbs. The stresses for the double and single arch mirrors are given in table 2.2. Fig. 2.16 compares the stresses of single and double arch mirrors as the mirror height is varied. For constant height, optimized double arch mirrors are lower in self-weight stress than optimized single arch mirrors. Fig. 2.17 compares the stresses of single and double arch mirrors as the mirror weight is varied. For constant weight optimized mirrors, the self-weight stress of double arch mirrors is lower than the stress of single arch mirrors.

Another important type of mirror is the lightweight sandwich mirror. The maximum bending stress in the faceplates of a lightweight sandwich structure is given by[43]:

$$\sigma_{max} = \frac{M_r}{t_f h} \tag{2.5}$$

where:

σ_{max}	is the maximum principle stress in the faceplate of the lightweight sandwich structure
M_r	is the moment applied to the sandwich structure
t_f	is the faceplate thickness
h	is the total thickness of the sandwich structure

The maximum moment in an edge supported right circular cylinder plate or mirror is given by:

$$M_r = \frac{P_o r_o^2}{16} (3 + \upsilon) \tag{2.6}$$

where:

P_o	is the area density of the applied load

The area density of a lightweight sandwich mirror is given by:

$$P_o = \rho (2t_f + \eta h_c) \tag{2.7}$$

where:

P_o	is the area density of the lightweight sandwich mirror
ρ	is the mirror material density
t_f	is the faceplate thickness
η	is the rib solidity ratio
h_c	is the shear core height

And the rib solidity ratio is given by:

$$\eta = \frac{(2B + t_w)t_w}{(B + t_w)^2} \tag{2.8}$$

where:

η	is the rib solidity ratio
B	is the diameter of a circle inscribed in the unit cell of the shear core
t_w	is the rib thickness

Substituting equations 6 and 7 into equation 5, the maximum global stress in an edge ring supported self-weight loaded sandwich mirror is given by:

$$\sigma_{max} = \frac{(3 + \upsilon)}{16} \frac{\rho r_o^2}{t_f h} (2t_f + \eta h_c) \tag{2.9}$$

where:

σ_{max}	is the maximum global stress in a self-weight loaded sandwich mirror

A similar derivation is used to find the maximum stress in an edge ring loaded solid right circular cylinder mirror, assuming self-weight loading:

$$\sigma_{max} = \frac{3}{8} \rho \frac{r_o^2}{h} (3 + \upsilon) \tag{2.10}$$

where:

σ_{max}	is the maximum stress in a self-weight loaded solid mirror
h	is the mirror thickness
ρ	is the mirror material density
r_o	is the mirror radius
υ	is the Poisson's ratio of the mirror material

A series of equations can be developed for other support conditions, assuming self-weight loading. Regardless of the type of support, the following expressions are used to scale stress as mirror parameters are varied:

$$\sigma_{SOLID} \propto \rho \frac{r_o^2}{h} \tag{2.11}$$

$$\sigma_{SANDWICH} \propto \rho \frac{r_o^2}{h} \frac{(2t_f + \eta h_c)}{t_f} \tag{2.12}$$

where:

σ_{SOLID}	is the stress in a solid mirror
ρ	is the mirror material density
h	is the mirror overall thickness
r_o	is the mirror radius
$\sigma_{SANDWICH}$	is the stress in a sandwich mirror
t_f	is the faceplate thickness
η	is the rib solidity ratio
h_c	is the shear core thickness ($h - 2t_f = h_c$)

The above scaling laws, along with equation 3, are useful for quickly estimating the effect of a change of the environment or mirror configuration on the mirror maximum stress. These expressions hold for stress due to the rigid body motion of the mirror vibration in the mirror. Using equations 11 and 12, an expression is developed which compares the stress in the same thickness solid and lightweight mirrors, assuming identical materials and diameters:

$$\frac{\sigma_{SOLID}}{\sigma_{SANDWICH}} = \frac{6t_f}{2t_f + \eta h_c} \tag{2.13}$$

Another source of stress in the mirror is vibration of the mirror itself. This is not rigid body motion, but rather the mirror vibrating at one of its modes. The Miles approximation is used to determine the stress developed by this vibration, but the fundamental frequency and Q are now for the mirror itself.

In addition to the self-weight stress equations, determination of the stress due to vibration of the mirror requires an expression for the fundamental frequency of the mirror. For a solid right circular cylinder mirror, the fundamental frequency is given by[44]:

$$f_n = \frac{J_1^2}{2\pi r_o^2} \left[\frac{gEh^2}{12\rho(1-\upsilon^2)}\right]^{1/2} \tag{2.14}$$

where:

f_n	is the mirror natural frequency
J_1	is the support condition constant (dimensionless)
r_o	is the mirror radius
g	is the acceleration due to earth's gravity
E	is the elastic modulus of the mirror material
h	is the mirror thickness
ρ	is the mirror material density
υ	is the Poisson's ratio of the mirror material

Equations 14 and 10 are substituted into equation 3 to produce an expression for the maximum global stress for conventional right circular cylinder mirrors due to vibration of the mirror itself:

$$\sigma_{solid} = C_o \frac{(3+\upsilon)}{[12(1-\upsilon^2)]^{1/4}} \rho^{3/4} E^{1/4} \frac{r_o}{h^{1/2}} g^{1/4} Q^{1/2} (PSD)^{1/2} \tag{2.15}$$

where:

σ_{SOLID}	is the maximum dynamic stress
C_o	is the support condition constant
ρ	is the mirror material density
E	is the mirror material elastic modulus
υ	is the Poisson's ratio of the mirror material
r_o	is the mirror radius
h	is the mirror thickness
g	is the acceleration due to earth's gravity
PSD	is the environmental power spectral density
Q	is the mirror transmissibility at resonance

Equation (15) is used to find an expression for the minimum mirror thickness necessary to keep the stress in the mirror due to vibration of the mirror itself below some allowable level. This thickness is then used to find the minimum weight mirror required to keep the mirror stress below some allowable level when the mirror itself vibrates when exposed to random vibration. The minimum mirror weight is then given by:

$$W_{min} = C_o \frac{(3+\upsilon)^2}{[12(1-\upsilon^2)]^{1/2}} (\rho/\sigma_A)^2 (\rho E)^{1/2} r_o^4 g^{1/2} (PSD) Q \tag{2.16}$$

where:

W_{min}	is the minimum mirror weight for a solid mirror
σ_A	is the allowable stress in the mirror

A similar approach is used to develop expressions for the maximum global stress due to vibration of the mirror itself for a sandwich mirror, when the mirror is exposed to random vibration. The maximum stress for the sandwich mirror is given by;

$$\sigma_{SANDWICH} = C_1 \frac{(3+\upsilon)}{[12(1-\upsilon^2)]^{1/4}} \frac{\rho r_o}{t_f h} (2t_f + \eta h_c) (PSD)^{1/2} Q^{1/2} \left\{ \frac{gE}{\rho} \left[\frac{h^3 - (1-\eta/2) h_c^3}{2t_f + \eta h_c} \right] \right\}^{1/4} \tag{2.17}$$

where:

$\sigma_{SANDWICH}$	is the maximum stress in the sandwich mirror
υ	is the Poisson's ratio of the mirror material
C_1	is the support condition constant
ρ	is the mirror material density
h	is the overall mirror thickness
η	is the rib solidity ratio
h_c	is the shear core thickness
t_f	is the faceplate thickness
PSD	is the environmental power spectral density
Q	is the mirror transmissibility at resonance
E	is the elastic modulus of the mirror material
g	is the acceleration due to the earth's gravity

Equation 17 is used to develop an expression for the minimum weight sandwich mirror. Minimum weight is defined as the weight required to keep the mirror stress below some allowable stress when the mirror is exposed to random vibration. Minimum weight for a sandwich mirror is given by:

$$W_{MIN} = C_1 \frac{(3+\upsilon)^2}{[12(1-\upsilon)^2]^{1/2}} (\rho/\sigma_A)^2 (\rho E)^{1/2} r_o^4 g^{1/2} (PSD) Q$$
$$x \frac{1}{\left(\frac{t_f}{h}\right)^2} \left\{1-(1-\eta)\left[1-2\left(\frac{t_f}{h}\right)\right]\right\}^{3/2} \left\{1-\left(1-\frac{\eta}{2}\right)\left[1-2\left(\frac{t_f}{h}\right)\right]^3\right\}^{1/2} \quad (2.18)$$

where:

W_{min} is the minimum weight of the sandwich mirror
σ_A is the allowable stress

Although complex, equations 16 and 18 provide insight into the behavior of mirrors subject to random vibration. Of particular interest is the relationship between mirror material properties and minimum weight. For minimum weight mirrors subject to excitation by random vibration, the following material parameter is important:

$$(\rho/\sigma_A)^2 (\rho E)^{1/2} \quad (2.19)$$

where:

ρ is the mirror material density
σ_A is the allowable stress
E is the mirror elastic modulus

For glass mirrors, the allowable stress is normally the fracture stress, modified by a safety factor. For metal mirrors, the allowable stress is the microyield stress, modified by a safety factor. (Microyield stress is defined as the stress necessary to produce a permanent strain of one part per million in the material.) Table 2.3 compares different mirror materials on the basis of this new dynamic material property. For minimum weight, this property should be as small as possible.

2.14. MOUNT STRESS ANALYSIS:

In addition to the global stress induced by random vibration, the local stress due to mounting must be considered in the SIRTF primary mirror mount design. Determination of the local stress due to the mount is a difficult problem if the finite element method is used. However, it is possible to derive closed form or analytical expressions for the local stress using some simple approximations.

Two types of mount are of interest: the flat pad mount, and the conical mount. Both types of mounts are likely to be used in a semi-kinematic design, where the individual mounts act as defining points. If semi-kinematic design is used, the mounts are likely to be employed as three equal spaced defining "points" on a common diameter.

The Miles approximation, equation 3, is used to provide the accelerations of the mirror, when the mirror is subject to random vibration. Local stress for a single circular flat pad mount is given by:

$$\sigma_{mount} = \frac{4 g_{max} F}{\pi D^2} = \frac{g_{max} F}{A} \tag{2.20}$$

where:

σ_{mount}	is the local stress in the mount
F	is the fraction of the mirror weight carried by the mount
g_{max}	is the acceleration acting perpendicular to the flat pad mount surface
A	is the flat pad area in contact with the mirror
D	is the diameter of the flat pad

Substituting equation 20 into equation 3, the local stress in a flat pad mount during random vibration is given by:

$$\sigma_{mount} = \frac{12F}{\pi D^2} \left[\frac{\pi}{2} f_n Q \, (PSD) \right]^{1/2} \tag{2.21}$$

where:

σ_{mount}	is the local stress in the mount
F	is the fraction of the mirror weight carried by the mount
D	is the flat pad diameter
f_n	is the natural frequency of the mirror mount
Q	is the transmissibility of the mirror mount
PSD	is the environmental power spectral density

If the flat pads are equal spaced about the circumference of the mirror, it is reasonable to assume that at some time during random vibration, a single pad will carry the full weight of the mirror. If this assumption is made, equation 21 can be solved for the minimum pad diameter required to keep the local mount stress below some allowable stress. The minimum pad diameter is given by:

$$D_{min} = \left\{ \frac{12 W_{mirror}}{\pi \sigma_A} \left[\frac{\pi}{2} f_n Q \, (PSD) \right]^{1/2} \right\}^{1/2} \tag{2.22}$$

where:

D_{min}	is the minimum pad diameter required to keep the mount stress below the allowable stress
σ_A	is the allowable stress in the mount

Fig. 2.18 shows the local stress versus mount natural frequency in flat pad mounts for a representative set of SIRTF design parameters. Pad diameter was fixed at 3.5 in. This pad diameter was selected because of the limitation on fused silica blank thickness of 4.0 in. The values of Q and the PSD were chosen from previous studies of the SIRTF. Fig. 2.18 shows how the stress varies with mirror weight.

An alternate approach is shown in fig. 2.19. This figure is based on equation 22, and shows how the minimum pad diameter varies with frequency for a variety of mirror weights. Both fig. 2.18 and 2.19 demonstrate that relatively low mount frequency are necessary if the pad diameter is kept small.

Although the flat pad mount has considerable promise for the SIRTF program, it has a great disadvantage in only permitting loading perpendicular to the mirror surface. The conical mount can handle loading both along the mount axis and transverse to the axis. Athermalization of the conical mount is very good; as the temperature changes the two conical surface slide so as to remain in contact.

The maximum local stress in a conical contact is given by[45,46]:

$$\sigma_{conical} = \frac{2F_A \cos\theta}{(D+d)\pi L(\mu\cos\theta + \sin\theta)} + \frac{4F_t}{\pi Ld} \tag{2.23}$$

where:

$\sigma_{conical}$	is the maximum local stress in the conical contact
F_A	is the axial load
F_t	is the tangential load (load normal to the axis of the mount)
D	is the maximum conical diameter
d	is the minimum conical diameter
L	is the conical length
μ	the friction coefficient of the contact
Θ	is the cone angle (measured from the axis)

Equation 23 can be substituted into equation 3, to derive an equation for the maximum local stress in a conical mount under random vibration. If the conical mounts are used as edge mounts, radially directed, and equal spaced about the circumference of the mirror, the maximum local stress is given by:

$$\sigma_{mount} = \frac{W}{\pi}\left[\frac{\pi}{2} f_r\, Q\, (PSD)\right]^{1/2} f(\mu,\theta,L,D,K) \tag{2.24}$$

$$f(\mu,\theta,L,D,K) = \frac{1}{L}\left[\frac{1}{4}\,\frac{\cos\theta}{(\mu\cos\theta + \sin\theta)}\,\frac{1}{(D - L\tan\theta)} + \left(12 + \frac{K^2}{9}\right)^{1/2}\frac{1}{(D - 2L\tan\theta)}\right] \tag{2.25}$$

where:

σ_{mount}	is the maximum local stress in the conical mount
W	is the mirror weight
f_R	is the radial natural frequency of the mirror mount
f_A	is the axial natural frequency of the mirror mount
K	is the mirror mount frequency ratio f_A/f_R
Q	is the mirror mount transmissibility
PSD	is the environmental power spectral density
Θ	is the mount conical socket angle (measured from the mount axis)
L	is the radial conical socket length
D	is the maximum socket diameter

Fig. 2.20 to 2.23 illustrate how the geometry factor given by equation 25 varies with the mount frequency ratio. A friction coefficient ("mu") of 0.3 and a maximum socket diameter of 3 in. were selected for this set of figures. For a given socket angle, there is usually an optimum conical socket length to minimize the geometry factor, and therefor minimize the local stress in the mount.

Equations 21 and 24 indicate that it is possible to use closed form solutions to evaluate the local stress in relatively complex mirror mounts subject to random vibration. These equations can be easily evaluated on a programmable calculator or micro-computer. Use of such economical computational devices permits rapid evaluation of mount performance for inexpensive optimization of mount design.

REFERENCES

1. R. M. Richard, D. Vukobratovich, L. W. Pollard, and M. K. Cho, SIRTF Primary Mirror Mount Flexure and Socket Design, Oct. 1986 - June 1987, Optical Sciences Center, University of Arizona, Tucson, AZ, 85721.

2. D. Vukobratovich and R. M. Richard, "Flexure mounts for high-resolution optical elements,"Proc. SPIE 959, pp. 18-36 (1988).

3. Chin, D., "Optical mirror-mount design and philosophy," Appl. Opt., Vol. 3, No. 7, pp. 895-901 (July, 1964).

4. J. W. Pepi, and R. J. Wollensak, "Ultra-lightweight fused silica mirrors for a cryogenic space optical system," Proc. SPIE 183, pp. 131-137 (1979).

5. J.W. Pepi, M. A. Kahan, W. H. Barnes, and R. J. Zielinski, "Teal Ruby-design, manufacture and test," Proc. SPIE 216, pp. 160-173 (1980).

6. W.P. Barnes, Jr., Fused Silica Mirror Development for SIRTF, NASA CR - 166522, July, 1983.

7. W. P. Barnes, Jr. and R. K. Melugin, "Fused silica mirror evaluation for the Shuttle Infrared Telescope Facility (SIRTF)," Proc. SPIE 364, pp. 110-122 (1983).

8. W. P. Barnes, Jr. and R. K. Melugin, "Fused silica mirror evaluation for the Shuttle Infrared Telescope Facility (SIRTF)," Proc. SPIE 444, pp. 200-210 (1983).

9. W. P. Barnes, Jr., "Connecting optics to supporting structures," Opt. Eng. Reports, No. 35, pp. 5A-6A, Nov., 1986.

10. E.W. Huang, "Thermal stress in a glass/metal bond with PR-1578 adhesive," Proc. SPIE 1303 (in press) (1990).

11. J. H. Miller, R. K. Melugin, G. C. Augason, S. D. Howard, and G. M. Pryor, "Ames Research Center cryogenic mirror testing program. A comparison of the cryogenic performance of metal and glass mirrors with different types of mounts," Proc. SPIE 973, pp. 62-70 (1988).

12. Tony Hull, Perkin-Elmer, private communication.

13. B. Iraninejad, D. Vukobratovich, R. M. Richard, and R. K. Melugin, "A mirror mount for cryogenic environments," Proc. SPIE 450, pp. 34-39 (1983).

14. R. Schlegelmilch et al, GIRL-German Infrared Laboratory Final Report of the Telescope Study, Phase B, NASA TM-75911, Jan., 1981.

15. R. Schlegelmilch and J. Altmann, "A cooled infrared telescope for the GIRL German infrared laboratory," Zeiss Inform., Vol. 28, No. 96 E, pp. 19-23 (Dec. 1985).

16. R. K. Melugin, J. H. Miller, "Infrared telescope design: Implications from cryogenic tests of fused silica mirrors," Proc. SPIE 433, pp. 171-177 (1983).

17. Bruce Kenyon, Boeing, private communication.

18. "Kinematic Mount," U.S. Patent No. 4,268,123, issued May 19, 1981, to Bernard Mesco, Playa Del Rey, CA.

19. W. P. Barnes, op. cit.

20. J. Espiard, J. Paseri, G. Cerutti-Maori, and C. Singer, "Lightweight cold mirror and fixation," Proc. SPIE 589, pp. 187-193 (1985).

21. "Mounting Device for Supporting a Component, Especially a Mirror or an Antenna Reflector in a Spacecraft," U. S. Patent 4,533,100, issued Aug. 6, 1985, to Jacques Paseri, Fontenay-les-Briis, France.

22. C. La Fiandra, A Non-Adhesive Glass to Metal Bonding Technique, PA 11078, Perkin-Elmer Corp., 100 Wooster Heights, Danbury, CT 06810.

23. B. Iraninejad, J. Lubliner, T. Mast, and J. Nelson, "Mirror deformations due to thermal expansion of inserts bonded to the glass," Proc. SPIE 748, pp. 206-214 (1987).

24. D. A. Crowe, R. K. Melugin, J. H. Miller, "Ultra lightweight mirror performance at 8 degrees kelvin," Proc. SPIE 509, pp. 179-190 (1984).

25. J. Ulmes, "Design of a catadioptric lens for long-range oblique aerial reconnaissance," Proc. SPIE 1113, pp. 116-125 (1989).

26. D. B. Pollock and J. B. Brown, "The fabrication of the Airborne Optical Adjunct (AOA) mirrors," Proc. SPIE 1113, pp. 160-177 (1989).

27. G. Sarver, NASA Ames, Moffett Field, CA, private communication.

28. M. Schreibman and P. Young, "Design of infrared astronomical satellite (IRAS) primary mirror mounts," Proc. SPIE 250, pp. 50-58 (1989).

29. P. Young and M. Schreibman, "Alignment design for a cryogenic telescope," Proc. SPIE 251, pp. 171-178 (1980).

30. N. R. Adsit, P. Dessau, and W. E. Witzell, "Flexural fatigue testing of titanium forging material in liquid hydrogen," Fatigue and Fracture Toughness, ASTM STP 556, American Society for Testing and Materials, 1974, pp. 44-54.

31. R. H. Van Stone, J. L. Shannon, W. S. Pierce, and J. R. Low, Jr., "Influence of composition, annealing treatment, and texture on the fracture toughness of Ti-5Al-2.5Sn plate at cryogenic temperatures," Toughness and Fracture Behavior of Titanium, ASTM STP 651, American Society for Testing and Materials, 1978. pp. 154-179.

32. T. Kawabata, S. Morita, and O. Izumi, "Deformation and fracture of Ti-5Al-2.5Sn ELI alloy at 4.2K - 291 K," in Titanium 80 Science and Technology, Plenum Press, New York, pp. 801-809 (1980).

33. C. F. Fiftal, D. A. Bolstad, and M. S. Misra, "Fracture resistance of Ti-5Al-2.5Sn extra-low interstitial castings," Toughness and Fracture Behavior of Titanium, ASTM STP 651, American Society for Testing and Materials, 1978, pp. 3-16.

34. H. Terada, E. Nakai, and Takamatsu, "Fracture toughness and fatigue behavior of Ti-6Al-4V and Ti-5Al-2.5Sn at cryogenic temperature," in Titanium 80 Science and Technology, Plenum Press, New York, pp. 1607-1615 (1980).

35. C. M. Carman and J. M. Katlin, "Plane strain fracture toughness and mechanical properties of 5Al-2.5Sn ELI and commercial titanium alloys at room and cryogenic temperatures," Applications Related Phenomena in Titanium Alloys, ASTM STP 432, American Society for Testing and Materials, 1968, pp. 124-144.

36. R.L. Tobler, "Fatigue crack growth and J-integral fracture parameters of Ti-6Al-4V at ambient and cryogenic temperatures," Cracks and Fracture, ASTM STP 601, American Society for Testing and Materials, 1976, pp. 346-370.

37. C. W. Fowlkes and R. L. Tobler, "Fracture testing and results for a Ti-6Al-4V alloy at liquid helium temperature," Eng. Fracture Mechanics, Vol. 8, pp. 487-500 (1976).

38. R. L. Tobler, "Low temperature fracture behavior of a Ti-6Al-4V alloy and its electron beam welds," Toughness and Fracture Behavior of Titanium, ASTM STP 651, American Society for Testing and Materials, 1978, pp. 267-294.

39. R. R. Altenhof, "The design and manufacture of large beryllium optics," Proc. SPIE 65, pp. 20-32 (1975).

40. G. Mikk, "cryogenic testing of a beryllium mirror," Proc. SPIE 65, pp. 89-96 (1975).

41. D. S. Steinberg, Vibration Analysis for Electronic Equipment, 2nd. Ed., J. Wiley and Sons, New York, 1988.

42. R. Bares, Tables for the Analysis of Plates, Slabs and Diaphragms Based on the Elastic Theory, 2nd Ed., Bauverlag GMBH, Wiesbaden, 1971 (German-English Edition).

43. Structural Sandwich Composites, MIL-HDBK-23A, 30 Dec. 1968, Department of Defense, Washington, D.C. 20025.

44. R. D. Belvins, Formulas for Natural Frequency and Mode Shape, Van Nostrand Reinhold Co., New York, 1979.

45. T. L. Angle, "Analyzing taper fits," Machine Design, Feb. 24, 1983, pp. 75-78.

46. W. Trylinski, Fine Mechanisms and Precision Instruments, Pergamon Press, Poland, 1971.

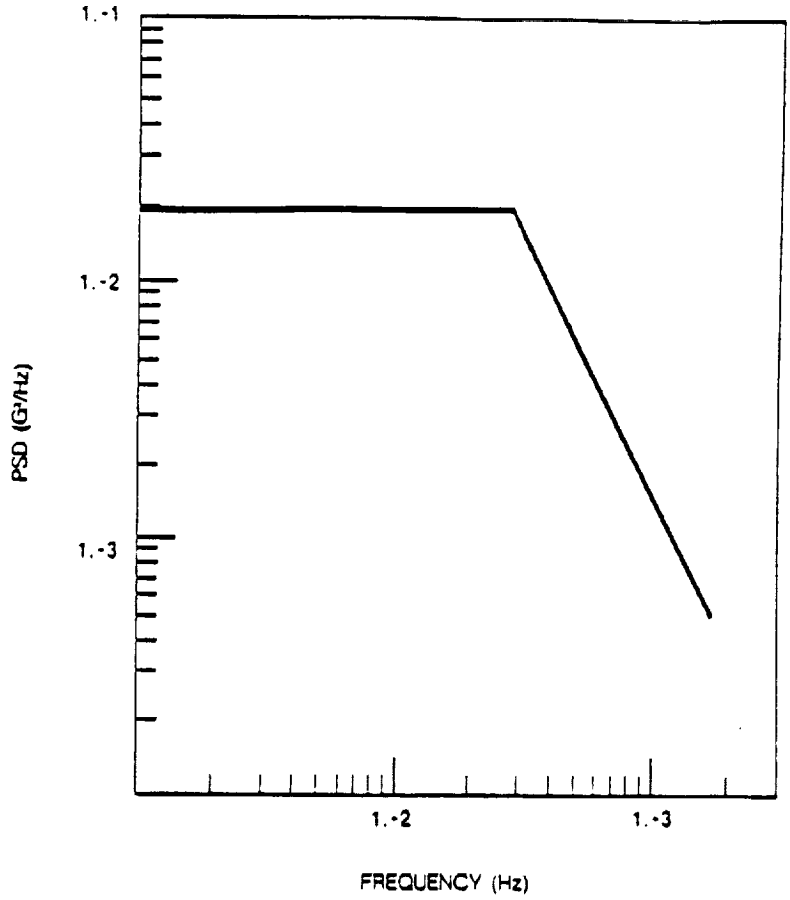

Figure 2.1. PSD Design curve.

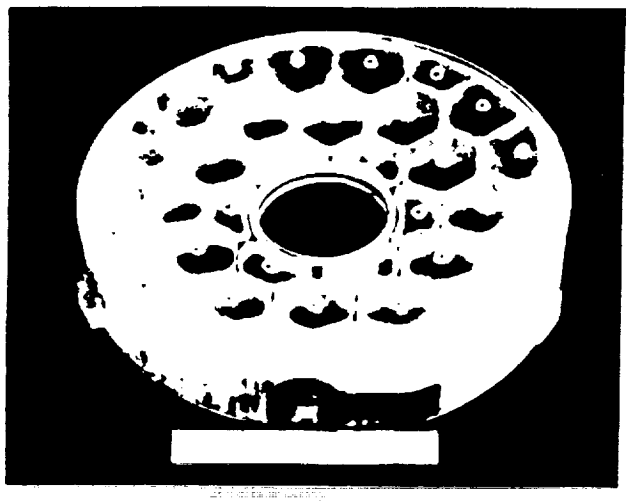

Figure 2.2 TEAL RUBY mirror and mount.

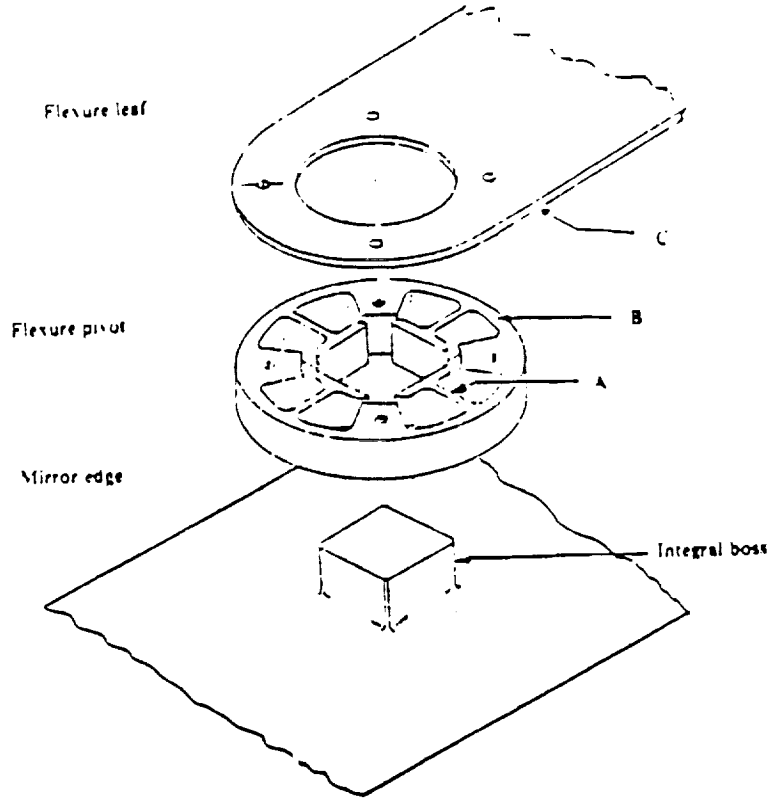

Figure 2.3. Metal to glass interface of bonded mount (ITEK mirror).

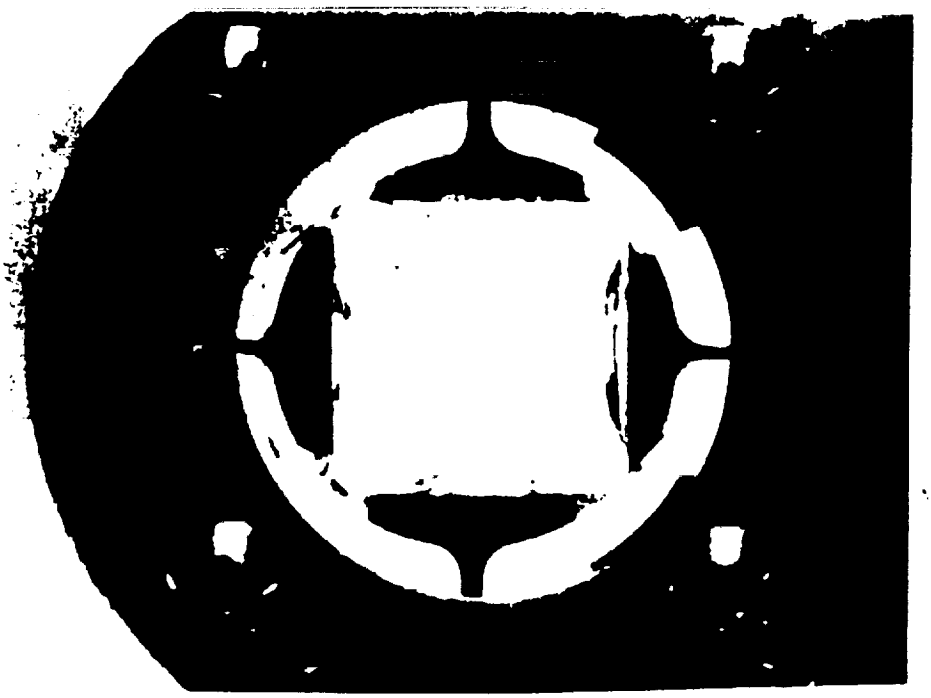

Figure 2.4. Failure of bonded mount after LN_2 immersion.

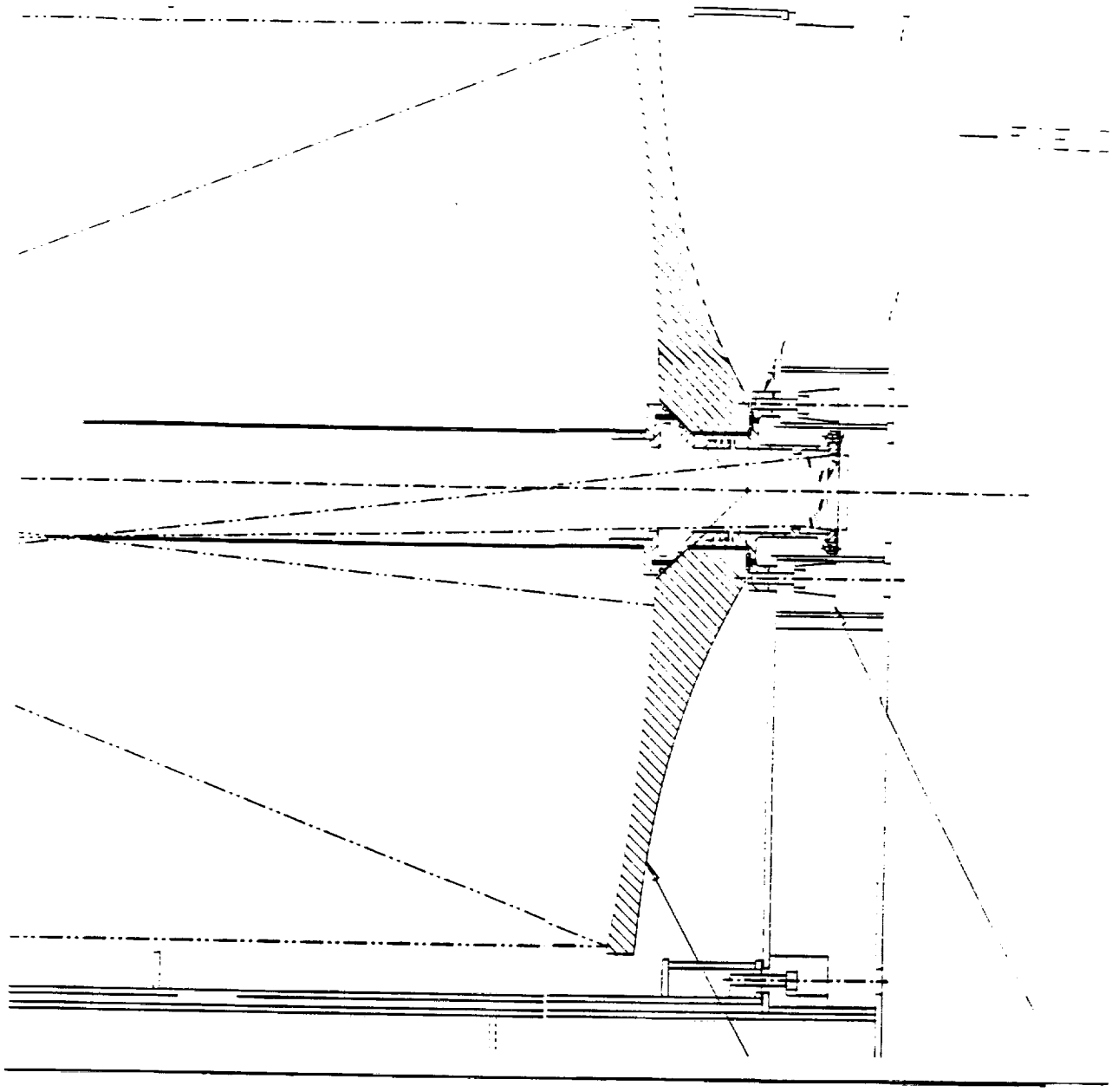

Figure 2.5. Mars Observer Camera (MOC) conical mirror mount.

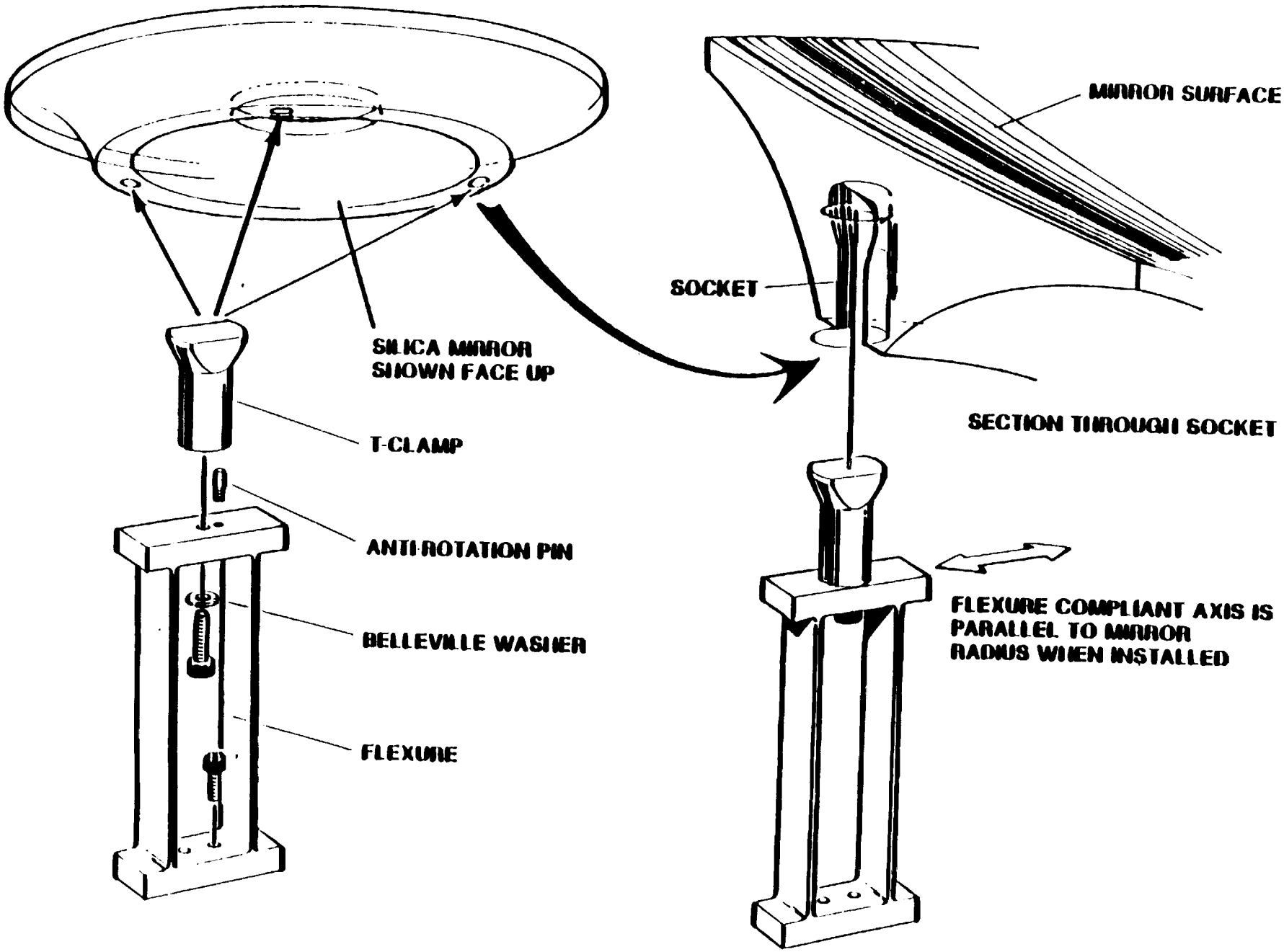

Figure 2.6. University of Arizona/Ames Research Center (UofA/ARC) three point conical mount with flexures.

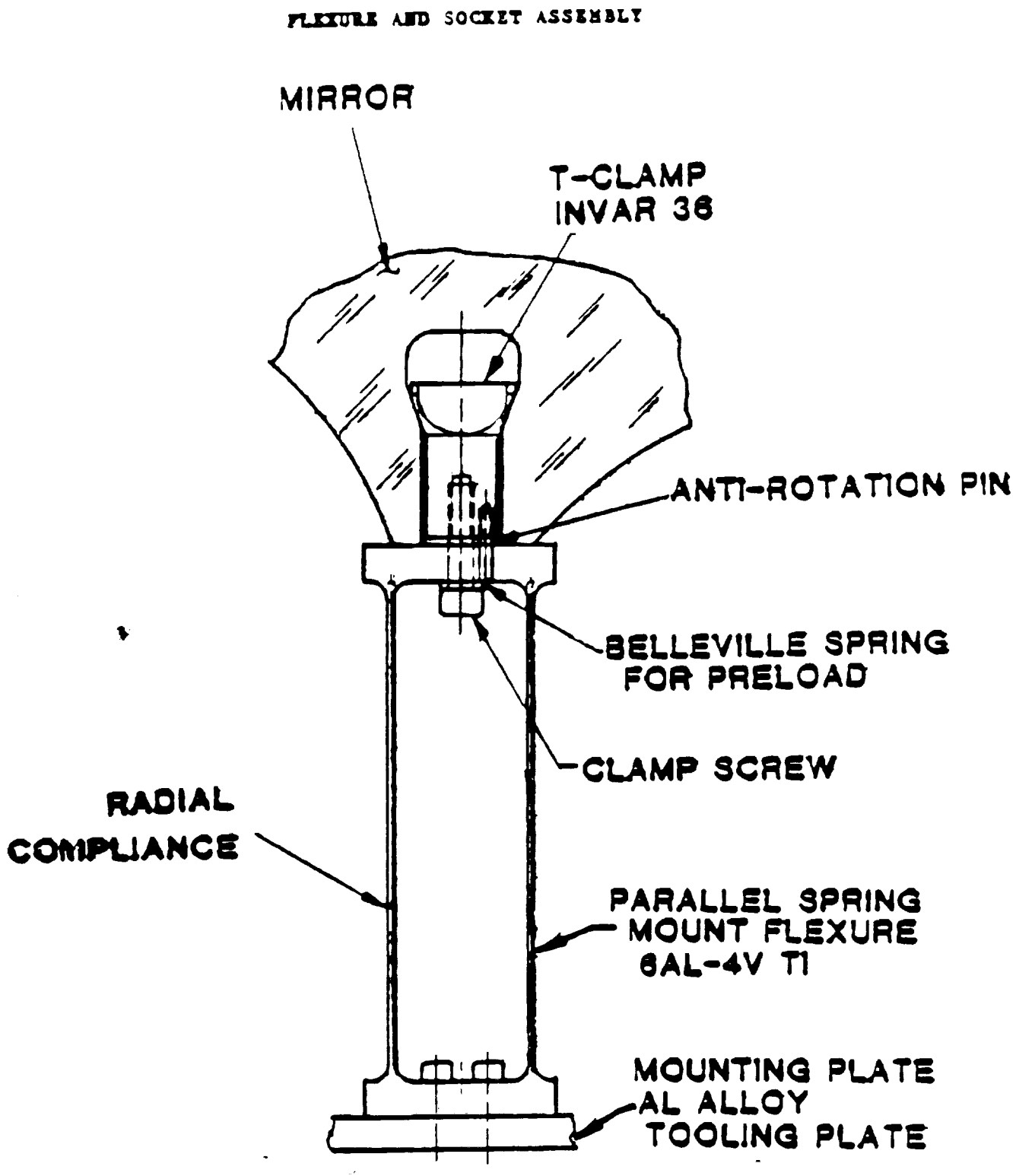

Figure 2.7. Details of UofA/ARC conical mirror mount.

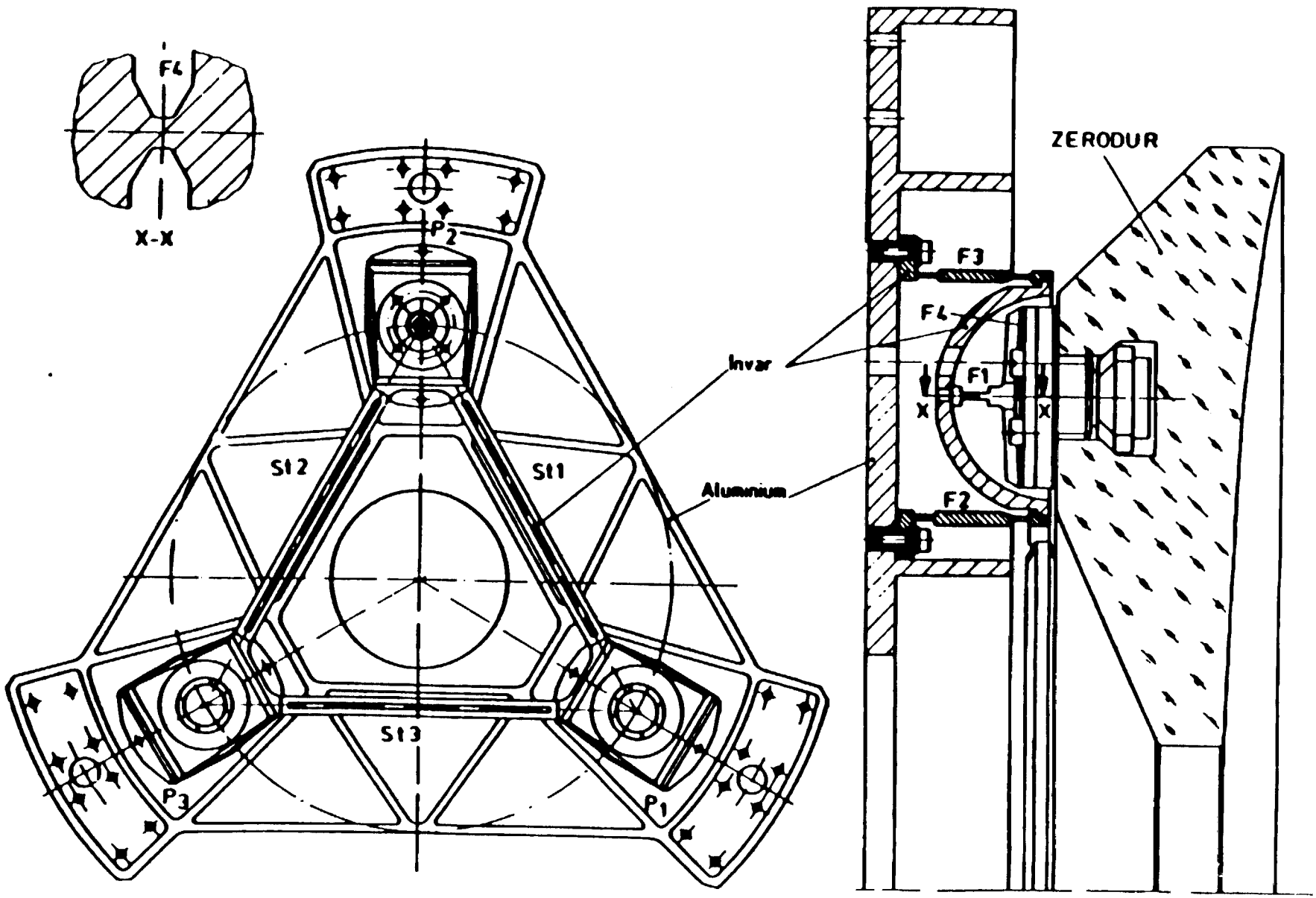

Figure 2.8. Three point conical mount for German Infrared Laboratory (GIL) mirror.

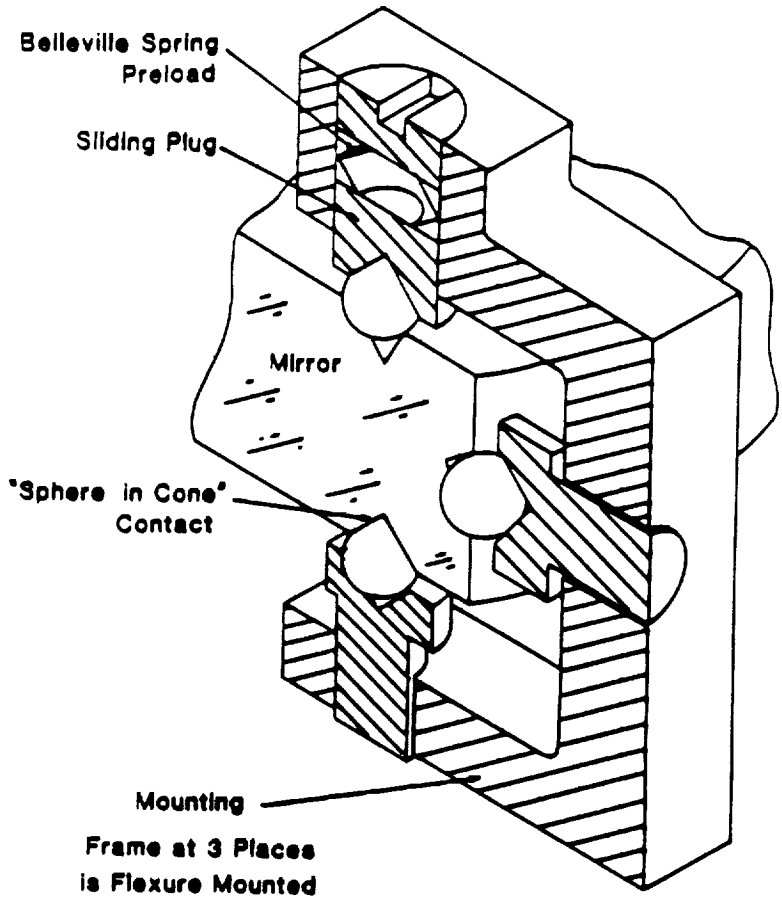

Figure 2.9. P-E BIRS sphere/cone mirror edge mount (conceptual).

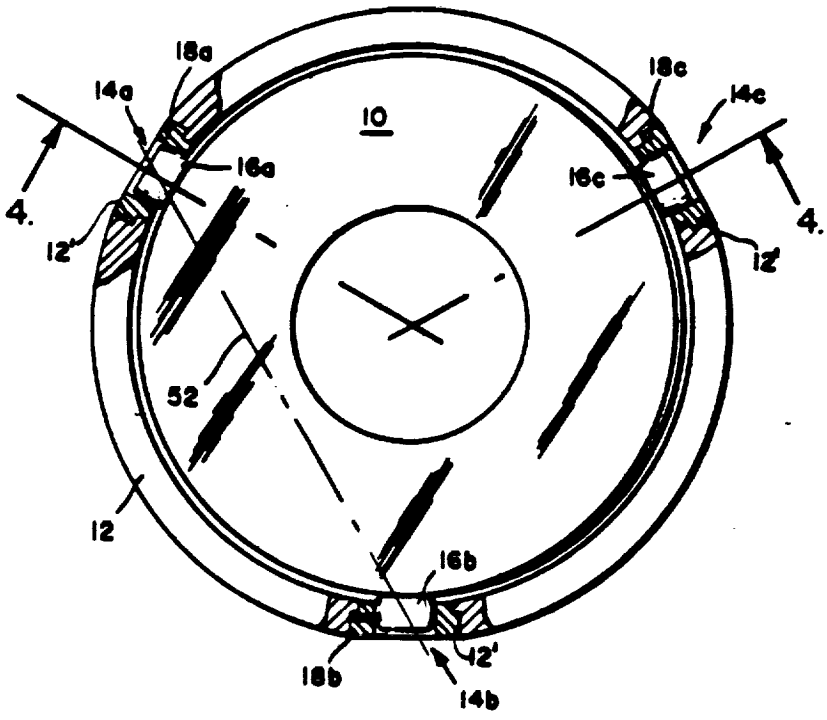

Figure 2.10. Sphere/cylinder mount patented by Mesco.

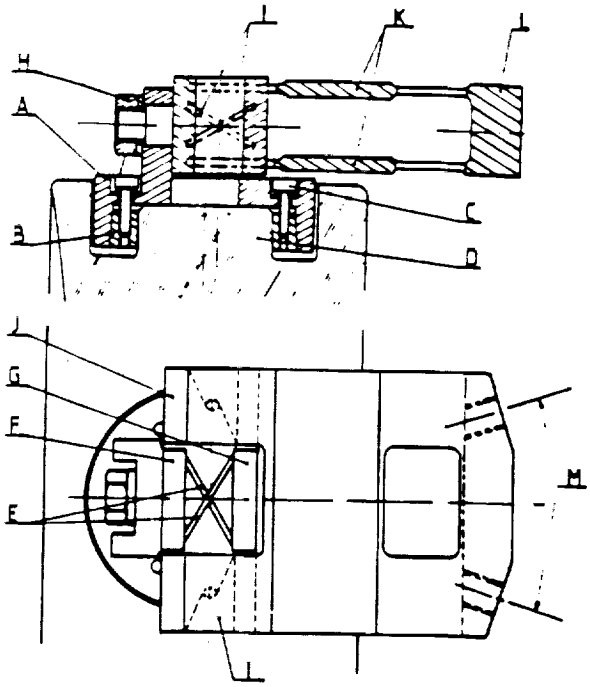

Figure 2.11. REOSC ISO cylindrical clamp mount.

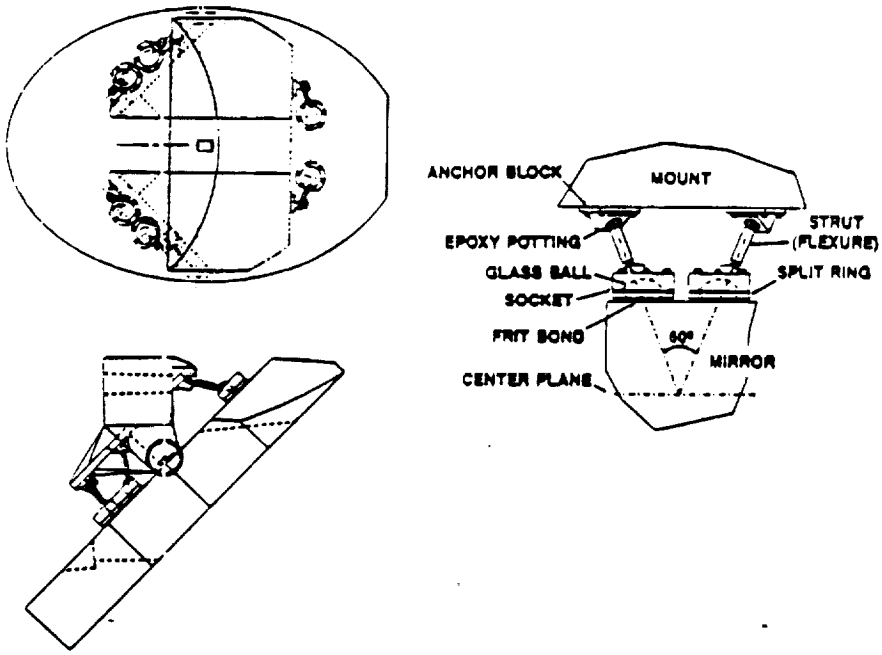

Figure 2.12. Ball foot clamp mount (with bipod).

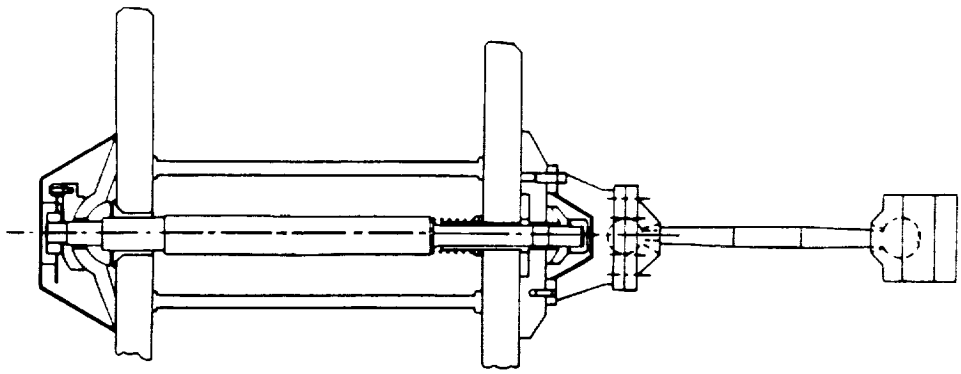

Figure 2.13. Hubble Space Telescope (HST) bolted mount.

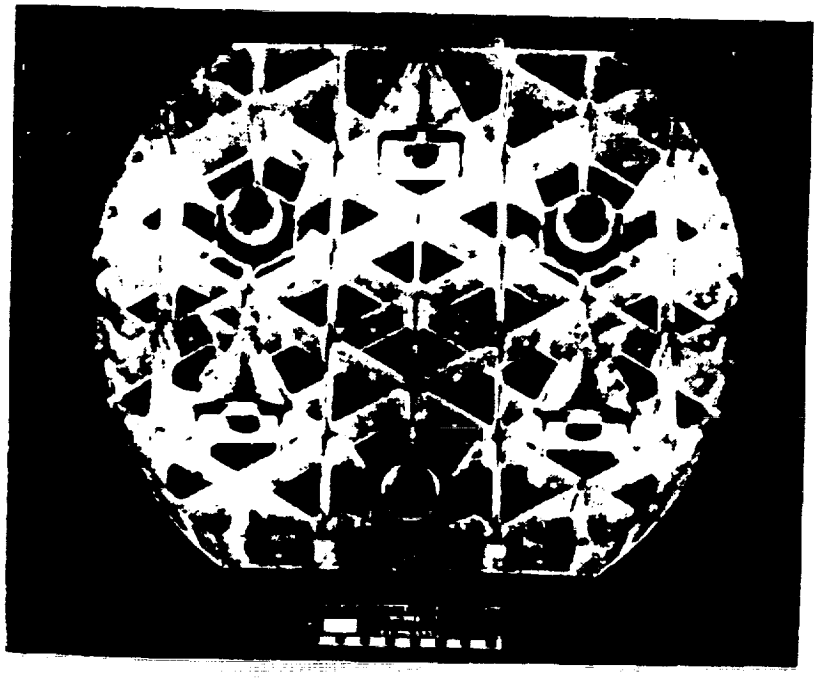

Figure 2.14. Bolted mount for Airborne Optical Adjunct (ADA) mirror.

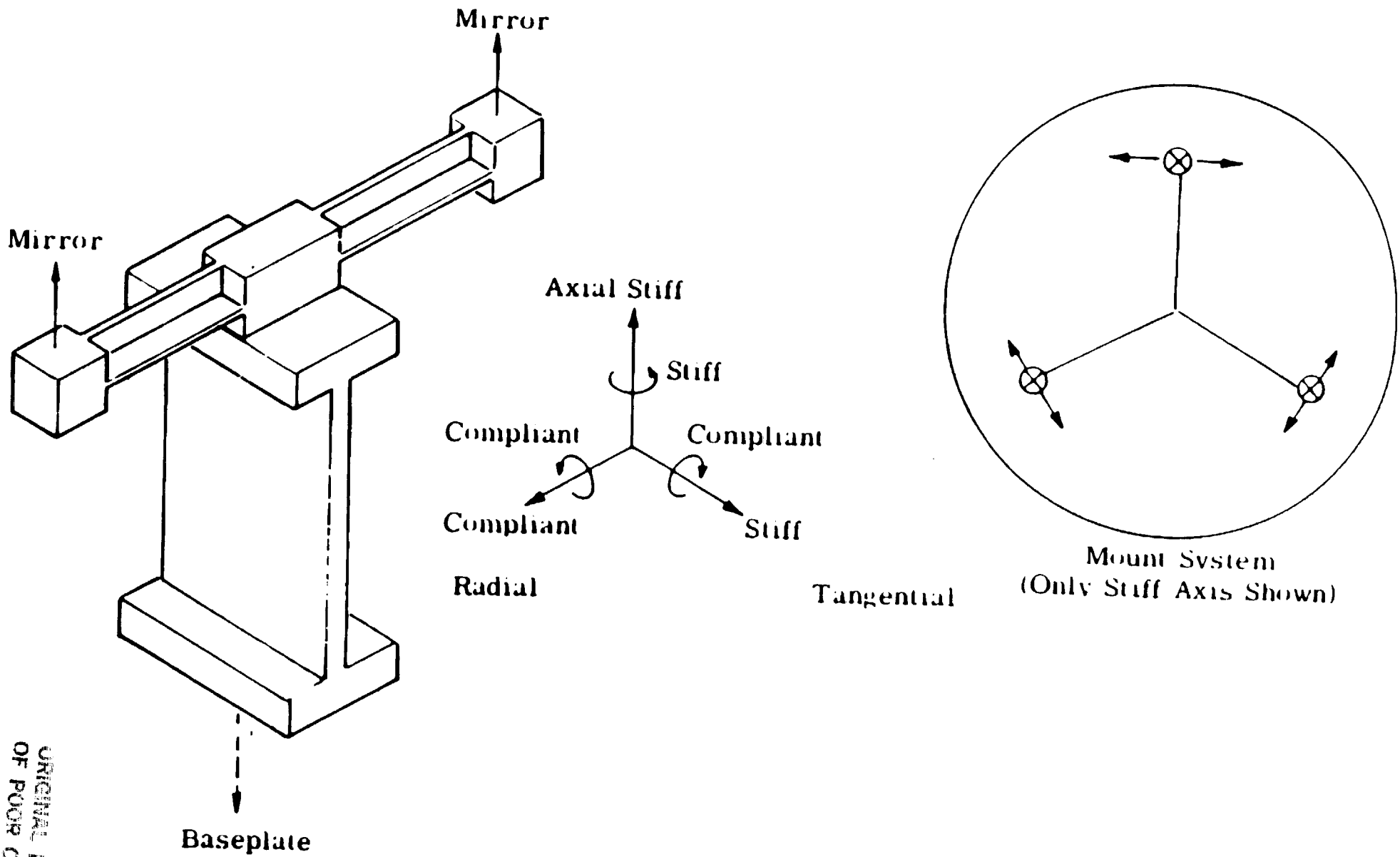

Figure 2.15. Infrared Astronomical Satellite (IRAS) bolted flexure mount.

COMPARISON OF SELF-WEIGHT STRESS FOR RIGHT CIRCULAR CYLINDER MIRRORS CALCULATED BY CLOSED FORM AND FINITE ELEMENT METHODS

3 INCHES THICK

Diameter	Support	Closed Form (PSI)	Finite Element (PSI)	Error
40 in.	ring 0.065R ring Edge	4.616 12.73	4.165 12.61	0.098 0.009
30 in.	ring 0.065R ring Edge	2.597 7.275	2.30 7.10	0.114 0.024
20 in.	ring 0.065R ring Edge	1.154 3.183	0.969 3.16	0.160 0.007

4 INCHES THICK

Diameter	Support	Closed Form (PSI)	Finite Element (PSI)	Error
40 in.	ring 0.065R ring Edge	3.46 9.55	3.06 9.46	0.116 0.009
30 in.	ring 0.065R ring Edge	1.95 5.37	1.665 5.33	0.114 0.008
20 in.	ring 0.065R ring Edge	0.865 2.39	0.687 2.38	0.160 0.003

5 INCHES THICK

Diameter	Support	Closed Form (PSI)	Finite Element (PSI)	Error
40 in.	ring 0.065R ring Edge	2.770 7.64	2.39 7.58	0.137 0.017
30 in.	ring 0.065R ring Edge	1.56 4.30	1.28 4.27	0.178 0.006
20 in.	ring 0.065R ring Edge	0.693 1.91	0.519 1.91	0.250 0.000

6 INCHES THICK

Diameter	Support	Closed Form (PSI)	Finite Element (PSI)	Error
40 in.	ring 0.065R ring Edge	2.308 6.364	1.938 6.323	0.160 0.006
30 in.	ring 0.065R ring Edge	1.298 3.580	1.031 3.568	0.206 0.003
20 in.	ring 0.065R ring Edge	0.577 1.591	0.408 1.61	0.293 0.012

Table 2.1.

EQUIVALENT HEIGHT CONTOURED BACK MIRRORS

Single Arch
Height = 4 in.
Max. principle stress = -16.0 psi
Max. deflection = -9.0×10^{-5} in.
Fundamental frequency = 330 Hz
Weight = 148 lb.

Double Arch
Height = 4 in.
Max. principle stress = -1.8 psi
Max. deflection = -4.25×10^{-6} in
Fundamental frequency = 1518 Hz
Weight = 208 lb.

Single Arch
Height = 5 in.
Max. principle stress = -13.0 psi
Max. deflection = -6.0×10^{-5} in.
Fundamental frequency = 404 Hz
Weight = 175 lb.

Double Arch
Height = 5 in.
Max. principle stress = -1.4 psi
Max. deflection = -3.20×10^{-6} in.
Fundamental frequency = 1749 Hz
Weight = 253 lb.

Single Arch
Height = 7 in.
Max. principle stress = -9.0 psi
Max. deflection = -3.2×10^{-5} in.
Fundamental frequency = 553 Hz
Weight = 239 lb.

Double Arch
Height = 7 in.
Max. principle stress = -1.2 psi
Max. deflection = -2.20×10^{-6} in.
Fundamental frequency = 2109 Hz
Weight = 340 lb.

EQUIVALENT WEIGHT CONTOURED BACK MIRRORS

Single Arch
Weight = 175 lb.
Max. principle stress = -13.0 psi
Max. deflection = -6.0×10^{-5} in.
Fundamental frequency = 404 Hz
Height = 5 in.

Double Arch
Weight = 175 lb.
Max. principle stress = -2.0 psi
Max. deflection = -5.5×10^{-6} in.
Fundamental frequency = 1334 Hz
Height = 3.3 in.

Single Arch
Weight = 206 lb.
Max. principle stress = -10.0 psi
Max. deflection = -4.25×10^{-5} in.
Fundamental frequency = 480 Hz
Height = 6.1 in.

Double Arch
Weight = 208 lb.
Max. principle stress = -1.8 psi
Max. deflection = -4.25×10^{-6} in.
Fundamental frequency = 1518 Hz
Height = 4.0 in.

Single Arch
Weight = 251 lb.
Max. principle stress = -8.0 psi
Max. deflection = -2.8×10^{-5} in.
Fundamental frequency = 591 Hz
Height = 7.7 in.

Double Arch
Weight = 253 lb.
Max. principle stress = -1.4 psi
Max. deflection = -3.2×10^{-6} in.
Fundamental frequency = 1749 Hz
Height = 5.0 in.

FUNDAMENTAL FREQUENCY ESTIMATE

$$f = \left[\frac{1}{2\pi}\right]\left[\frac{g}{\delta_s}\right]^{\frac{1}{2}} \text{ Hz.}$$

Where : f = fundmental frequency
g = acceleration due to gravity
δ_s = maximum static deflection

Table 2.2. Self-weight stress in contoured back mirrors.

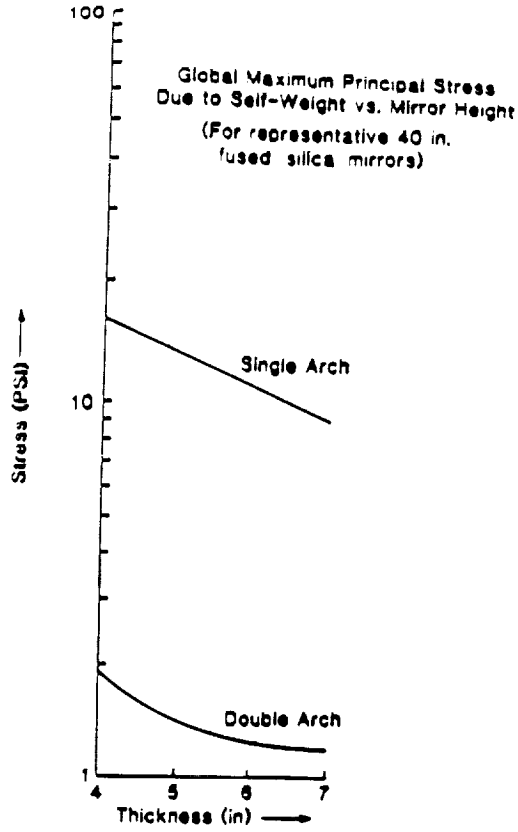

Figure 2.16.

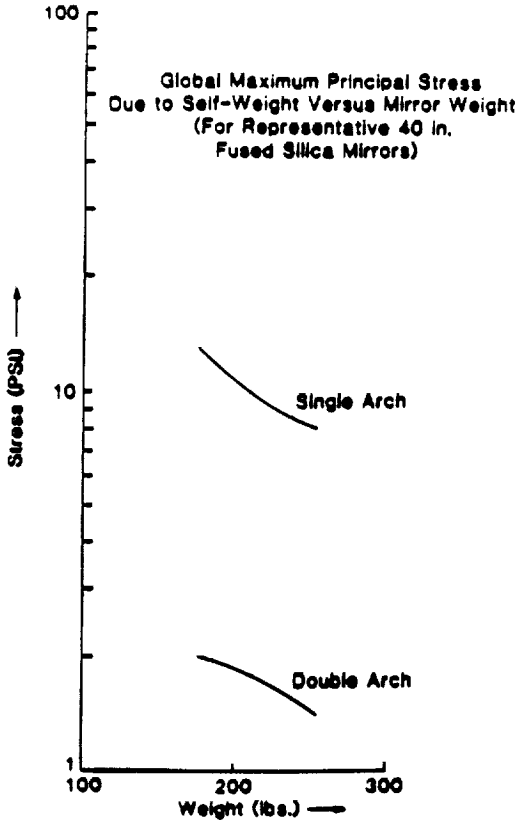

Figure 2.17.

DYNAMIC PROPERTIES OF MIRROR MATERIALS

MATERIAL	$\frac{\rho}{Kg/m^3 x 10^3}$	E GPa	σ MPa	$(\rho\sigma_{MAX})^2(\rho E)^{1/2}$ $(Kg/m^7 \times 10^{-3})$
1. AL 6061-T6	2.71	69	65	23.8
2. Be 1-70	1.85	304	17	280.8
3. Invar 36	8.03	145	69	462.1
4. AL/SiC SXA®	2.91	117	117	11.4 (Lightest)
5. Pyrex 7740	2.23	65.5	7	1226 (Heaviest)
6. Fused Silica ULE	2.20	67.7	10	590.7
7. Fused Silica 7940	2.20	73.2	10	614.2
8. Zerodur	2.53	91	10	971.2
9. Silicon	2.53	131	34	82.0
10. SiC	2.92	311	68	55.6

Table 2.3.

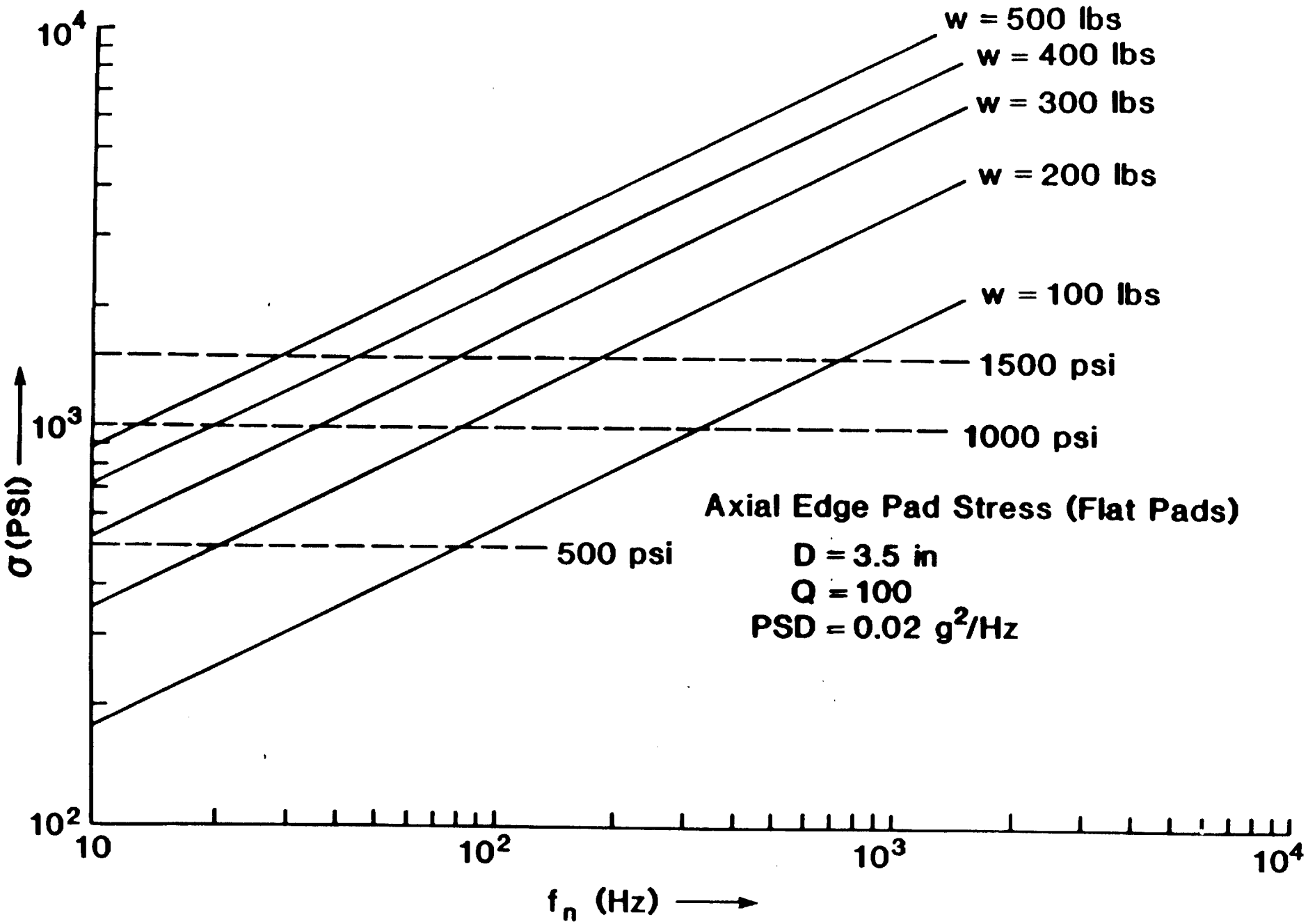

Figure 2.18. Maximum local stress versus mount natural frequency for flat pad mounts.

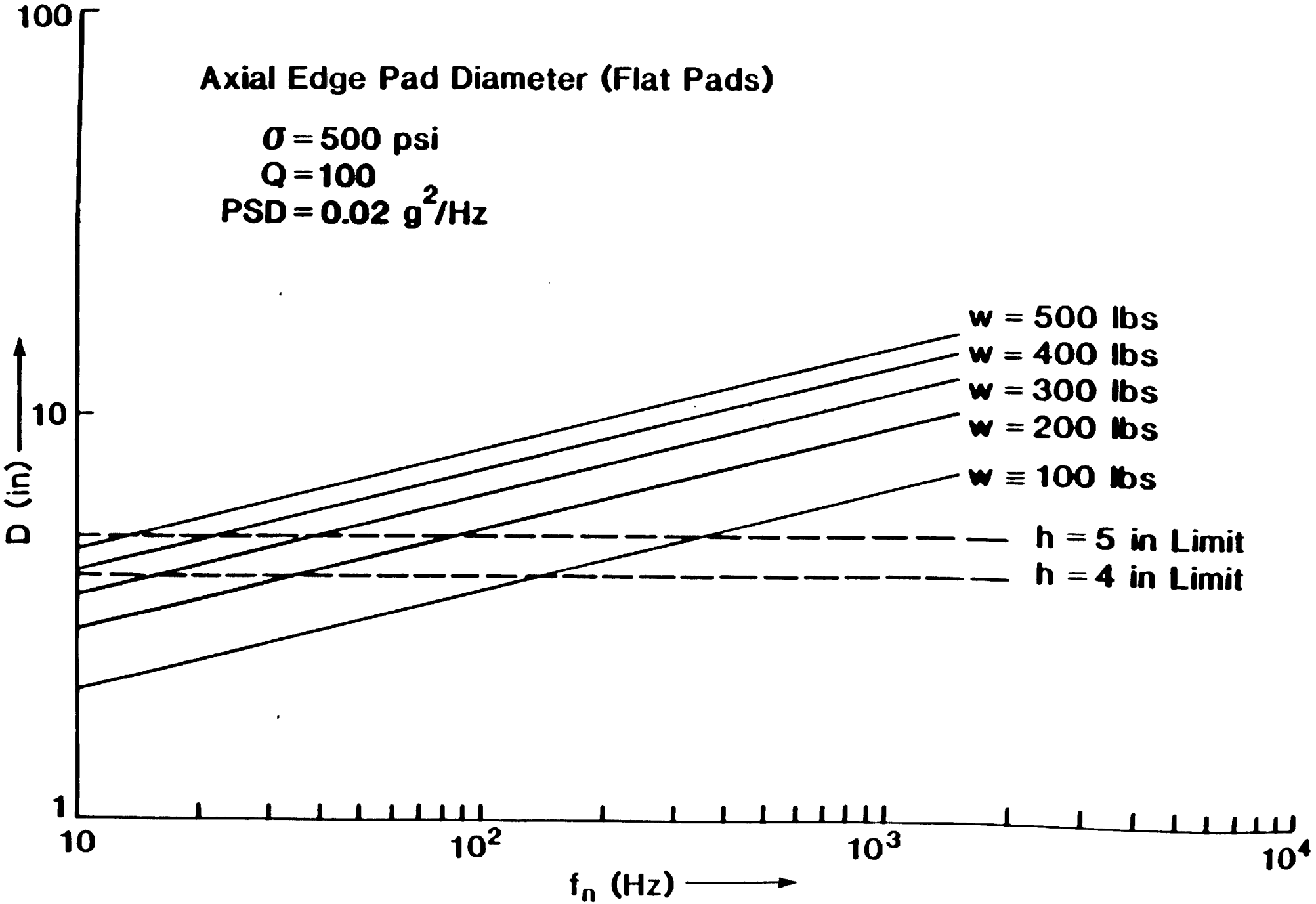

Figure 2.19. Maximum flat pad diameter versus mount natural frequency for flat pad mounts.

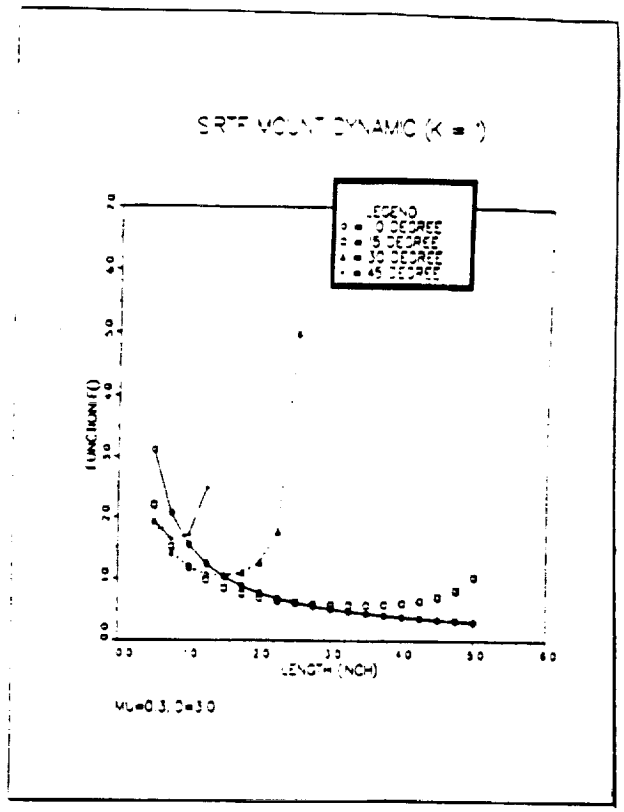

Figure 2.20. Conical mount geometry factor.

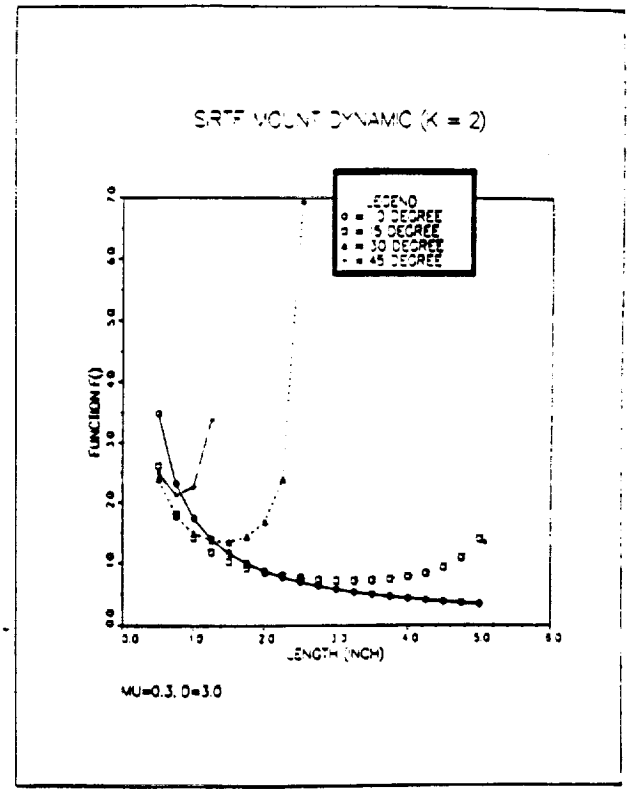

Figure 2.21. Conical mount geometry factor.

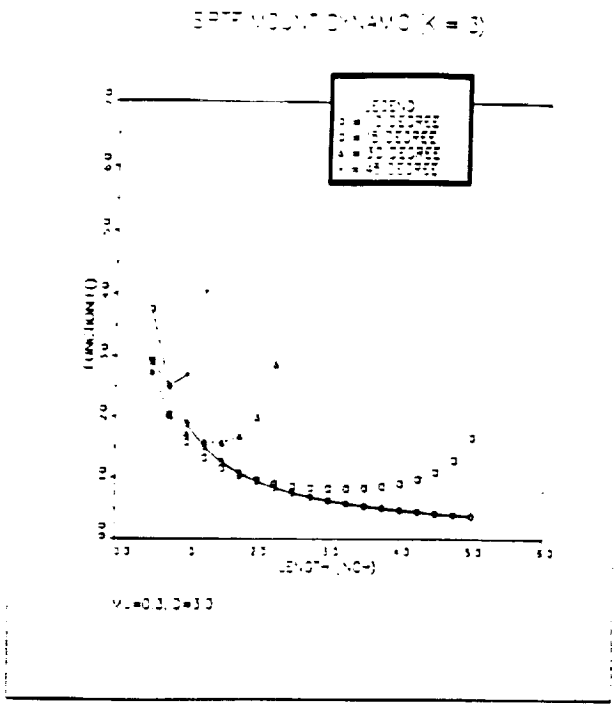

Figure 2.22. Conical mount geometry factor.

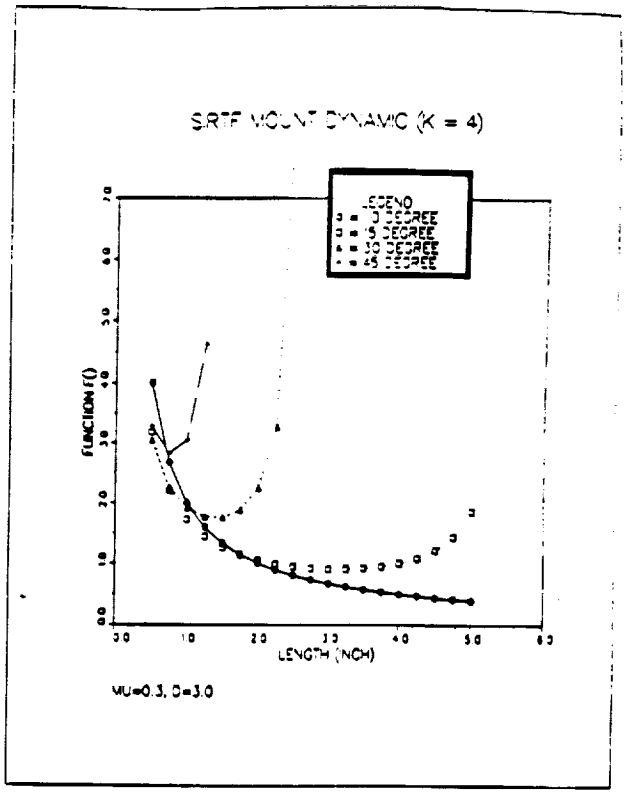

Figure 2.23. Conical mount geometry factor.

LIGHTWEIGHT BERYLLIUM MIRROR PERFORMANCE

Mirror	Date	Size (m)	Weight (Kg)	Alloy	Structure	Test Temp. (K)	Test Figure (nm)	Hysteresis (nm)	Note	Ref.
IRAS (P-E)	1983	0.62	12.6	KBI HP81	Open back radial & circumfer ribs	25	215 RMS	YES	Polishing corrosion	5
ARC (P-E)	1988	0.5	-	B-W HIP I-70	Meniscus	8	215 RMS	82 RMS (3 Cycles)	-	1
BALL RME	1990	0.6	9	B-W HIP I-70	Open back triangular cells	77	-	1580 P-V (10 Cycles)	-	2
P-E TEST	1989	1.02	18	B-W HIP 0-50	Sandwich hex cells	108	160 RMS	52 RMS (3 Cycles)	Polishing corrosion cracked	6
Hughes TEST	1989	0.5	-	B-W HIP I-70	Soild	97	120 RMS	25 RMS (2 Cycles)	-	4
ITT TEST	1989	.48 x .31	-	-	-	287-309	380 P-V	25	Nickel plated	3
P-E TEST	1988	0.241	-	-	-	83	63 RMS	-	Flat	7
P-E TEST	1988	0.431	3.3	B-W HIP I-70	Sandwich hex cells	110	41 RMS	-	Sphere	7

Appendix 1. Lightweight beryllium mirror performance.
(Note -- use version with references!)

Sources

1) Melugin; R.K., Miller, J.H.; Young, J.A.; Howard, S.D.; and Pryor, G.M.; "Cryogenic Optical Lightweight HIP Beryllium Mirror," Proc. SPIE 973 (1988).

2) Killpatrick, D.H., Mirror Deformation Due to Thermal Cycling, (Unpublished).

3) Weinswig, S., "Thermal Effects on Beryllium Mirrors," Proc. SPIE 1118.

4) Gossett, E.W., Jr.,; Marder, J.; Kendrick, R. and Cross, O., "Evaluation of Isostatic Pressed Beryllium for Low Scatter Cryogenic Optics," Proc. SPIE 1118 (1989).

5) SIRTF Free Flyer Phase A System Concept Description, Document No. PD-1006, May 3, 1984, NASA Ames Research Center, Moffett Field, CA 94035.

6) One Meter Beryllium Mirror Polishing and Characterization Program, PR B11-95, Tobin, E.; Gardopee, G.; Fink, R.; Petrie, W.; Vernold, C. and Carbone, F.; Perkin-Elmer Comporation, 100 Wooster Heights Road, Danbury, CT 06810, May 1989.

7) Roger Paquin, Private Communication.

Appendix 1b. Sources.

Appendix 2. Derivation of global stress equations.

SOLID MIRROR

CONSIDER A UNIFORMLY LOADED SOLID FLAT CIRCULAR PLATE, SIMPLY SUPPORTED AT THE EDGE ALL AROUND. THE MAXIMUM DEFLECTION IS GIVEN BY:

$$\delta_r = \frac{p r_0^2}{D} (3 + \nu) \quad (1)$$

WHERE: δ_r = MAXIMUM RADIUS DEFLECTION
p = LOAD PER UNIT AREA
r_0 = PLATE EDGE RADIUS
ν = POISSON'S RATIO

NOW FOR A CELLO-WEIGHT LOADED PLATE THE LOAD PER UNIT DEFLECTION IS THE AREAL DENSITY GIVEN BY:

$$D_0 = \rho h \quad (2)$$

WHERE: ρ = MATERIAL DENSITY
h = PLATE THICKNESS

SUBSTITUTING INTO EQ (1)

$$M_r = \frac{\rho h r_0^2}{6} (3 + \nu) \quad (3)$$

THE BENDING STRESS IN THE PLATE IS FOUND BY:

$$\sigma = \frac{6 M_r}{h^2} \quad (4)$$

WHERE: σ = BENDING STRESS

SUBSTITUTING EQ (3) INTO EQ (4) THE MAXIMUM PLATE BENDING STRESS IS:

$$\sigma_{max} = \frac{3}{8} \rho \frac{r_0^2}{h} (3 + \nu) \quad (5)$$

SITE DYNAMIC RESPONSE

ACCORDING TO "3-SIGMA" RESPONSE THE ACCELERATION LOADING ON THE PLATE DUE TO RANDOM VIBRATION IS GIVEN BY:

$$g_{max} = 3 \left[\frac{\pi}{2} f_n (PSD) Q \right]^{1/2}$$

WHERE: g_{max} = ACCELERATION (DIMENSIONLESS)
f_n = PLATE NATURAL FREQUENCY
PSD = POWER SPECTRAL DENSITY AT f_n
Q = TRANSMISSIVITY AT RESONANCE

THE EFFECT OF RANDOM VIBRATION IS TO MODIFY THE SELF-WEIGHT LOADING BY g_{max}. SUBSTITUTING EQ 6 INTO EQ (5)

$$\sigma_{max} = \frac{9}{8} \rho \frac{r_0^2}{h} (3+\upsilon) \left[\frac{\pi}{2} f_n (PSD) Q \right]^{1/2} \qquad (7)$$

THE PLATE NATURAL FREQUENCY IS GIVEN BY:

$$f_n = \frac{\lambda_{11}^2}{2\pi r_0^2} \left[\frac{g E h^2}{12 \rho (1-\upsilon^2)} \right]^{1/2} \qquad (8)$$

WHERE: λ_{11} = CONSTANT
g = ACCELERATION DUE TO EARTH'S GRAVITY
E = MATERIAL ELASTIC MODULUS

SUBSTITUTING EQ (8) INTO EQ (7):

$$\sigma_{max} = \frac{9}{8} \rho \frac{r_0^2}{h} (3+\upsilon) \left\{ \frac{\lambda_{11}^2}{4 r_0^2} \left[\frac{g E h^2}{12 \rho (1-\upsilon^2)} \right]^{1/2} (PSD) Q \right\}^{1/2}$$

$$= \frac{9}{16} \frac{\lambda_{11} (3+\upsilon)}{[12 (1-\upsilon^2)]^{1/4}} \rho^{3/4} E^{1/4} \frac{r_0}{h^{1/2}} g^{1/4} (PSD)^{1/2} Q^{1/2}$$

SOLVING FOR h:

$$h = \frac{81}{256}\frac{\lambda_{11}^2 (2+\upsilon)^2}{[12(1-\upsilon^2)]^{1/2}} \rho^{3/2} E^{1/2} \frac{r_o^2}{\sigma_{max}^2} g^{1/2} \quad (9)$$

- = PLATE WEIGHT IS GIVEN BY

$$W = \gamma \rho r_o^2 h \quad (10)$$

WHERE W = PLATE WEIGHT

SUBSTITUTING EQ (10) INTO EQ (9)

$$W = \frac{81 \pi \lambda_{11}^2 (2+\upsilon)^2}{256[12(1-\upsilon^2)]^{1/2}} \frac{\rho^{3/2} E^{1/2}}{\sigma_{max}^2} r_o^4 g^{1/2} \quad (12)$$

$$= \frac{81 \pi \lambda_{11}^2 (2+\upsilon)^2}{256[12(1-\upsilon^2)]^{1/2}} \left(\frac{\rho}{\sigma_{max}}\right)^2 (\rho E)^{1/2} r_o^4 g^{1/2} \quad (13)$$

CHECKING EQ (13) USING DIMENSIONAL ANALYSIS:

$$F = \left(\frac{F}{L^3}\frac{L^2}{F}\right)^2 \left(\frac{F}{L^3}\frac{F}{L^2}\right)^{1/2} \left(\frac{L}{T^2}\right)^{1/2} L^4 T$$

$$= \frac{1}{L^2}\frac{F}{L^{3/2}}\frac{L^{1/2}}{T} L^4 T = F \quad \text{CHECKS}$$

CONCLUSION: FOR MINIMUM WEIGHT, THE MATERIAL PARAMETER

$$\left(\frac{\rho}{\sigma_{max}}\right)^2 (\rho E)^{1/2}$$

OR

$$\frac{(\rho E)^{1/2}}{(\text{SPECIFIC STRENGTH})^2}$$

IS IMPORTANT.

FOR GLASSES, σ_{max} = YIELD STRESS, FOR METALS, σ_{max} = MICRO-YIELD STRESS. COMPARING SOME MATERIALS OF INTEREST FOR SIRTF:

MATL	$\frac{\rho}{lb/in^3 \times 10^2}$	$\frac{E}{GPa}$	$\frac{\sigma_{max}}{MPa}$	$\left(\frac{\sigma_{max}}{E}\right)^2 \left(\frac{E}{\rho}\right)$ in^2/sec^2
1. AL 6061-T6	3.7	69	65	22.3 $\times 10^{-3}$
2. Be I-70	.30	304	217	280.9 $\times 10^{-3}$
3. INVAR 36	3.02	145	69	62.1 $\times 10^{-3}$
4. GLASS SXA	2.91	117	117	11.4 $\times 10^{-3}$ (LIGHTEST)
5. PYREX 7740	2.23	65.5	7	1.20 (HEAVIEST)
6. FUSED SILICA ULE	2.20	67.7	10	5 90.7 $\times 10^{-3}$
7. FUSED SILICA 7940	2.20	73.2	10	614.2 $\times 10^{-3}$
8. ZERODUR	2.53	91	10	7 71.2 $\times 10^{-3}$
9. SILICON	2.33	131	34	82.0 $\times 10^{-3}$

CONCLUSIONS: IN THE METALS, SXA IS BEST, ALUMINUM NEXT BEST, Be IS ~ 25 TIMES WORSE THAN SXA, 12 TIMES WORSE THAN ALUMINUM.

IN THE GLASSES (EXCLUDING SILICON), ULE IS BEST, FOLLOWED CLOSELY BY 7940. PYREX IS TWICE AS BAD AS 7940.

STRUCTURED MIRROR

THE AREAL DENSITY OF A SANDWICH MIRROR IS GIVEN BY:

$$\rho_0 = \rho\,(2t_f + \eta h_c)$$

WHERE: t_f = FACE SHEET THICKNESS
η = RIB SOLIDITY RATIO
h_c = CORE HEIGHT

SUBSTITUTING EQ (17) INTO EQ (1)

$$M_r = \frac{(3+\nu)}{16}\,\rho\, r_0^2\,(2t_f + \eta h_c)$$

THE BENDING STRESS IN THE FACE-SHEET IS GIVEN BY:

$$\sigma = \frac{M_r}{t_f\, h} \qquad (16)$$

SUBSTITUTING EQ (15) INTO EQ (16)

$$\sigma = \frac{(3+\nu)}{16}\,\frac{\rho\, r_0^2}{t_f\, h}\,(2t_f + \eta h_c) \qquad (17)$$

THE FUNDAMENTAL FREQUENCY OF A SANDWICH PLATE IS GIVEN BY:

$$f_n = \frac{\lambda_{11}^2}{2\pi r_0^2}\left[\frac{g\,D}{\rho_0}\right]^{1/2} \qquad (18)$$

WHERE: D = FLEXURAL RIGIDITY OF THE SANDWICH PLATE

SANDWICH PLATE FLEXURAL RIGIDITY IS GIVEN BY:

$$D = \frac{E}{12(1-\nu^2)}\left[(2t_f + h_c)^3 - \left(1 - \frac{\eta}{2}\right)h_c^3\right] \qquad (19)$$

SUBSTITUTING EQ (14) & (19) INTO EQ (5),

$$\sigma_r = \frac{\lambda_{11}^2}{2\pi r_0^2}\left\{\frac{gE\left[(2t_f+h_c)^2-(1-\frac{\eta}{2})h_c^2\right]}{12(1-\nu^2)(2t_f+\eta h_c)}\right\}^2$$

NOTING THAT $2t_f+h_c = h$, EQ (20) BECOMES

$$\sigma_r = \frac{\lambda_{11}^2}{2\pi r_0^2}\left\{\frac{gE}{12(1-\nu^2)\rho}\left[\frac{h^2-(1-\frac{\eta}{2})h_c^3}{2t_f-\eta h_c}\right]\right\}^{1/2} \quad (21)$$

SUBSTITUTING EQ (6) INTO EQ (17);

$$\sigma = \frac{3(3+\nu)}{16[12(1-\nu^2)]^{1/4}}\frac{\rho r_0^2}{t_f h}(2t_f+\eta h_c)\left[\frac{\pi}{2}\lambda_{11}(PSD)Q\right]^{1/2}$$

SUBSTITUTING EQ (21) INTO EQ (22)

$$\sigma = \frac{3(3+\nu)\lambda_{11}}{32[12(1-\nu^2)]^{1/4}}\frac{\rho r_0}{t_f h}(2t_f+\eta h_c)(PSD)^{1/2}Q^{1/2} \times\left\{\frac{gE}{\rho}\left(\frac{h^3-(1-\frac{\eta}{2})h_c^3}{2t_f+\eta h_c}\right)\right\}^{1/4} \quad (23)$$

NOW $2t_f+\eta h_c = 2t_f+h_c-(1-\eta)h_c$

SINCE $2t_f+h_c = h$, $2t_f+\eta h_c = h-(1-\eta)h_c$

SUBSTITUTING

$$\sigma = \frac{3(3+\nu)\lambda_{11}}{32[12(1-\nu^2)]^{1/4}}\frac{\rho r_0}{t_f h}\left[h-(1-\eta)h_c\right]PSD^{1/2}Q^{1/2} \times\left\{\frac{gE}{\rho}\left[\frac{h^3-(1-\frac{\eta}{2})h_c^3}{h-(1-\eta)h_c}\right]\right\}^{1/4} \quad (24)$$

NOW $h_c = h - 2t_F$

LET $t_F = Kh$, THEN $h_c = h - 2Kh = h(1-2K)$

SUBSTITUTING:

$$\sigma = \frac{9(3+\nu)\lambda_{11}}{32[12(1-\nu^2)]^{1/4}} \frac{r_0}{Kh^2}\left[h-(1-\eta)h(1-2K)\right](PSD)^{1/2}Q^{1/2} \times \left\{\frac{gE}{\rho}\left[\frac{h^3-(1-\frac{\eta}{2})h^3(1-2K)^3}{h-(1-\eta)h(1-2K)}\right]\right\}^{1/4}$$

$$= \frac{9(3+\nu)\lambda_{11}}{32[12(1-\nu^2)]^{1/4}}\rho^{3/4}E^{1/4}\frac{r_0}{h^{1/2}}(PSD)^{1/2}Q^{1/2}g^{1/4} \times \frac{1}{K}\left[1-(1-\eta)(1-2K)\right]\left[\frac{1-(1-\frac{\eta}{2})(1-2K)^3}{1-(1-\eta)(1-2K)}\right]^{1/4}$$

$$= \frac{9(3+\nu)\lambda_{11}}{32(12(1-\nu^2))^{1/4}}\rho^{3/4}E^{1/4}\frac{r_0}{h^{1/2}}(PSD)^{1/2}Q^{1/2}g^{1/4} \times \frac{1}{K}\left[1-(1-\eta)(1-2K)\right]^{3/4}\left[1-(1-\frac{\eta}{2})(1-2K)^3\right]^{1/4} \quad (25)$$

EQ (25) IS SIMILAR TO EQ (9), BUT WITH A CORRECTION FOR THE MIRROR STRUCTURE.

THE MIRROR WEIGHT IS GIVEN BY:

$$W = 2\pi r_0^2 \rho\,(2t_F + \eta h_c) \quad (26)$$

OR

$$W = 2\pi\rho\, r_0^2 h\left[1-(1-\eta)(1-2K)\right]. \quad (27)$$

EIRT DYNAMIC RESPONSE 14 NOV 89 DAN VUKOBRATOVICH

SOLVING EQ (25) FOR h:

$$h = \frac{81}{1024}\frac{(3+\nu)^2\lambda_{11}^2}{[12(1-\nu^2)]^2}\rho^{2/2}\frac{E^{1/2}}{\sigma^2}\eta_0^2(PSD)\lambda_0^{1/2}$$

$$\times \frac{1}{k^2}\left[1-(1-\eta_2)(1-2\zeta)\right]^{2/2}\left[1-(1-\frac{\eta}{2})(1-2\zeta)\right]^{-1/2}$$

SUBSTITUTING EQ (23) INTO EQ (24)

$$W = \frac{1024}{1024}\frac{(3+\nu)^2\lambda_{11}^2}{[12(1-\nu^2)]^{1/2}}\rho^{5/2}\frac{E^{1/2}}{6^2}\eta_0^4(PSD)\lambda_0^{1/2}$$

$$\times \frac{1}{k^2}\left[1-(1-\eta_2)(1-2\zeta)\right]^{5/2}\left[1-(1-\eta/2)(1-2\zeta)\right]^{-1/2}$$

$$= \frac{162\pi}{1024}\frac{(3+\nu)^2\lambda_{11}}{[12(1-\nu^2)]^{1/2}}\left(\frac{\rho}{6}\right)^2(\rho E)^{1/2}\eta_0^4(PSD)\lambda_0^{1/2}$$

$$\times \frac{1}{k^2}\left[1-(1-\eta_2)(1-2k)\right]^{5/2}\left[1-(1-\frac{\eta}{2})(1-2\zeta)\right]^{-1/2}$$

CONCLUSIONS: FOR A SANDWICH MIRROR, THE MATERIAL PARAMETER

$$\frac{(\rho E)^{1/2}}{(\text{SPECIFIC STRENGTH})^2}$$

IS CRITICAL

REFERENCES

1.) BLEVINS R. D., FORMULAS FOR NATURAL FREQUENCY & MODE SHAPE, VAN NOSTRAND REINHOLD CO, NEW YORK, N.Y., 1979.

2.) ROARK, R.C. & YOUNG, W.C., FORMULAS FOR STRESS & STRAIN, 5TH ED., MCGRAW-HILL, ETC.

3.) THE BASICS OF BONDED SANDWICH CONSTRUCTION, TSD 24, HEXCEL, DUBLIN, CA, 1984.

4.) VALENTE, T. M. & VUKOBRATOVICH D, "A COMPARISON OF THE MERITS OF OPEN-BACK, SYMMETRIC SANDWICH, AND CONTOURED BACK MIRRORS AS LIGHT-WEIGHTED OPTICS," PROC. SPIE 1167 (1989).

Appendix 3. Derivation of mount local stress equations.

SIRTF MOUNT DYNAMICS — 14 NOV 99 — DAD — DECORATION

FOR A CIRCULAR MIRROR, AND A 3 POINT SEMI-KINEMATIC MIRROR MOUNT, THE MINIMUM EFFECTIVE CONTACT AREA IS THREE CIRCLES:

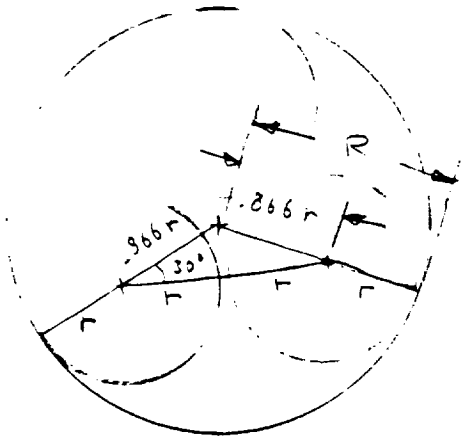

$$r + r = R$$

$$r = \frac{R}{.966}$$

$$r \simeq 0.536\,R$$

$$A = 3\pi r^2$$

$$A \simeq 2.707\,R^2$$

THIS REPRESENTS AN UPPER LIMIT.

THE STRESS IN THE CONTACT IS:

$$\sigma = \frac{W\, g_{max}}{A_c} \qquad (1)$$

WHERE: W = MIRROR WEIGHT
g_{max} = MAXIMUM ACCELERATION
A_c = CONTACT AREA
σ = STRESS IN CONTACT AREA

THE "3 - SIGMA" ACCELERATION IS:

$$g_{max} = 3\left[\frac{\pi}{2} f_n Q\,(PSD)\right]^{1/2} \qquad (2)$$

WHERE: f_n = MOUNT NATURAL FREQUENCY
Q = TRANSMISSARILITY AT RESONANCE
PSD = POWER SPECTRAL DENSITY AT f_n

TO AVOID COUPLED OSCILLATION, F_n FOR THE MOUNT SHOULD BE 0.6 OF F_n FOR THE MIRROR. THE MIRROR MODAL FREQUENCY IS APPROXIMATELY

$$F_{n\ MIR} = \frac{1}{2\pi}\left(\frac{g}{\delta}\right)^{1/2} \qquad (2)$$

WHERE g = ACCELERATION DUE TO EARTH'S GRAVITY

δ = MIRROR SELF-WEIGHT DEFLECTION

USING EQ (2) IN EQ (1):

$$g_{max} = \frac{3}{2}\left[\frac{1}{2}\left(\frac{g}{\delta}\right)^{1/2} Q\ (PSD)\right]^{1/2} \qquad (4)$$

SUBSTITUTING EQ (4) INTO EQ (1)

$$\sigma = \frac{3}{2}\frac{W}{A_c}\left[\frac{1}{2}\left(\frac{g}{\delta}\right)^{1/2} Q\ (PSD)\right]^{1/2} \qquad (5)$$

SOLVING FOR A_c

$$A_c = \frac{3}{2}\frac{W}{\sigma}\left[\frac{1}{2}\left(\frac{g}{\delta}\right)^{1/2} Q\ (PSD)\right]^{1/2} \qquad (6)$$

EXAMPLE:

W = 300 LBS
σ = 500 PSI
g = 386 IN/SEC^2
δ = 1 MIN
Q = 100
PSD = 0.02 g^2/hz

$$A_c = \frac{3}{2}\frac{300}{500}\left[\frac{1}{2}\left(\frac{386}{10^{-6}}\right)^{1/2}(100)(.02)\right]^{1/2}$$

$$= 126.15\ IN^2$$

AN ALTERNATE APPROACH: FOR A SINGLE DEGREE OF FREEDOM (SDOF) SYSTEM THE FUNDAMENTAL FREQUENCY IS GIVEN BY:

$$f_n = \frac{1}{2\pi}\left(\frac{K}{W}\right)^{1/2} \quad (8)$$

WHERE: K = MOUNT STIFFNESS

USING THE OCTAVE RULE, AND SOLVING FOR:

$$\frac{1}{4}\left(\frac{K}{W}\right) = \frac{1}{2\pi}\left(\frac{2}{\delta}\right)^{1/2} \quad (9)$$

$$\frac{1}{4}\,\frac{K}{W} = \frac{2}{\delta} \quad (10)$$

SOLVING FOR K:

$$K = \frac{4W}{\delta} \quad (10)$$

THIS IS THE <u>HIGHEST</u> ACCEPTABLE MOUNT STIFFNESS.

MOUNT STRUCTURE

1) FLAT CONTACT AREA
2.) CONICAL CONTACT
3.) SPHERICAL CONTACT
4.) CYLINDRICAL CONTACT

1.) FOR A FLAT CONTACT AREA:

$$\sigma = \frac{F}{A} = \frac{F}{\pi r^2}$$

WHERE F IS THE APPLIED FORCE

2.) FOR A CONICAL CONTACT

$$\sigma = \frac{2F_A \cos\theta}{(D+d)\pi L(\mu\cos\theta+\sin\theta)} + \frac{4F_T}{\pi L d} \quad (2)$$

WHERE: F_A = AXIAL FORCE
F_T = TANGENTIAL FORCE
D = MAXIMUM CONICAL DIAMETER
d = MINIMUM CONICAL DIAMETER
L = CONICAL LENGTH
μ = FRICTION COEFFICENT
θ = CONE ANGLE (MEASURED TO AXIS)

3) SPHERICAL CONTACT

$$\sigma = \frac{F}{\frac{\pi R^2}{2} + \frac{R^2}{2}\sin(2\phi) + R^2(\phi)} \quad (3)$$

WHERE: R = SPHERICAL RADIUS
ϕ = SPHERICAL SECTOR ANGLE

4) CYLINDRICAL CONTACT

$$\sigma = \frac{2F}{\pi r L} \quad (4)$$

WHERE: r = CYLINDRICAL RADIUS
L = LENGTH OF CYLINDER

EDGE MOUNTS

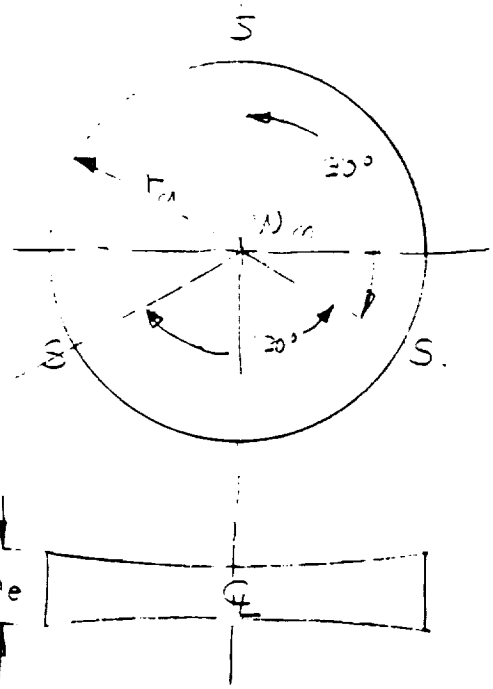

1) EDGE PADS

IF THE MIRROR IS CONSTRAINED RADIALLY BY 3 FLAT EDGE PADS OF DIAMETER D THE STRESS IN THE PADS IS GIVEN BY:

$$\sigma = \frac{12 W_m}{\pi D^2} \left[\frac{\pi}{2} f_n Q (PSD) \right]^{1/2} \qquad (15)$$

SOLVING FOR D

$$D = \left\{ \frac{12 W_m}{\pi \sigma} \left[\frac{\pi}{2} f_n Q (PSD)_{\cdot} \right]^{-1/2} \right\}^{1/2} \qquad (16)$$

LET S = 500
D = 100
PSD = 0.02

F_n	100	200	300	400	500
10	[illegible]	[illegible]	2.33	[illegible]	[illegible]
50	[illegible]	[illegible]	5.30	[illegible]	[illegible]
100	[illegible]	[illegible]	[illegible]	[illegible]	[illegible]
200	[illegible]	[illegible]	[illegible]	[illegible]	[illegible]
300	[illegible]	[illegible]	[illegible]	[illegible]	[illegible]
500	[illegible]	[illegible]	[illegible]	[illegible]	[illegible]
700	[illegible]	[illegible]	[illegible]	[illegible]	[illegible]
1000	[illegible]	[illegible]	[illegible]	[illegible]	[illegible]
1200	[illegible]	[illegible]	[illegible]	[illegible]	[illegible]
1500	[illegible]	[illegible]	[illegible]	4.48	[illegible]

LET D = 2.5
G = 100
PSD = 0.02

F_n	100	200	300	400	500
10	195	350	524	699	874
50	391	782	1172	1563	1954
100	553	1105	1658	2211	2763
200	782	1563	2345	3126	3905
300	957	1915	2872	3829	4786
500	1236	2472	3707	4943	6179
700	1462	2924	4387	5849	7311
1000	1748	3495	5243	6991	8739
1200	1915	3829	5744	7658	9573
1500	2140	4281	6422	8562	10703

LET D = 4.5"

F_n	100	200	300	400	500
10	106	211	317	423	529
50	236	473	709	946	1182
100	334	669	1003	1337	1672
200	473	946	1418	1891	2364
300	579	1158	1737	2316	2895
500	746	1495	2243	2990	3738
700	835	1769	2654	3538	4423
1000	1057	2115	3172	4229	5286
1200	1158	2316	3475	4633	5791
1500	1295	2590	3885	5179	6474

2) EDGE CONE

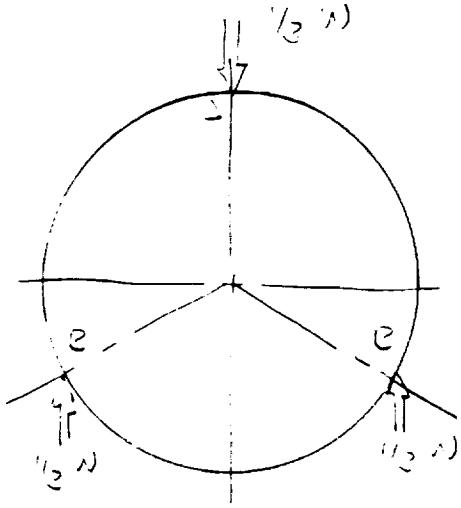

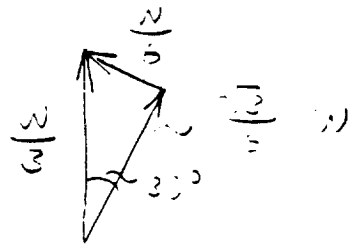

THE STRESS IN CONE A IS:

$$\sigma = \frac{2}{3} W \frac{\cos\theta}{(D-d)\pi L (N\cos\theta + \sin\theta)} \quad (9)$$

THE STRESS IN CONE B IS

$$\sigma = W \left[\frac{1}{6\pi} \frac{1}{(D-d)} \frac{\cos\theta}{(N\cos\theta - \sin\theta)} + \frac{2\sqrt{3}}{3\pi} \frac{1}{Ld} \right] \quad (11)$$

NOTING THAT:

$$d = D - 2L\tan\theta \quad (10)$$

SUBSTITUTING INTO EQ (9)

$$\sigma = \frac{1}{3\pi} W \frac{\cos\theta}{(N\cos\theta + \sin\theta)} \frac{1}{(D - L\tan\theta)L} \quad (20)$$

SUBSTITUTING INTO EQ (11)

$$\sigma = \frac{W}{3\pi} \left[\frac{1}{4} \frac{\cos\theta}{(N\cos\theta + \sin\theta)} \frac{1}{(D - L\tan\theta)L} + 2\sqrt{3} \frac{1}{(D-2L\tan\theta)L} \right] \quad (12)$$

SIRE MOUNT DYNAMICS 14 NOV 89 DAN VUKOBRATOVICH

DYNAMICS EFFECTS INCREASE W/ [illegible] ESTIMATION [illegible] EQ (20)

$$G = \frac{1}{2} W_{max} \frac{2\cos\theta}{(4\cos\theta - \sin\theta)} \frac{1}{(1 - L\tan\theta)}$$

$$= \frac{1}{2} \frac{W}{L} \frac{2\cos\theta}{(4\cos\theta - \sin\theta)} \frac{1}{(1 - L\tan\theta)} \left[\frac{\pi}{2} f_n Q\,(PSD)\right]^{1/2}$$

SIMILARLY, FOR EQ (21)

$$G = \frac{1}{2} \frac{W}{L} \left\{ \frac{1}{2} \frac{2\cos\theta}{(4\cos\theta + \sin\theta)} \frac{1}{(1 - L\tan\theta)} + \frac{2\cos\theta}{(1 - 2L\tan\theta)} \right\} \times \left[\frac{\pi}{2} f_n Q\,(PSD)\right]^{1/2}$$

LET; $Q = 100$
$PSD = 0.02\ g_n^2/Hz$
$D = 3.0$
$W = 1.0$

ORIGINAL PAGE IS OF POOR QUALITY

$\theta = 15°$, $L = 0.5"$, $D = 3.0"$

F	100	200	300	400	500
10	477	954	1431	1908	2385
20	675	1349	2024	2698	3372
50	1067	2133	3200	4266	5333
100	1508	3017	4525	6033	7542
200	2133	4266	6399	8533	10666
300	3373	6746	10118	13491	16864
500	4770	9540	14310	19079	23849
1000	6745	13490	20235	26980	33725
1500	8262	16524	24786	33048	41310

$\theta = 15°$, $L = 1.0$, $D = 3.0"$

F	100	200	300	400	500
10	264	527	791	1055	1318
20	373	746	1119	1492	1865
50	590	1179	1769	2359	2948
100	834	1668	2502	3335	4169
200	1179	2359	3538	4717	5896
500	1865	3729	5594	7458	9323
1000	2637	5274	7911	10546	13185
1500	2989	5977	8966	11954	14943
2000	3230	6459	9689	12918	16148

SIRTF MOUNT DYNAMICS   14 NOV 89   DAN VUKOBRATOVICH

$\theta = 15°$, $L = 1.5''$, $D = 3.0'$

F	100	200	300	400	500
10	197	292	590	737	932
20	273	336	[illegible]	[illegible]	[illegible]
50	440	979	1319	1759	[illegible]
100	622	[illegible]	[illegible]	2437	[illegible]
200	[illegible]	[illegible]	2623	[illegible]	[illegible]
500	1290	[illegible]	[illegible]	5562	[illegible]
1000	[illegible]	[illegible]	5399	[illegible]	[illegible]
1200	[illegible]	4303	6462	9616	[illegible]
1500	[illegible]	4817	7225	[illegible]	[illegible]

$\theta = 15°$, $L = 2.0''$, $D = 3.0$

F	100	200	300	400	500
10	167	335	502	670	837
20	237	473	710	947	1184
50	374	749	1123	1497	1872
100	529	1059	1589	2117	2647
200	749	1497	2246	2995	3742
500	1184	2367	3551	4735	5919
1000	1674	3349	5022	6696	8370
1200	1834	3668	5501	7335	9169
1500	2050	4100	6151	8201	10251

NOW THE MIRROR WILL EXPERIENCE AXIAL LOADS AS WELL. THE MAXIMUM STRESS IS GIVEN BY (GERE) [illegible]

$$\sigma = \frac{W}{\pi} \left\{ \frac{1}{4} g_R \frac{\cos\theta}{(N\cos\theta + \sin\theta)} \frac{1}{(D - L\tan\theta)} + \left[\left(12 + \frac{\kappa^2}{9}\right) g_R^2 \frac{1}{(D - 2L\tan\theta)^2} \right]^{1/2} \right\}$$

IF $g_A = \kappa g_R$, THEN

$$\sigma = \frac{W}{\pi} N G \frac{1}{L} \left\{ \frac{1}{4} \frac{\cos\theta}{(N\cos\theta + \sin\theta)} \frac{1}{(D - L\tan\theta)} + \left(12 + \frac{\kappa^2}{9}\right)^{1/2} \frac{1}{(D - 2L\tan\theta)} \right\} \quad (25$$

NOTING THAT

$$f(N, \theta, L, D, \kappa) = \frac{1}{L} \left[\frac{1}{4} \frac{\cos\theta}{(N\cos\theta + \sin\theta)} \frac{1}{(D - L\tan\theta)} + \left(12 + \frac{\kappa^2}{9}\right)^{1/2} \frac{1}{(D - 2L\tan\theta)} \right] \quad (25.$$

$$g_R = 3 \left[\frac{\pi}{2} f_R Q (PSD) \right]^{1/2} \quad (2$$

THEN EQ (25) IS:

$$\sigma = \frac{1}{\pi} W \left[\frac{\pi}{2} f_R Q (PSD) \right]^{1/2} f(N, \theta, L, D, \kappa) \quad (2$$

A GEOMETRIC CONCERN

$$D - 2L \tan\theta > 0$$

SO

$$\arctan\left(\frac{D}{2L}\right) = \theta$$

IF $D = 3$

θ	L
71.565°	.5
56.30	1.0
36.870	2.0
26.565	3.0
20.556	4.0
16.699	5.0

$\theta =$ [illegible] 30, 35, 45, 60

SIRTF MOUNT DYNAMICS — 22 NOV 87 — DAN VUKOBRATOVICH

2) REVISED EDGE CONEC

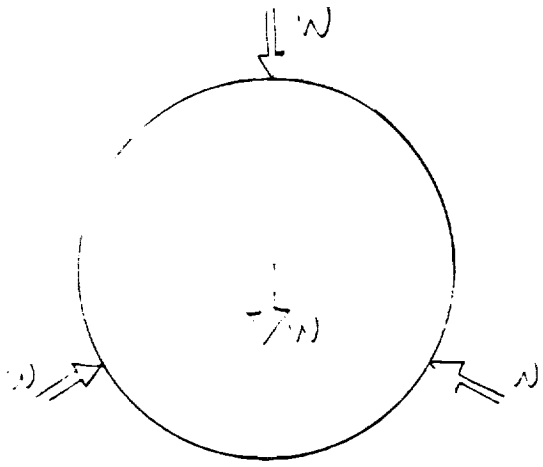

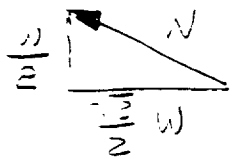

IF THE AXIAL LOADS ARE INCLUDED, THE STRESS BECOMES

$$\sigma = \frac{2 F_R \cos\theta}{(D-d)\pi L (\mu\cos\theta + \sin\theta)} + \frac{4 F_A}{3\pi L d} \qquad (31)$$

LET $d = D - 2L\tan\theta$; SUBSTITUTING

$$\sigma = \frac{2 F_R \cos\theta}{(D + D - 2L\tan\theta)\pi L (\mu\cos\theta + \sin\theta)} + \frac{4 F_A}{3\pi L (D - 2L\tan\theta)}$$

$$= \frac{1}{\pi}\frac{1}{L}\left[\frac{F_R \cos\theta}{(D - L\tan\theta)(\mu\cos\theta + \sin\theta)} + \frac{4}{3}\frac{F_A}{(D - 2L\tan\theta)}\right] \qquad (32)$$

NOW:

$$F_R = W g_R = 3\left[\frac{\pi}{2} f_R Q (PSD)\right]^{1/2}$$

$$= 3 W f_R^{1/2}\left[\frac{\pi}{2} Q (PSD)\right]^{1/2} \qquad (32)$$

$$F_A = W g_A = 3\left[\frac{\pi}{2} f_A Q (PSD)\right]^{1/2}$$

$$= 3 W f_A^{1/2}\left[\frac{\pi}{2} Q (PSD)\right]^{1/2} \qquad (33)$$

LET $F_\Delta = \zeta F_R$, THEN EQ 22 BECOMES

$$F_\Delta = 2W \zeta^{1/2} f_{12}^{1/2} \left[\frac{\pi}{2} Q(PSD) \right]^2 \qquad (24)$$

SUBSTITUTING EQ 23 INTO EQ 24:

$$\sigma = \frac{2}{\pi} W f_R^{1/2} \frac{1}{L} \left[\frac{\cos\theta}{(D - L\tan\theta)(M\cos\theta - L\sin\theta)} - \frac{4}{3} \frac{\zeta^{1/2}}{D - 2L\tan\theta} \right] \times \frac{\pi}{2} Q(PSD) \Big]^2 \qquad (25)$$

LET:

$$F(M, \theta, D, L, \zeta) = \frac{1}{L} \left[\frac{\cos\theta}{(D - L\tan\theta)(M\cos\theta + L\sin\theta)} + \frac{4}{3} \frac{\zeta^{1/2}}{(D - 2L\tan\theta)} \right] \qquad (26)$$

THEN EQ (25) BECOMES:

$$\sigma = \frac{2}{\pi} W f_R^{1/2} \left[\frac{\pi}{2} Q(PSD) \right]^{1/2} F(M, \theta, D, L, \zeta)$$

3. LIGHTWEIGHT MIRROR AND MOUNT DESIGNS

3.1. SINGLE ARCH MIRROR AND MOUNT STUDIES

Two lightweight mirror and mount studies were completed. The single arch design provided by George Sarver of NASA Ames is shown in Figure 3.1. This hub mounted design is athermalized by the hub geometry as shown in Figure 3.2 Two back contour shapes which optimize the weight to rms wavefront error for gravity loading in the zenith direction were used. A 150 pound mirror with an outer 1/2 inch edge thickness and a 187 pound mirror with an outer 1 inch edge thickness were modeled and analyzed. Both of these mirrors were supported at three points with a semi-kinematic mount comprising three circular pads on the mirror land. Two different pad diameters were used to demonstrate the effect of pad size on this semi-kinematic mount. A 60 degree pie finite element model of these mirrors is shown in Figure 3.3. Shown in Figures 3.4 and 3.5 are the optical performances of the 150 pound mirror for gravity load pointing zenith and horizon, respectively, and shown in Figure 3.6 is the effect of a 1-g clamping load. Shown in Figures 3.7 and 3.8 are the optical path differences for combinations of a 5-g preload and a 1-g selfweight load in the zenith and horizon directions, respectively. Summarized in Table 3.1 are the results for both the 187 pound and 150 pound mirrors with different sized supporting pads. The 5-g preload was used as typical to prevent the mirror from moving in its mount during normal transportation and handling environments. In all load cases the interface between the glass and the invar hub was assumed smooth with no friction forces acting between these elements. This, of course, is a modeling assumption that should be validated.

These results on the optical performances of a single arch design indicate the heavier 187 lb. design with the one inch edge thickness is significantly better than the lighter 150 lb. design with the 1/2 inch edge thickness for the self-weight zenith pointing position. However, the preload clamping effects on the optical performances is essentially the same for both mirrors. When these loadings, i.e. gravity and preload are combined, the optical performances are again essentially identical at about 0.50λ rms. Decreasing the sizes of the 3 point pad supports improved the surfaces to 0.37λ rms.

The Sarver design philosophy departs radically from the design constraints placed on the double arch design proposed by the University of Arizona. The latter design, which was neither caged or clamped, was preloaded to completely offset launch loads of approximately 50 g's along the optical axis and 42 g's normal to the optical axis. The critical damping coefficient used was 0.004 for the 6AL-TiV flexural system at cryogenic temperature. The Sarver design philosophy was to use a very low preload to allow the slippage of the mirror in its mount during the launch environment to increase the system damping and reduce the magnitude of the launch loads. A keyway in the hub is designed to keep the mirror from being decentered after the launch loads have ceased. From this study it is apparent that the preload for the Sarver design should not exceed about 2 g's to keep the wavefront error less that 0.25λ rms in the zenith pointing position.

No dynamic analyses were performed on these single arch designs. It is apparent that these studies along with full scale dynamic testing of the mirror in its mount are required to validate this design concept.

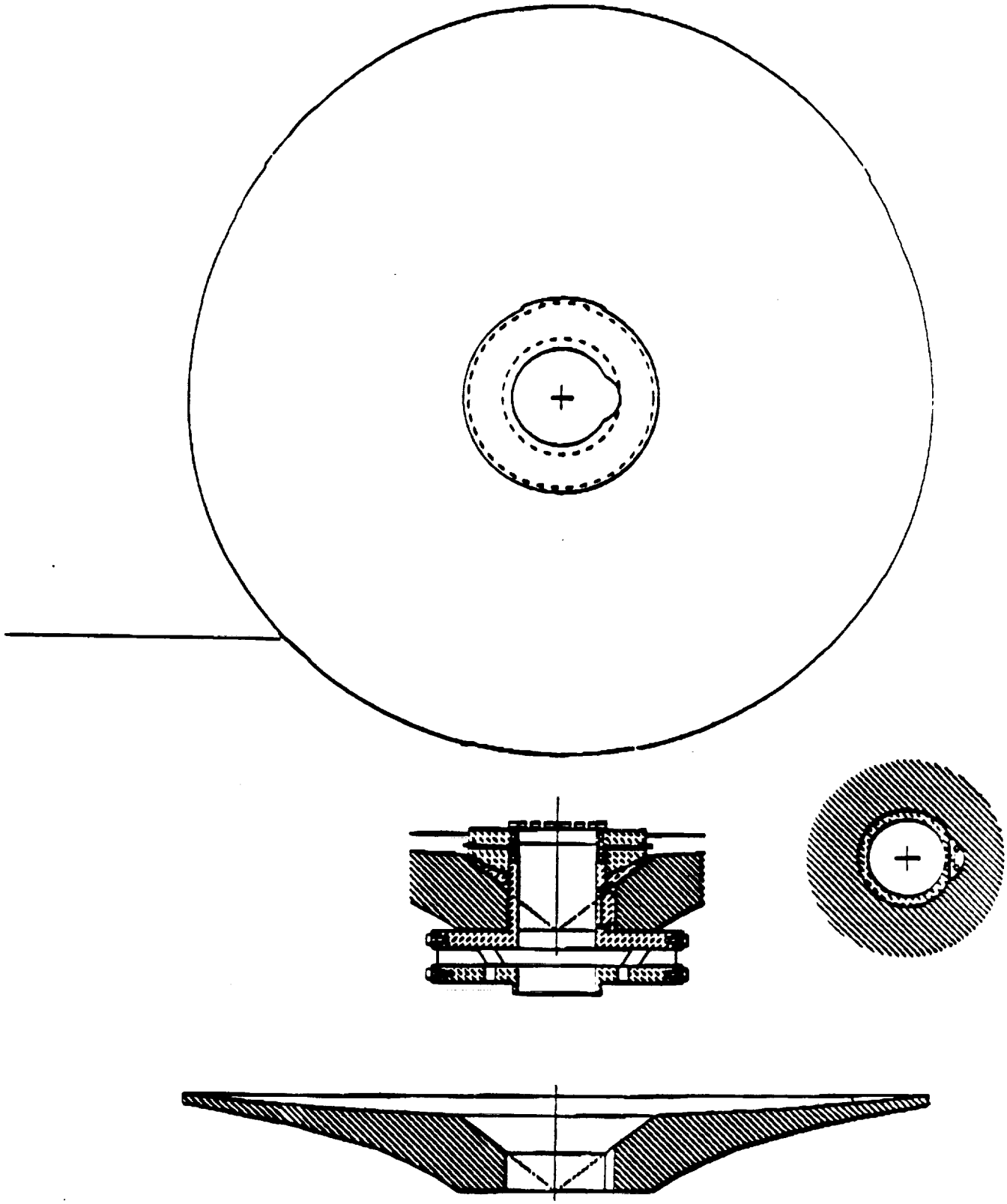

Figure 3.1. The NASA Ames Sarver Design

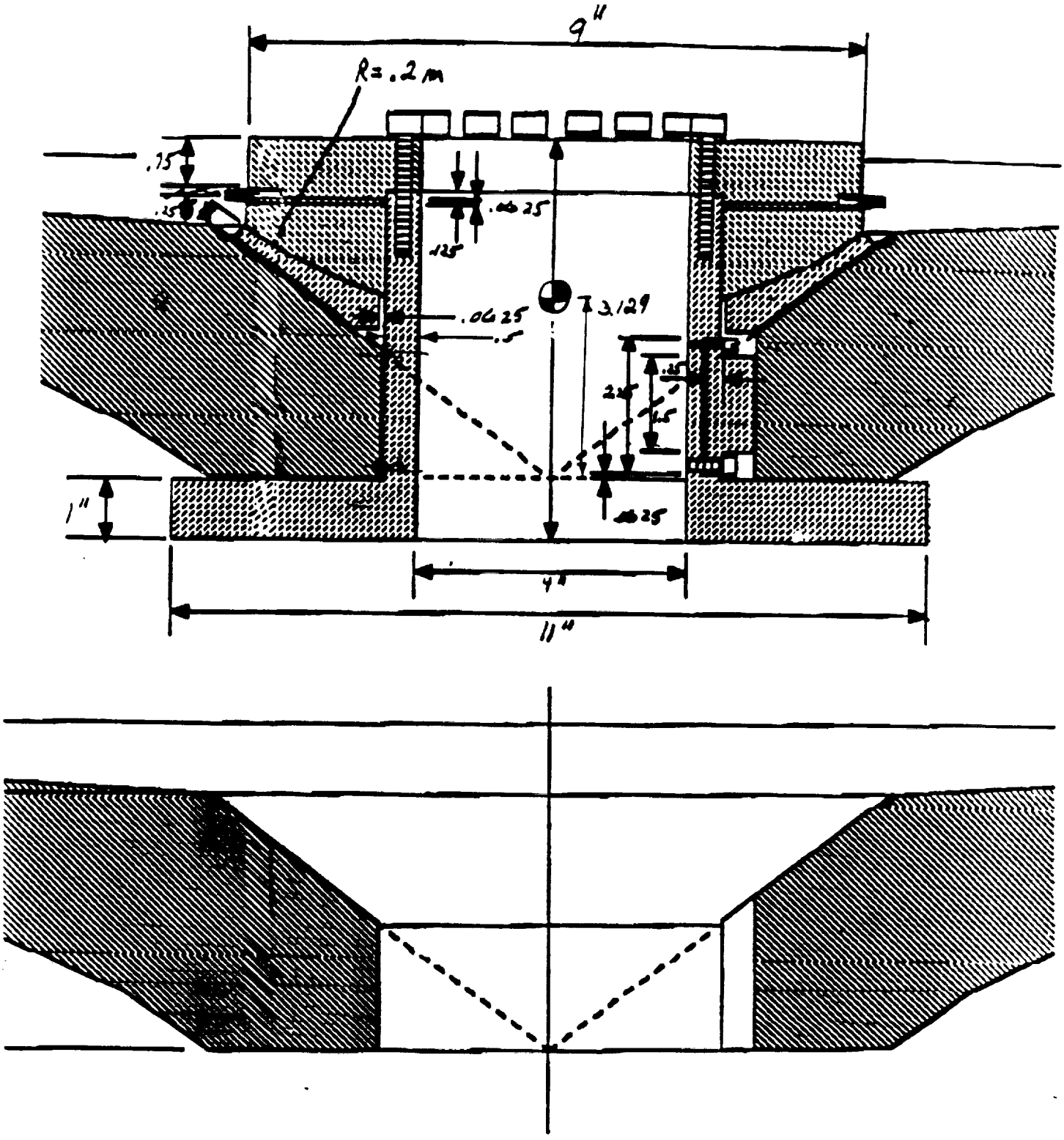

Figure 3.2. Hub Geometry

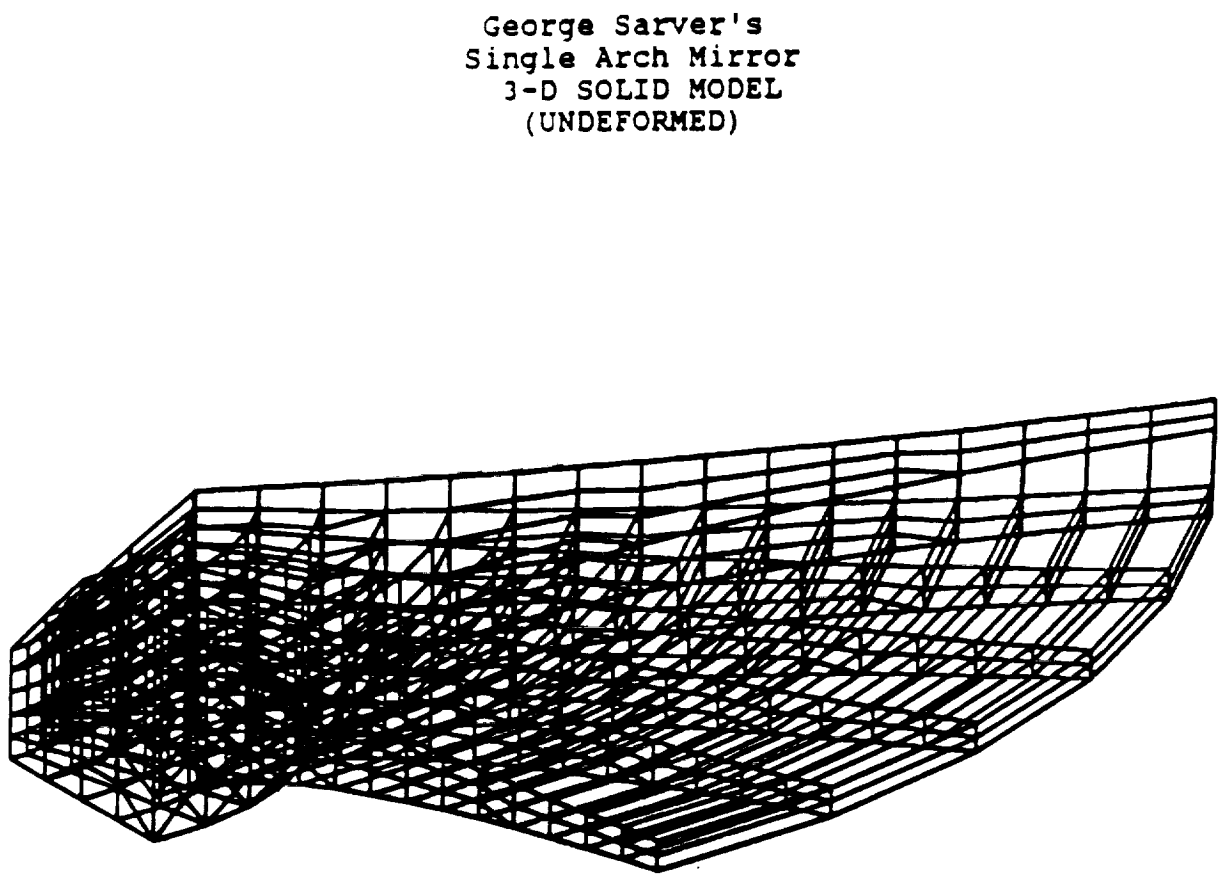

Figure 3.3. Sarver Design 60 degree pie finite element model undeformed

SIRTF SINGLE ARCH MIRROR

LOADING:

5G-PRELOAD +
1G_ZENITH

OPTICAL PERFORMANCE:
(tilt & focus removed)

RMS = .513 wave
P/V = 2.227 wave
SPOT RADIUS = 1.89 arcsec

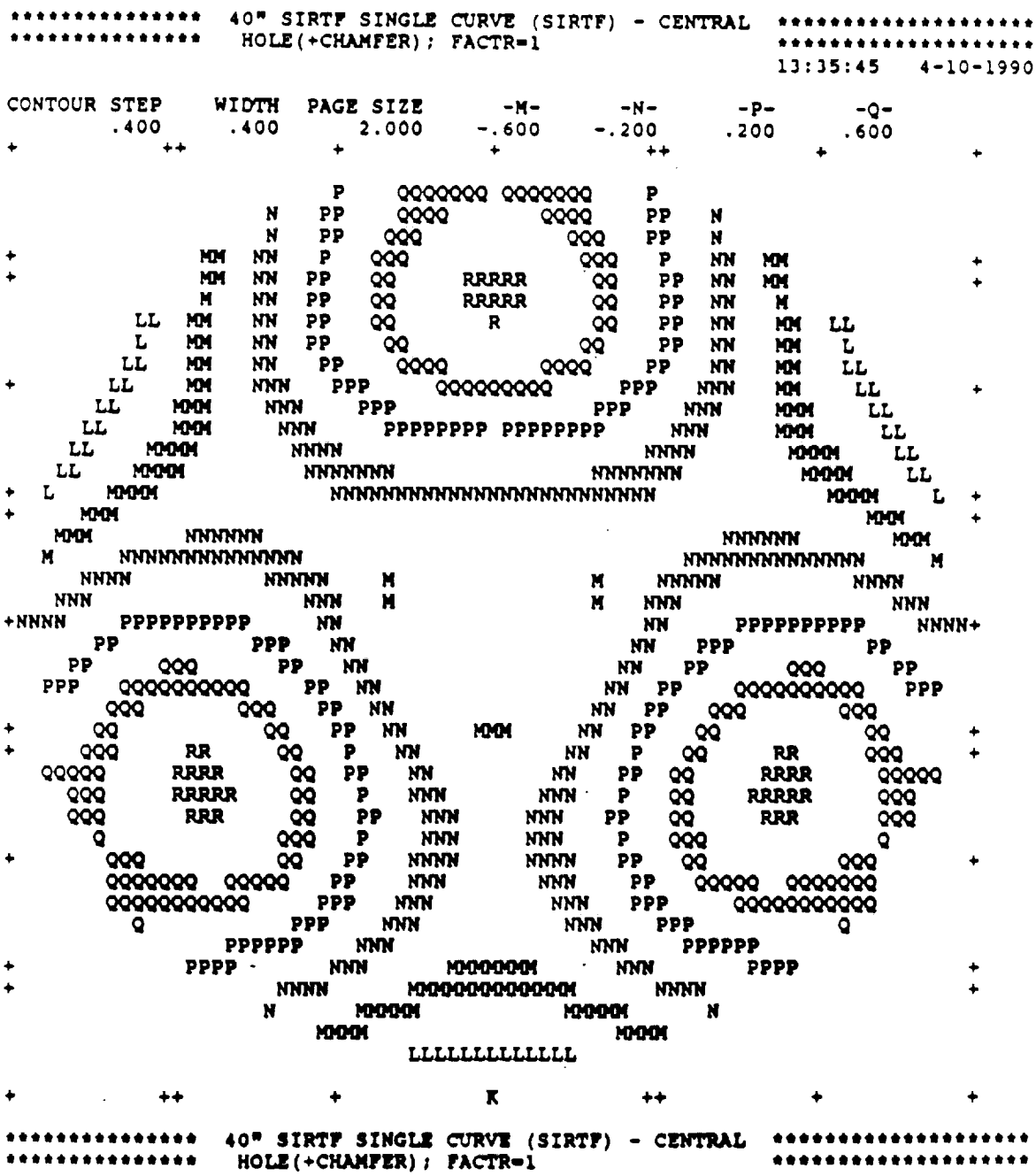

Figure 3.4. 150 lb mirror optical performances (zenith)

SIRTF SINGLE ARCH MIRROR

LOADING:

1G - HORIZON

OPTICAL PERFORMANCE:
(tilt & focus removed)

RMS = .345 wave

P/V = 1.686 wave

SPOT RADIUS = .72 arcsec

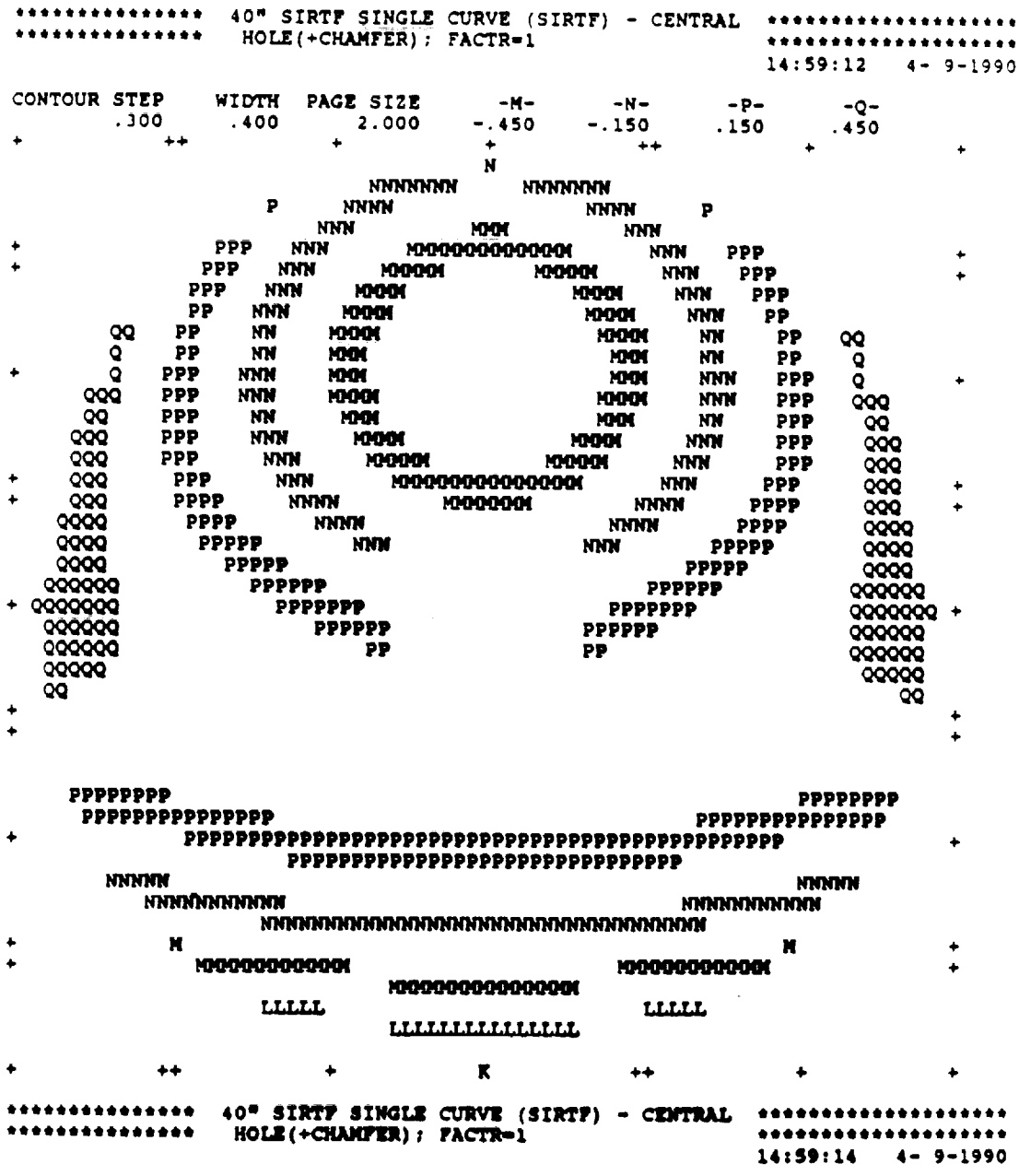

Figure 3.5. 150 lb mirror optical performances (horizon)

C-2

SIRTF SINGLE ARCH MIRROR

LOADING:

1G - PRELOAD

OPTICAL PERFORMANCE:
(tilt & focus removed)

RMS = .070 wave

P/V = .310 wave

SPOT RADIUS = .31 arcsec

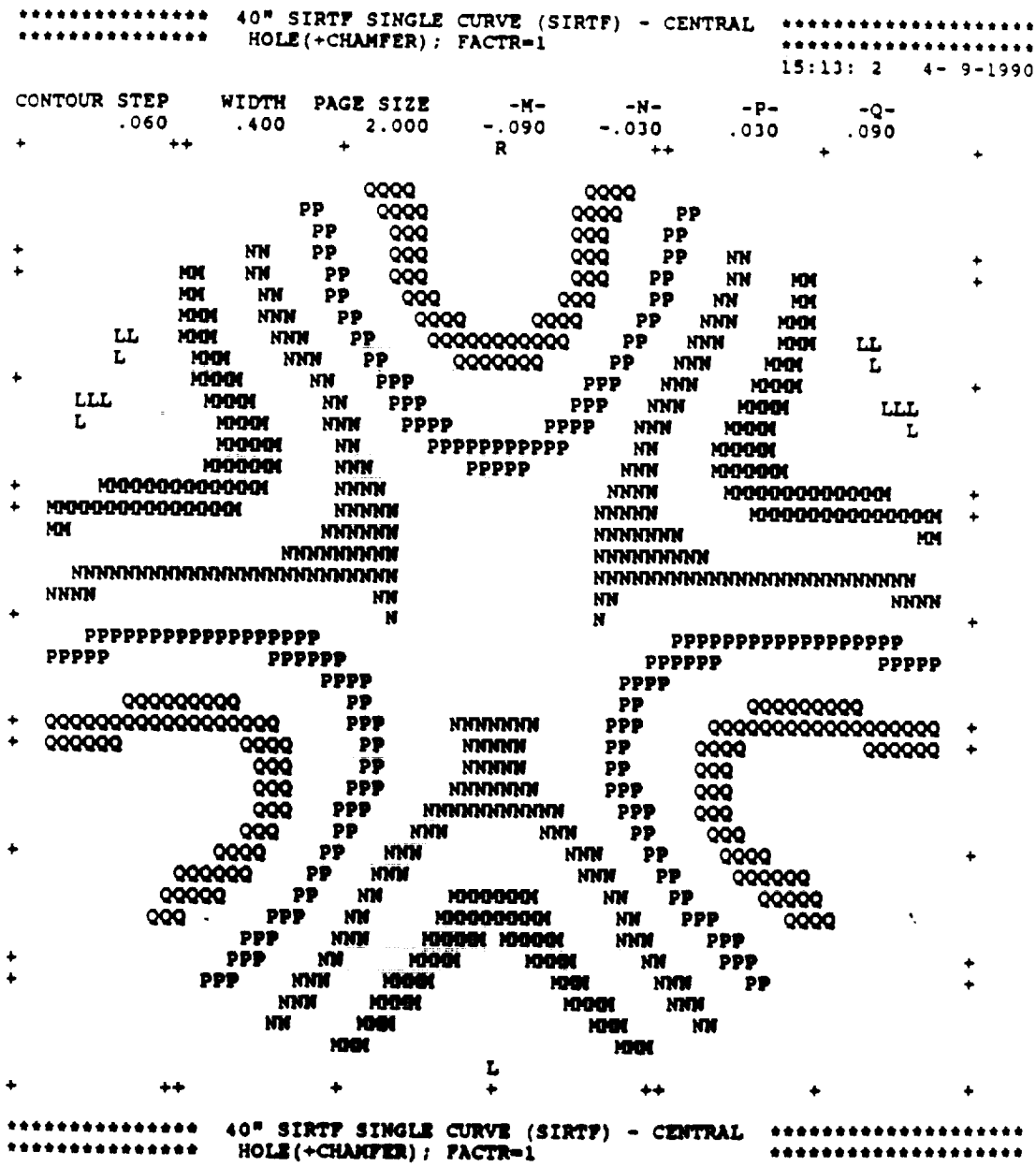

Figure 3.6. 150 lb mirror optical performance (1-g clamping load)

SIRTF SINGLE ARCH MIRROR

LOADING:

5G-PRELOAD +
1G_ZENITH

OPTICAL PERFORMANCE:
(tilt & focus removed)

RMS = .513 wave

P/V = 2.227 wave

SPOT RADIUS = 1.89 arcsec

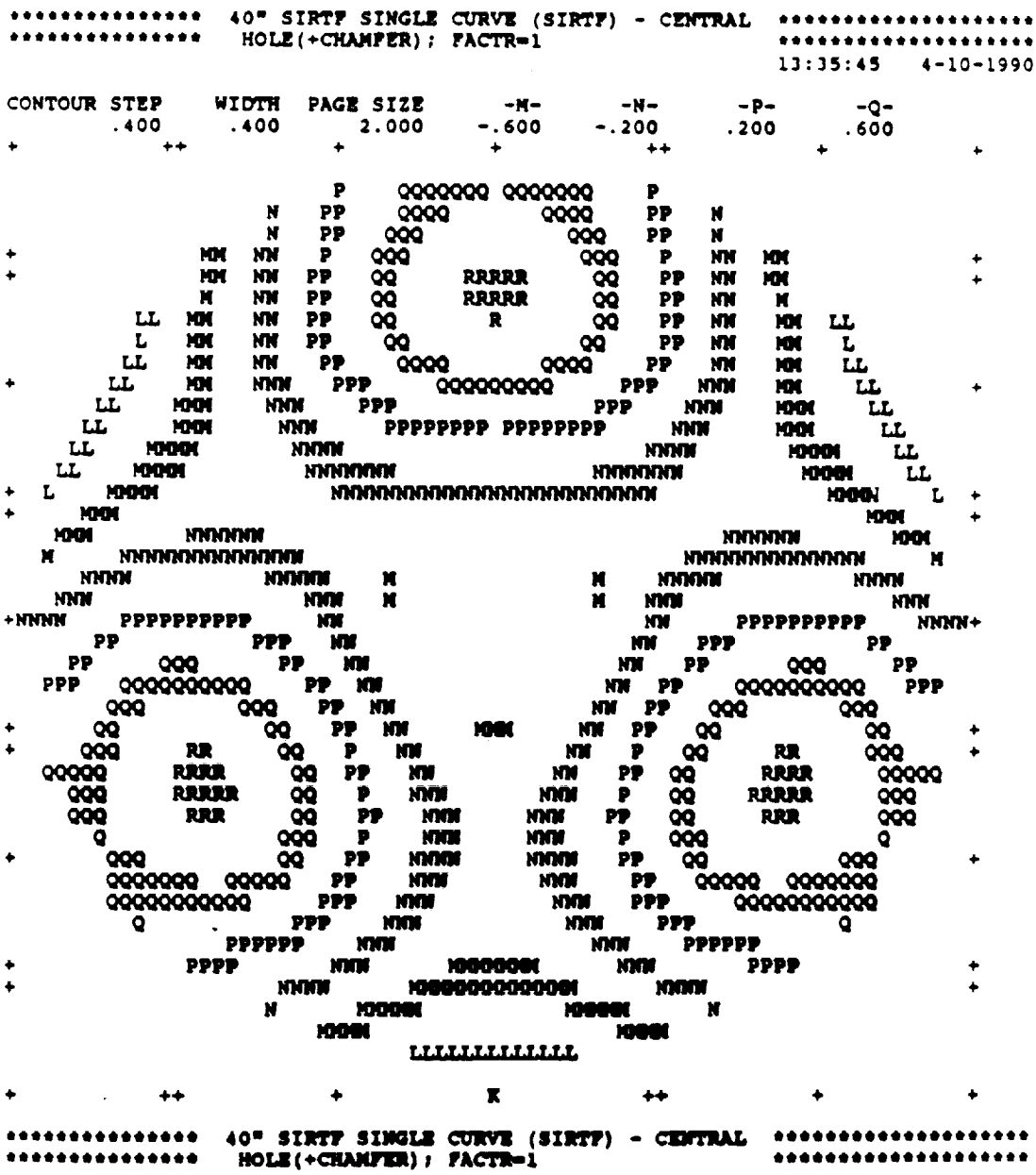

Figure 3.7. 150 lb mirror opt. performance (5-g preld., 1-g self ld. Zenith)

SIRTF SINGLE ARCH MIRROR

LOADING:

5G_PRELOAD +
1G_HORIZON

OPTICAL PERFORMANCE:
(tilt & focus removed)

RMS = .491 wave

P/V = 2.797 wave

SPOT RADIUS = 2.01 arcsec

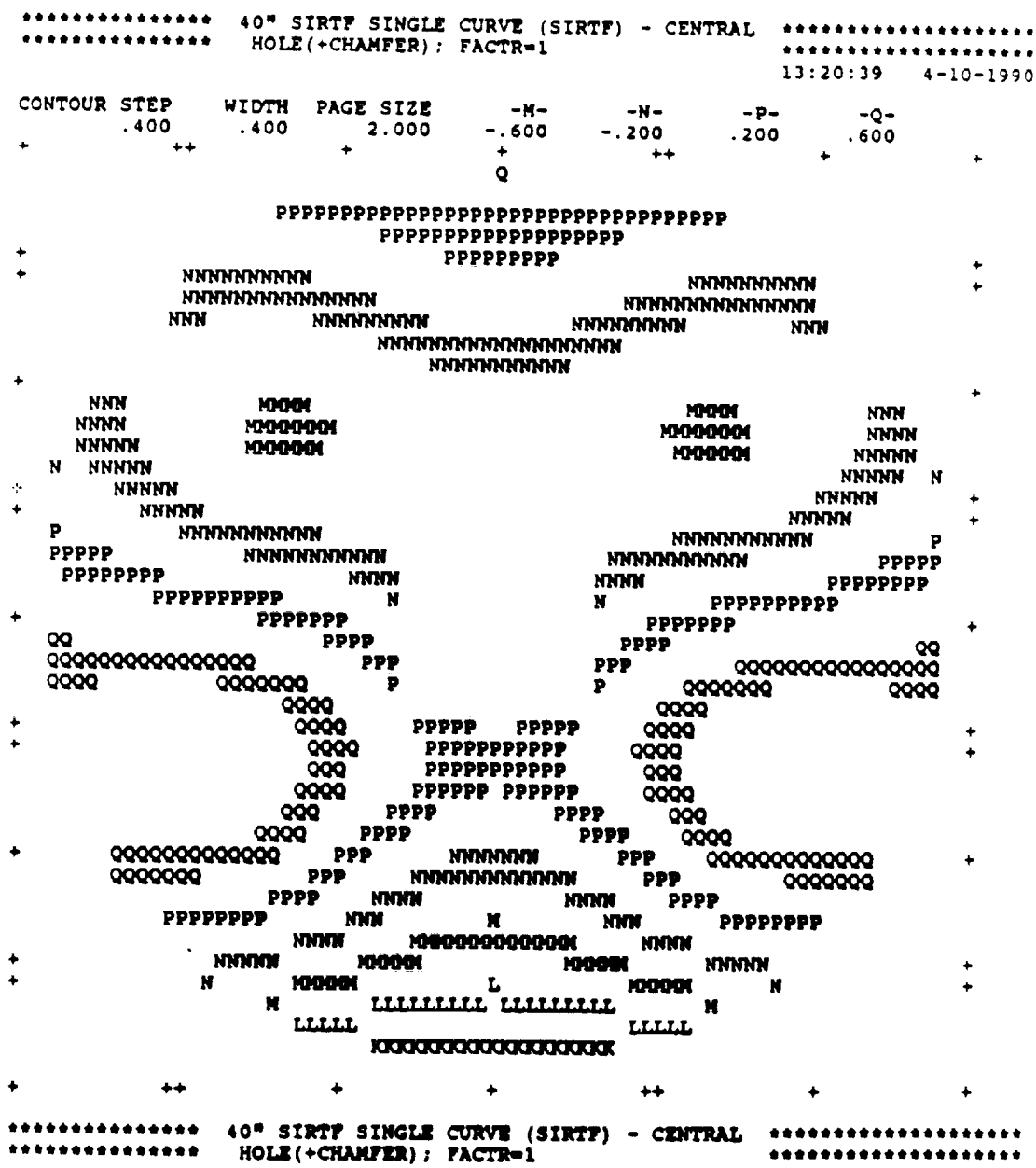

Figure 3.8. 150 lb mirror opt. performance (5-g preld., 1-g self ld. Horizon)

TABLE 3.1

SIRTF PRIMARY MIRROR STUDY

Sarver Single Arch

RMS Wavefront (lambda = 0.633)

MODEL (3 pt pad supt)	187# 3.5" pad	187# 2.25" pad	150# 3.5" pad
LOADING			
1-g Zenith	0.13	0.089	0.22
1-g Horizon	--	--	0.34
1-g Clamp	0.069	0.058	0.07
5-g Clamp + 1-g Horizon	--	--	0.51
5-g Clamp + 1-g Zenith	0.47	0.37	0.49

Table 3.1. Sarver single arch design optical performance summary

3.2. CELLULAR SANDWICH LIGHTWEIGHT MIRROR AND MOUNT STUDIES

An alternative design of a lightweight primary mirror and mirror cell for SIRTF uses a cellular sandwich mirror design. The severe launch load effects on the mirror are circumvented by clamping the mirror in the cell during launch. This preliminary design is a recommendation only and requires further analysis and testing.

This light-weight cellular mirror using tangent bar mounts is a cellular sandwich with triangular cells and weighs approximately 135 lbs. The mirror design has three socket inserts machined into blocks near the edge for the tangent bar mount. Metal bellows pressurized using He_3 which liquifies at 2°K are used for the clamping action and will release when the SIRTF is deployed. Tangent bar flexures connected to the sockets and the inside of the mirror cell will then support and position the mirror during space operations.

3.3. CONSTRAINTS

During the course of this study, the following assumptions and constraints were made. The design of the cellular mirror was limited to a total mirror weight of 135 lbs. The diameter was one meter and radius of curvature was four meters. Fused Silica, Corning code 7940, was chosen as the mirror material with the following material properties:

E = 10.7E6 psi

$v = 0.17$

$p = 0.092$ lb/in3

Additional design constraints for both the mirror and cell were:

1) The outside diameter of the mirror cell is not to exceed 42 in.

2) The temperature range the system will experience is room temperature 4°K.

3) The PSD design envelope specified for the launch environment is 0.02 g2/Hz along all axes for 20 to 250 Hz with a decrease of 9 db/octave above 250 Hz.

4) The sigma design factor for the microyield stress is 3.

Using these constraints, optimization of the cellular mirror, and a conceptual design for the mount and cell were made.

3.4. CELLULAR MIRROR OPTIMIZATION

In order to optimize the lightweight mirror, a two step approach was followed. Analytical, or strength of material (SOM) solutions were utilized to get an approximate optimum mirror geometry design in terms of stiffness to weight. With this information, Program MAP, a finite element program for wavefront error analysis of sandwich mirrors, was used to further refine the design. Lastly, a finite element model was developed using GIFTS for dynamic and static stress analysis. Shown in Figure 3.9 is the optimized design as determined by MAP and SOM solutions. The mirror design has the following physical dimensions:

faceplate thickness = .3 in.

backplate thickness = .2 in.

rib thickness = .2 in.

edge thickness = .25 in.

overall height = 4.0 in.

overall height = 4.0 in.

cell geometry = triangular

weight w/o socket blocks = 100 lbs.

weight w/ socket blocks = 135 lbs

3.5. ANALYTICAL DESIGN

Using a strength of materials approach developed by Mehta, sandwich mirror geometry can be optimized for the best possible stiffness to weight ratio. A 35 lb core evolved in this design. Table 3.2 lists various mirror designs investigated for the two different core weights when 10 cells were used across the mirror diameter. As the rib solidity ratio, n, increases then the cell size, B, decreases and

the three point edge support deflection increases. Although the SIRTF mirror will not be supported at the extreme outer edge, this maximum deflection calculation gives an indication of how the cell geometry will affect deflection. In the actual mounting case, as the support radius moves to the center of the socket blocks the deflection will actually decrease.

Another important deflection term which must be considered is the quilting deflection of the cells or the "print-through" due to polishing. The last column of Table 3.2 tabulates the quilting deflection for a .3 in. faceplate with triangular cells and .3 psi of polishing pressure. This deflection is influenced by all of these factors. Shown in Figures 3.10, 3.11, and 3.12 is the relationship of quilting deflection to faceplate thickness and cell geometry. A summary of the quilting equations as well as the other SOM equations used in this analysis are given in APPENDIX 3.A.

A review of lightweight mirror geometry indicated that a triangular rib pattern would provide symmetry and would be relatively east to fabricate. Although this geometry does not produce the smallest quilting deflection, the deflection is small enough with a .3 in faceplate to cause no major concern (on the order of 1/10 of a wave). As stated earlier, it was also decided to use a 35 lb. core for light-weight purposes. Further analyses also showed that a deeper core yielded a stiffer mirror, thus it was decided to increase the overall thickness to 4 in. from the previous 3.5 in. consideration.

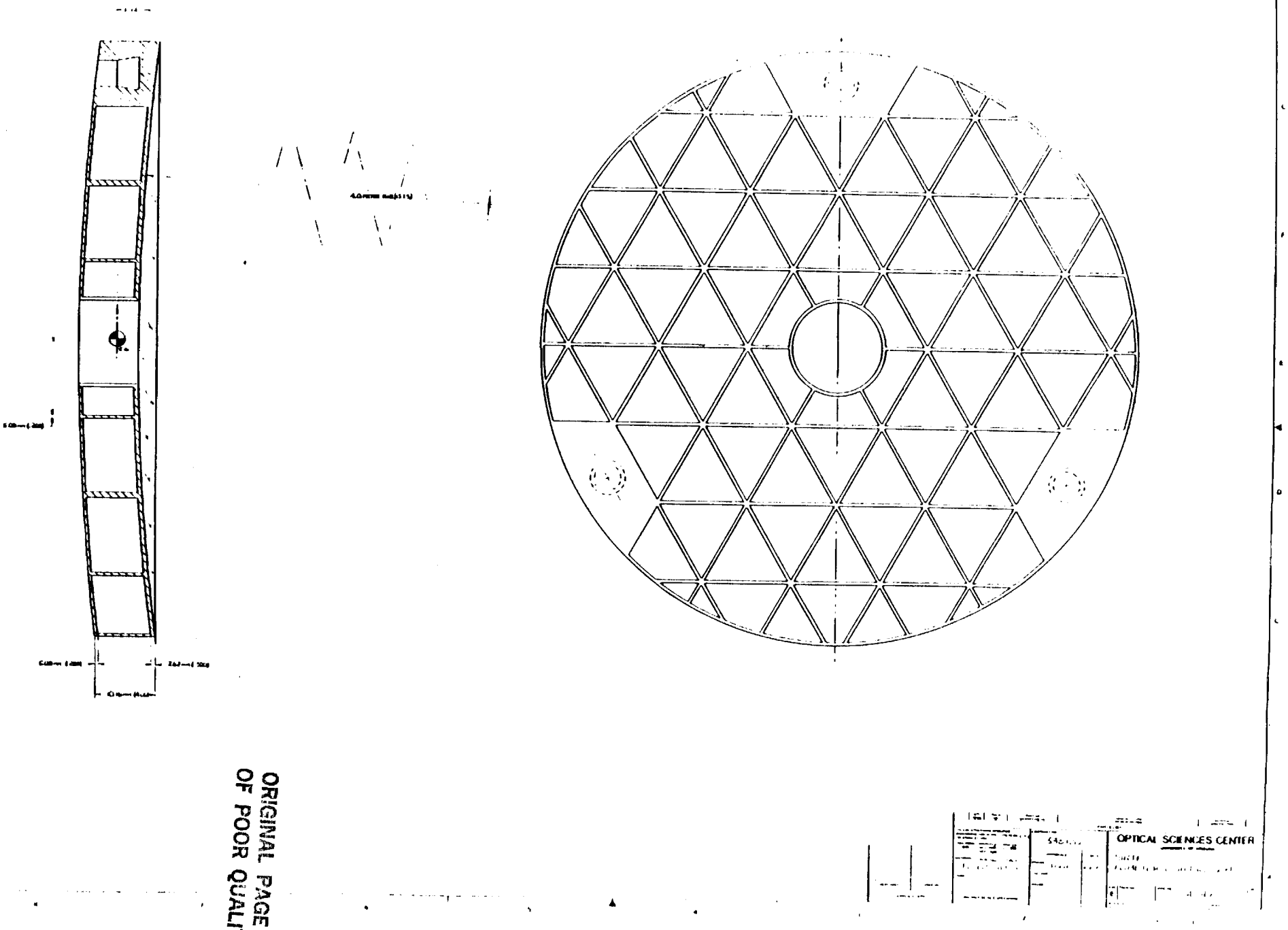

Figure 3.9. Mirror Geometry

Core Weight = 70lb (overall wt = 137.5 lb) 10 cells tf = .3 in.						Core Weight = 35lb (overall wt = 102.5 lb) 10 cells tf = .3 in.					
n	hc	tw	B	3 pt. Δ(E-5)	quilt. Δ(E-6)	n	hc	tw	B	3 pt. Δ(E-5)	quilt Δ(E-6)
0.1	6.66	.20	3.72	2.83	4.05	0.1	3.33	.20	3.72	8.63	4.05
0.15	4.44	.31	3.60	6.17	3.56	0.15	2.22	.31	3.60	18.2	3.56
0.20	3.33	.41	3.48	10.6	3.12	0.20	1.66	.41	3.48	30.5	3.12
0.25	2.66	.52	3.36	16.2	2.71	0.25	1.33	.52	3.36	44.7	2.71
0.30	2.22	.63	3.24	22.6	2.34	0.30	1.11	.63	3.24	60.5	2.34

Table 3.2. Analytical Mirror Design

3.6. PROGRAM MAP

The MAP program, developed by Dr. Ralph M. Richard, is a program which autogenerated models for light-weight structured mirrors using finite elements. This program was used to model the 1 m. mirror. The SOM solutions were used as a baseline and MAP was used to obtain a refined design with a high stiffness-to-weight ratio. Additionally a GIFTS finite element model was generated to provide a means of evaluating both the static and dynamic stresses. For comparison, the proposed design which was obtained by MAP was also evaluated using the SOM approach. For a 3 pt. edge support with sockets, the following weights and gravity loading deflections were determined.

	Structural Max. Deflection	Weight	Optical Axes Frequency	Max. Global Stress
MAP	7.6E-5 in.	135 lb	406 Hz	12.6 psi
SOM	8.6E-5 in.	135 lb	--	--
GIFTS	8.0E-5 in.	140 lb	--	14.0 psi

*MAP Wavefront RMS = 0.82λ

The SOM deflection calculations for this model are given in APPENDIX 3.A. A program MAP output from a model run is presented in APPENDIX 3.B.

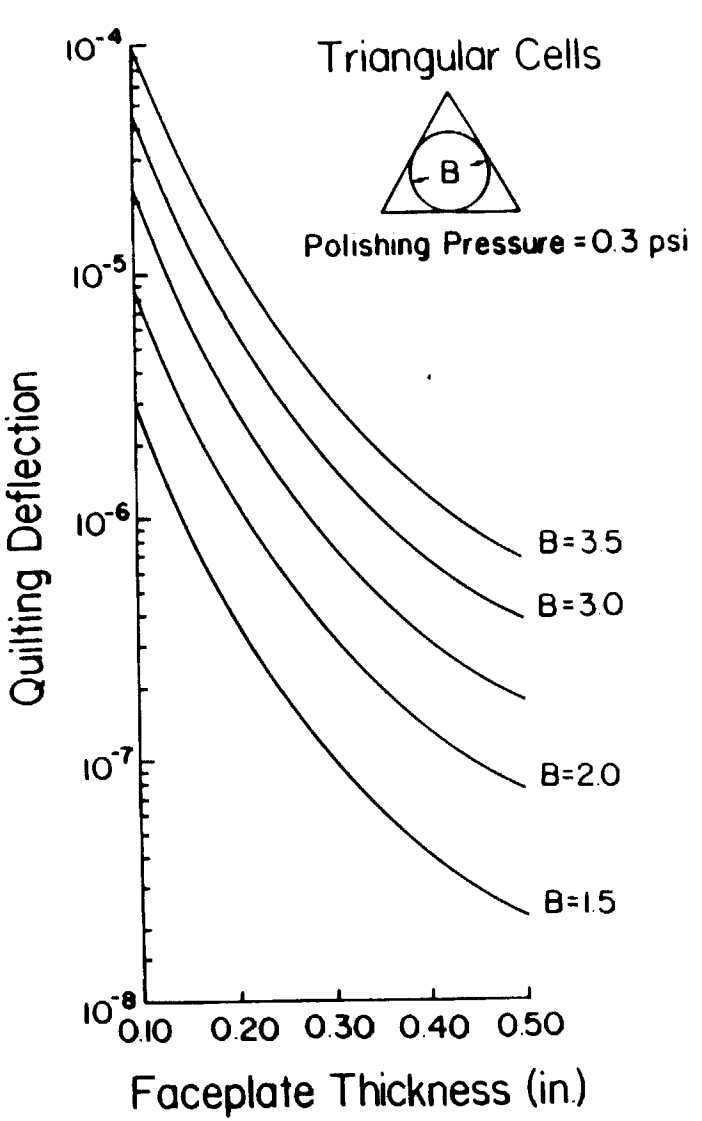

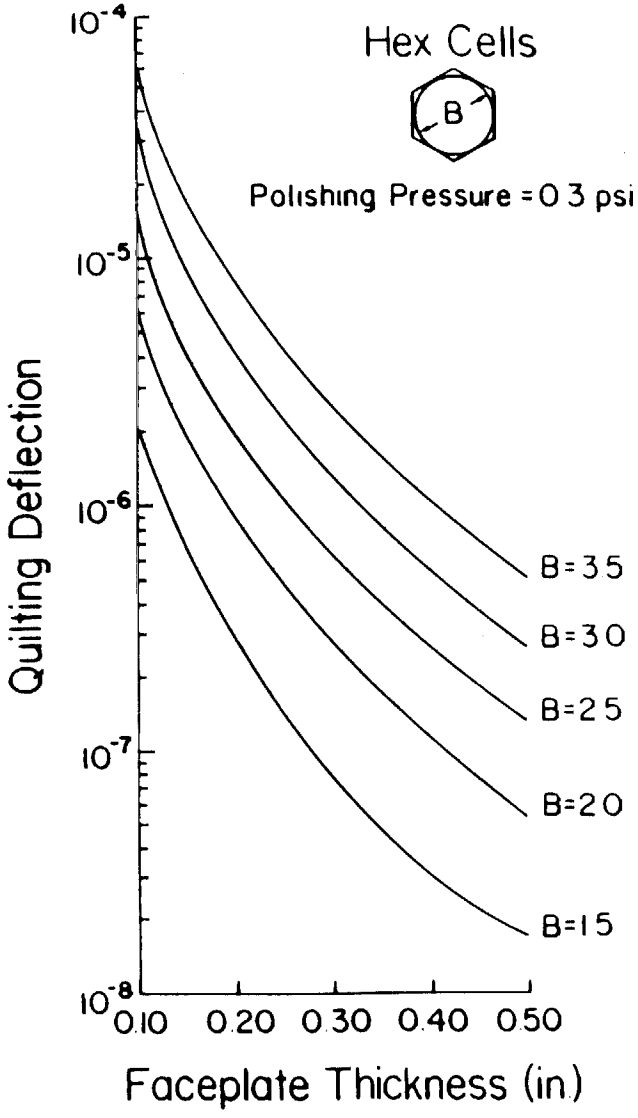

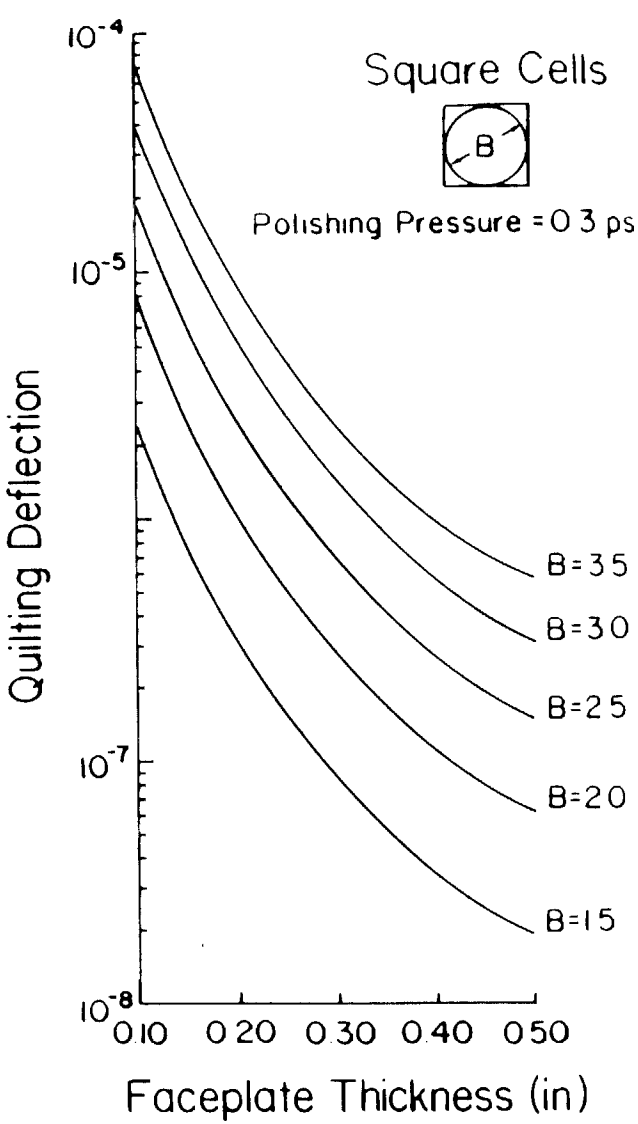

Figures 3.10, 3.11, and 3.12. Quilting Deflection for Triangular, Square and Hex Cells

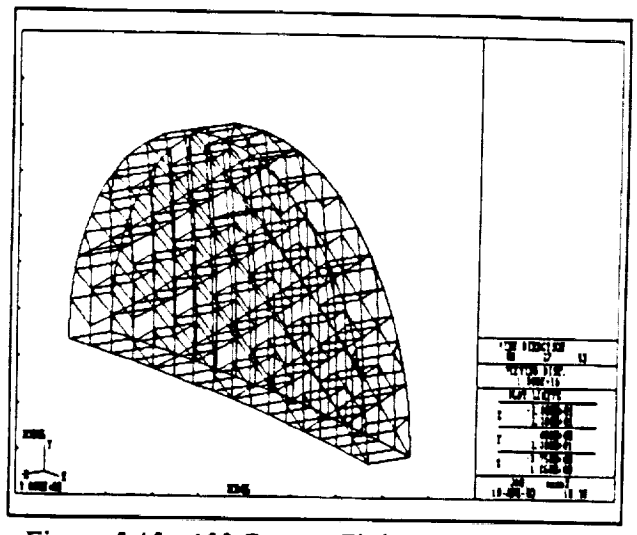

Figure 3.13. 180 Degree Finite Element Model

3.7. FINITE ELEMENT DESIGN

Further static and dynamic modeling of the 1 meter mirror is necessary to examine the effects of clamping during launch. Figure 3.13 shows a finite element model of a 180 degree segment of the mirror. For future analysis, this model should be refined and its performance evaluated for the design PSD.

3.8. 18 POINT MOUNTING SYSTEM FOR POLISHING

An important consideration is 0.25 rms wavefront error placed on the mirror. While in space, this constraint is not difficult to meet since gravity loading will not be present, only distortions due to the mount itself and the residual quilting due to polishing will be of concern. While polishing and testing the mirror under gravity loading however, it is extremely important to minimize self-weight included deflections to get a true measure of the mirror's optical surface. The 3 pt. support proposed for launch is insufficient for this purpose, therefore, an 18 pt. support system for polishing and testing is recommended. An 18 point polishing setup using oilpad belloframs exists at the Optical Sciences Center and has been successfully used for polishing high precision lightweight mirrors of the 1-m class.

3.9. MIRROR MOUNTING SYSTEM

Based upon the experience this design team has had with (SIRTF) double arch design, it was concluded that a clamped mirror mount system would be required for the lightweight mirror. The SIRTF design envelope, specified by NASA Ames for the space shuttle cargo bay was 0.02 g^2/Hz over the frequency range 20-250 Hz with a drop of 9 db/octave from that level for the higher frequencies. This design envelope resulted in approximately a 50g loading along the optical axis and a 40g loading normal to the optical axis for a 258 lb fused silica mirror with flexure mounts designed to accommodate cryo-cool down. It is very apparent that a lightweight mirror could not withstand loads of this magnitude.

The clamping system is a highly reliable design concept which circumvents a very difficult design, if even possible, for an unclamped flexure design.

This system results in a mirror design with a fundamental frequency along the optical axis of 400 Hz when supported by the flexures, and a frequency of 600 Hz with the clamped support system.

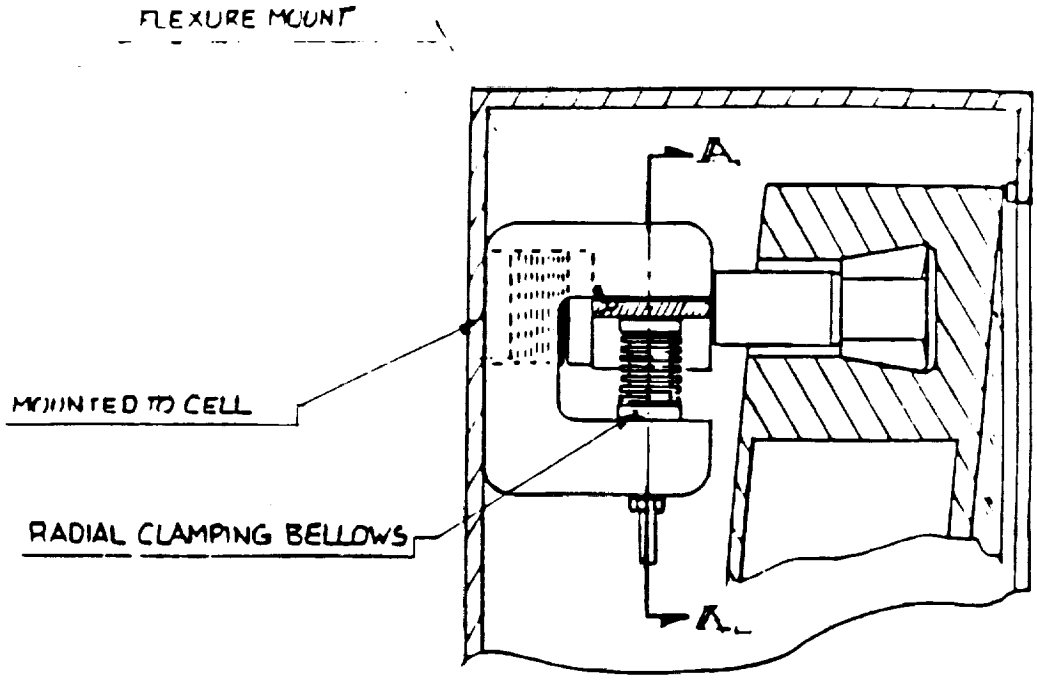

Figure 3.14. Socket Design

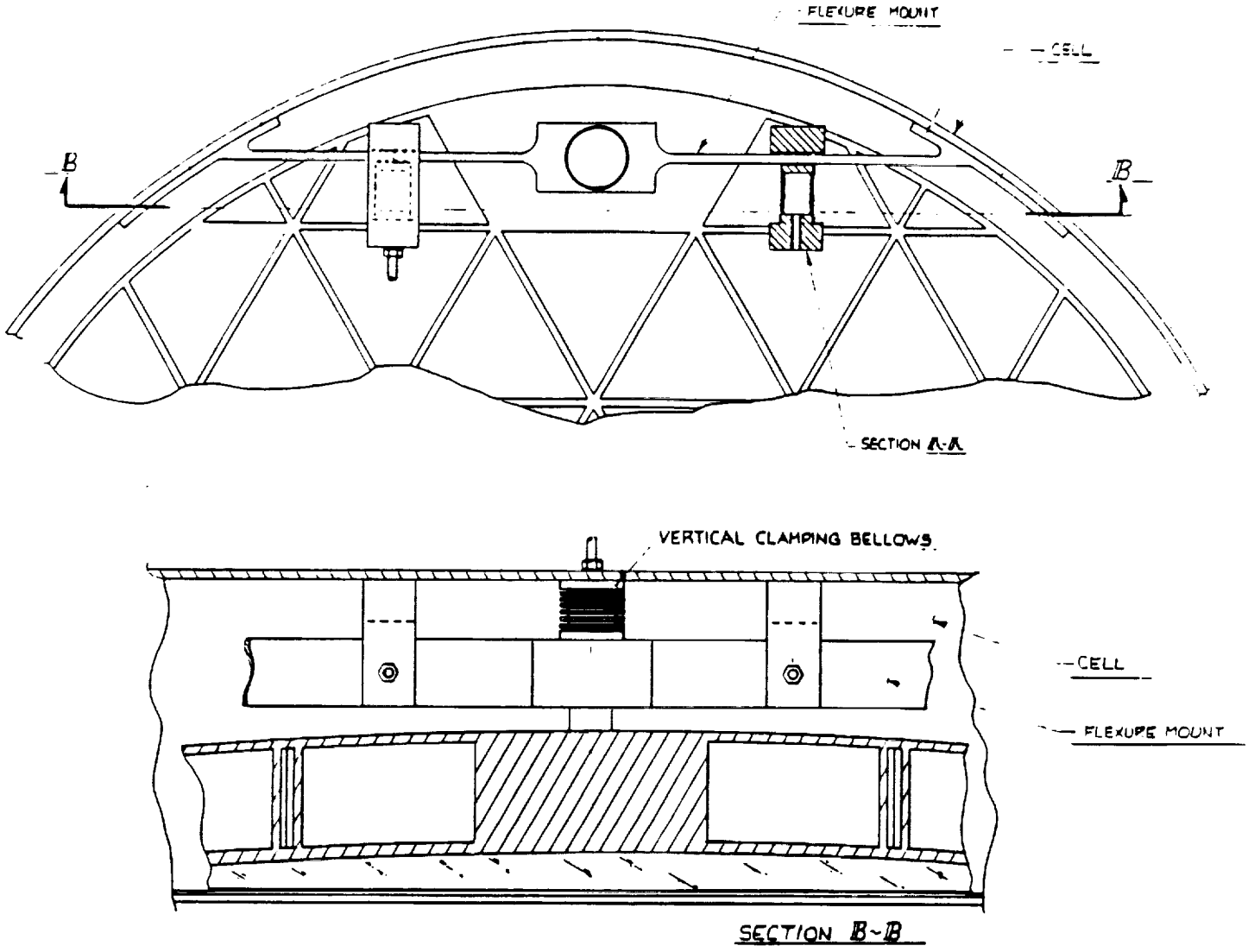

Figure 3.15. Mirror and Cell with Tangent Bars

3.10. SOCKET DESIGN

A preloaded tapered invar socket which has a large glass to metal contact area is proposed. Three of these inserts provide the interference between the mirror socket blocks and the tangent bar flexures. This design is similar to the proposed SIRTF double arch socket design. A Conceptual drawing of the socket design is shown in Figure 3.14.

3.11. TANGENT BAR FLEXURES

These invar flexures, attached to the tapered socket inserts, provide the support for normal handling of the mirror in its cell under 1 g loading and also provide both optical axis and lateral positioning of the mirror in space. This flexure design is similar to that used for the German Infrared Laboratory (GIRL) design. Shown in Figure 3.15, is a preliminary layout of the tangent bar concept with the lightweight mirror and mirror cell.

3.12. CLAMPED (BELLOWS) DESIGN FOR LAUNCH

This design comprises bellows located on the back of the mirror sockets which presses the mirror top outer edge against the mirror cell. Also a circumferential bellow design provides lateral constraint of the mirror in the cell from the effects of the lateral loads, i.e. loads normal to the optical axis. These bellows clamping conceptual designs are shown with the sockets in Figure 3.14.

3.13. FUTURE DESIGN STUDIES AND TESTS REQUIRED

Finite element analysis of the mirror, stress analyses of the sockets and flexure assemblies are required to determine stress levels, both clamped and unclamped due to static and dynamic loadings, and wavefront errors due to support conditions of a 1-g loading and the 18 point polishing support system.

With a final or near final design completed, a full scale qualification test would be made at the Fort Huachuca Environmental Test Facility to simulate the dynamic launch loads and verify the integrity of the design.

REFERENCES

Barnes, W.P., Jr., "Optimal design of cored mirror structures," *Applied Optics*, Vol. 8, No. 6, June 1969.

Cho, M.K., Richard, R.M., and Vukobratovich. D., " Study on mirror shape for a lightweight mirror subjected to self-weight," *Pro. SPIE*, Vol 1167, 1989.

Mehta, P.K., "Flexural rigidity characteristics of light-weighted mirrors," *Proc. SPIE*, Vol. 748, 1987.

Nelson, J.E., Lubliner, J., Mast, T.S., "Telescope mirror supports: Plate deflections on point supports," *Proc. SPIE*, Vol. 332, 1982.

Pepi, J.W., Kahan, M.A., Barnes, W.H., Zielinski, R.J., "Teal Ruby - design, manufacture and test," *Proc. SPIE*, Vol. 216, 1980.

Richard, R.M., and Malvick, A.J., "Elastic deformation of lightweight mirrors," *Applied Optics*, 12(6), 1973.

Richard R.M., and Malvick, A.J., "User's manual for program MAP (Mirror Analysis Program), University of Arizona, Tucson 85721, 1980.

Schlegelmilch r., et al., "GIRL - German Infrared Laboratory Final Report of the telescope study, phase B, "*NASA technical memorandum*, NASA TM-75911, January, 1981.

Appendix 3.A. Analytical Mirror Analysis

MIRROR GEOMETRY OPTIMIZATION

SANDWICH MODEL

$$W = \rho A (2 t_f + \eta h_c)$$

$$\eta = \frac{(2 t_b - [illegible])}{([illegible] - h^2)}$$

$t_b = $ [illegible]

$$\rho A \left[2 [illegible] \sqrt{1 - \eta/2} - [illegible] \sqrt{[illegible] - \eta)^2} \right]$$

$$D = \frac{E t_b^3}{12(1 - \nu^2)}$$

$$t_c^3 = (2 t_f - h_c)^3 - \left[1 - \frac{\eta}{2}\right] h_c^3$$

WHERE:

W = WEIGHT
ρ = DENSITY
η = RIB SOLIDITY RATIO
h_c = CORE HEIGHT
t_f = FACEPLATE THICKNESS
A = AREA
E = YOUNG'S MODULUS
ν = POISSON'S RATIO
t_b = EQUIVALENT BENDING THICKNESS
D = FLEXURAL RIGIDITY

ORIGINAL PAGE IS
OF POOR QUALITY

QUILTING FACEPLATE DEFLECTION

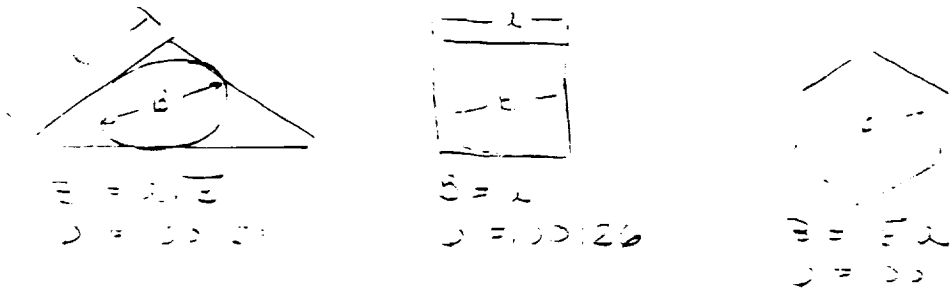

$$\delta_q = \frac{\psi \cdot 2(1-\gamma^2)}{E} \frac{(P)(\ell^4)}{t_f^3}$$

δ_q = QUILTING DEFLECTION
ψ = CONSTANT
P = POLISHING PRESSURE
ℓ = CELL INSCRIBED CIRCLE
E = YOUNG'S MODULUS
γ = POISSONS RATIO
t_f = FACEPLATE THICKNESS

DEFLECTION EQUATIONS

3 POINT EDGE SUPPORT

$$\delta = .0562 \frac{F_K r_o^2}{D}$$

WHERE: F_K = WEIGHT
r_o = MIRROR RADIUS
D = FLEXURAL RIGIDITY

18 POINT SURFACE DEFLECTION

$$\delta_{RMS} = \gamma_N \frac{\rho h}{D}\left(\frac{\pi r^2}{N}\right)^2 \left[1 + 2\left(\frac{h}{u}\right)^2\right] \qquad \delta_{MAX} = K \delta_{RMS}$$

WHERE: δ_{RMS} = DEFLECTION
ρ = DENSITY
h = EFFECTIVE THICKNESS
D = FLEXURAL RIGIDITY
E = YOUNG'S MODULUS
$u = r/N$
N = NUMBER OF SUPPORT POINTS
r = MIRROR RADIUS
$\gamma_N = 1.89 \times 10^{-3}$
$K = 5.5$

$t_f = .3$
$t_b = .2$

WINGLID c/p

CORE WEIGHT = 70 lb
(OVERALL WT = 137.5 lb)

10 CELLS

n	h_c	t_w	B	δ (3PT)	$\delta\Delta$
.1	3.66	.201	3.72	2.83	4.05
.15	2.44	.275	3.60	6.17	3.56
.20	1.83	.411	3.43	10.6	3.12
.25	1.46	.520	3.30	16.2	2.71
.30	1.22	.633	3.24	22.6	2.34

CORE WT = 35 lb
(OVERALL WT = 102.5 lb)

10 CELLS

n	h_c	t_w	B	δ (3PT)	$\delta\Delta$
.1	3.33	.201	3.72	2.83	4.05
.15	2.22	.275	3.60	6.17	3.56
.20	1.66	.411	3.43	10.6	3.12
.25	1.33	.520	3.30	16.2	2.71
.30	1.11	.633	3.24	22.6	2.34

12 CELLS

n	h_c	t_w	B	δ (3PT)	$\delta\Delta$ ($\times 10^{-6}$)
.1	3.66	.169	3.10	2.83	1.96
.15	2.44	.256	3.00	6.17	1.72
.20	1.83	.346	2.91	10.6	1.52
.25	1.46	.438	2.81	16.2	1.32
.30	1.22	.533	2.70	22.6	1.13

12 CELLS

n	h_c	t_w	B	δ (3PT)	$\delta\Delta$
.1	3.33	.169	3.10	2.83	1.96
.15	2.22	.256	3.00	6.17	1.72
.20	1.66	.346	2.91	10.6	1.52
.25	1.33	.438	2.81	16.2	1.32
.30	1.11	.533	2.70	22.6	1.13

15 CELLS

n	h_c	t_w	B	δ (3PT)	$\delta\Delta$ ($\times 10^{-6}$)
.1	3.66	.134	2.48	2.83	.803
.15	2.44	.204	2.41	6.17	.717
.20	1.83	.275	2.33	10.6	.626
.25	1.46	.349	2.25	16.2	.544
.30	1.22	.424	2.17	22.6	.471

15 CELLS

n	h_c	t_w	B	δ (3PT)	$\delta\Delta$
.1	3.33	.134	2.48		.803
.15	2.22	.204	2.41		.717
.20	1.66	.275	2.33		.626
.25	1.33	.349	2.25		.544
.30	1.11	.424	2.17		.471

SUGGEST;
10 CELLS $n = .17$
$t_f = .3$ $t_b = .2$
$h_c \cong 4.0$
$t_w \cong .375$
DEFLECTION (3PT) $\cong 7 \times 10^{-5}$ IN
DEFLECTION QUILTING $\cong 3.3 \times 10^{-6}$ IN

SUGGEST:
10 CELLS $n = .17$
$t_f = .3$ $t_b = .2$
$h_c \cong 2.0$
$t_w \cong .35$
DEFLECTION (3PT) $\cong 12 \times 10^{-5}$ IN
DEFLECTION QUILTING $\cong 3.3 \times 10^{-6}$ IN

TEST FOR COMPUTER PROGRAM MAP

$t_f = .2$
$\phi = 39.37$
WT = 1351b
OVERALL HT = 4.0IN
$\sigma = .28$
$E = 10.1 \times 10^6$
$\nu = .17$
RIB THICKNESS = .2

B = CELL DIA

$135 = .08 A (2t_f + \eta h_c)$

$135 = .08 (\pi 20^2 \times .5 + \eta h_c)$

$h_c = 3.5 \quad \eta = .341$

D = FLEXURAL RIGIDITY

$$D = \frac{E t_b^3}{12(1-\nu^2)}$$

$$t_b^3 = (2t_f + h_c)^3 - \left[1 - \frac{\eta}{2}\right] h_c^3$$

$$t_b^3 = (.5 + 3.5)^3 - \left[1 - \frac{.341}{2}\right] 3.5^3 \Rightarrow t_b^3 = 26.2914$$

$$D = \frac{(10.1 \times 10^6 \times 26.2914)}{12(1-.17^2)} \Rightarrow 22.7871 \times 10^6$$

3 POINT EDGE DEFLECTION

DEFLECTION $w = .0362 \frac{P^* r_0^2}{D}$

$$w = \frac{.0362 (135 \times 20^2}{22.7871 \times 10^6} \Rightarrow w = 8.579 \times 10^{-5}$$

$w_{MAP} = 7.58 \times 10^{-5}$
WT = 1331b.

$w_{SOM} = 8.579 \times 10^{-5}$
WT = 135 lb

Appendix 3.B. Program Map Output

1 INPUT DATA FOR NASA 3 POINT EDGE SUPPORT

NELEMS,NODES,NLOADS,NSUPTS,LMODE,MSOL
0 0 0 3 1 1
OSTRUCTURE ORIENTATION ANGLES IN DEGREES - TX AND TY
0. 0.

MATL E PR WT
1 .101E+08 .170E+00 .800E-01
RADCURVE= .16E+031D= .0000= 39.37DEPTH= 4.00
OTTOP= .300TBOTT= .200TRIB= .132TEDGE= .200

NODE PT.	X COORD	Y COORD	Z COORD	TEMPERATURE
1	.000E+00	-.197E+02	-.278E+01	.000E+00
2	.000E+00	-.197E+02	-.784E+00	.000E+00
3	.000E+00	-.197E+02	.122E+01	.000E+00
358	.000E+00	.197E+02	-.278E+01	.000E+00
359	.000E+00	.197E+02	-.784E+00	.000E+00
360	.000E+00	.197E+02	.122E+01	.000E+00

SUPPRESSED DEGREES OF FREEDOM

264 521 1074
OTOTAL WEIGHT OF STRUCTURE
.48801E+02
THE C.G. OF THE MIRROR IS AT Z= -1.145
THE RALEIGH FREQUENCY IS .406E+03 HERTZ
1 OUTPUT DATA
TRANSLATIONS

NODE POINT	ALONG X-AXIS	ALONG Y-AXIS	ALONG Z-AXIS
1	.00E+00	-.99E-06	-.59E-04
2	.00E+00	.12E-06	-.59E-04
3	.00E+00	.12E-05	-.59E-04
172	.00E+00	.16E-06	-.76E-04
173	.00E+00	.11E-06	-.76E-04
174	.00E+00	.00E+00	-.76E-04
358	.00E+00	.69E-05	.00E+00
359	.00E+00	-.39E-05	-.57E-05
360	.00E+00	-.13E-04	-.74E-05

OELEMENT NO.				SIGMA XX	SIGMA YY	SIGM A XY
3	15	18	1	-.675E+01	.895E-01	-.192E+00
15	18	6	1	.920E-01	-.675E+01	.217E+00
18	6	3	1	-.671E+01	.100E+00	-.213E+00
147	174	177	1	-.309E+01	-.280E+01	.152E+00
174	177	150	1	-.280E+01	-.309E+01	-.510E+00
177	150	147	1	-.395E+01	-.294E+01	.509E+00
150	147	174	1	-.295E+01	-.395E+01	-.151E+00
145	172	175	2	.560E+01	.526E+01	-.292E+00
172	175	148	2	.519E+01	.559E+01	.772E+00

168	195	198	1	.492E-02	-.408E+01	.214E+01
195	198	171	1	-.457E+01	-.840E-01	-.201E+01
198	171	168	1	-.461E-01	-.425E+01	.251E+01
171	168	195	1	-.402E+01	.339E+00	-.237E+01
166	193	196	2	.426E+00	.388E+01	-.335E+01
193	196	169	2	.355E+01	.377E+00	.318E+01
196	169	166	2	.320E+00	.307E+01	-.322E+01
169	166	193	2	.380E+01	-.100E-01	.321E+01
174	201	204	1	-.239E+01	-.344E+01	.190E+00
201	204	177	1	-.343E+01	-.239E+01	-.537E+00
204	177	174	1	-.322E+01	-.358E+01	.536E+00
177	174	201	1	-.358E+01	-.322E+01	-.189E+00
172	199	202	2	.454E+01	.607E+01	-.289E+00
199	202	175	2	.599E+01	.453E+01	.800E+00
202	175	172	2	.576E+01	.620E+01	-.768E+00
175	172	199	2	.628E+01	.578E+01	.256E+00
177	204	207	1	-.232E+01	-.342E+01	.898E+00
204	207	180	1	-.344E+01	-.232E+01	-.122E+01
207	180	177	1	-.310E+01	-.357E+01	.123E+01
180	177	204	1	-.356E+01	-.310E+01	-.904E+00
175	202	205	2	.443E+01	.597E+01	-.135E+01
202	205	178	2	.577E+01	.439E+01	.184E+01
205	178	175	2	.556E+01	.597E+01	-.175E+01
178	175	202	2	.617E+01	.560E+01	.127E+01
195	222	225	1	-.373E+00	-.464E+01	.224E+01
222	225	198	1	-.503E+01	-.435E+00	-.212E+01
225	198	195	1	.116E+00	-.522E+01	.197E+01
198	195	222	1	-.459E+01	-.873E-01	-.239E+01
193	220	223	2	.815E+00	.450E+01	-.306E+01
220	223	196	2	.405E+01	.733E+00	.294E+01
223	196	193	2	.129E+00	.436E+01	-.252E+01
196	193	220	2	.446E+01	.530E+00	.287E+01
345	360	363	1	.714E+01	-.919E+00	.121E+01
360	363	348	1	-.327E+00	.703E+01	-.293E+01
363	348	345	1	.438E+01	-.117E+01	.235E+01
348	345	360	1	-.140E+01	.434E+01	-.112E+01
343	358	361	2	-.967E+01	.533E+01	-.266E+01
358	361	346	2	.187E+01	-.981E+01	.493E+01
361	346	343	2	-.690E+01	.303E+01	-.298E+01
346	343	358	2	.589E+01	-.642E+01	.153E+01

1 EQUILIBRIUM CHECK

0 SUM FORCES X SUM FORCES Y SUM FORCES Z

.91035E-04 -.36904E-04 .14902E-02

VARIABLE 3

-.5898E-04	-.5782E-04	-.5438E-04	-.4877E-04	-.6100E-04	-.5969E-04	-.5579E-04	-.4948E-04	-.4226E-04	-.6334E-04
-.6201E-04	-.5804E-04	-.5150E-04	-.4250E-04	-.2748E-04	-.6593E-04	-.6461E-04	-.6063E-04	-.5402E-04	-.4474E-04
-.3266E-04	-.1451E-04	-.6862E-04	-.6735E-04	-.6353E-04	-.5715E-04	-.4816E-04	-.3639E-04	-.2148E-04	-.5577E-05
-.7123E-04	-.7006E-04	-.6655E-04	-.6072E-04	-.5262E-04	-.4233E-04	-.3015E-04	-.1723E-04	-.1282E-04	-.7349E-04
-.7246E-04	-.6939E-04	-.6433E-04	-.5742E-04	-.4892E-04	-.3931E-04	-.2950E-04	-.2303E-04	-.7511E-04	-.7425E-04
-.7168E-04	-.6750E-04	-.6187E-04	-.5507E-04	-.4755E-04	-.3994E-04	-.3331E-04	-.7574E-04	-.7506E-04	-.7303E-04
-.6975E-04	-.6536E-04	-.6010E-04	-.5432E-04	-.4840E-04	-.4271E-04	-.7505E-04	-.7455E-04	-.7308E-04	-.7069E-04
-.6749E-04	-.6363E-04	-.5934E-04	-.5488E-04	-.5073E-04	-.7272E-04	-.7242E-04	-.7152E-04	-.7002E-04	-.6797E-04
-.6543E-04	-.6253E-04	-.5940E-04	-.5701E-04	-.6846E-04	-.6838E-04	-.6809E-04	-.6754E-04	-.6667E-04	-.6544E-04
-.6389E-04	-.6206E-04	-.6123E-04	-.6202E-04	-.6220E-04	-.6265E-04	-.6316E-04	-.6354E-04	-.6368E-04	-.6554E-04
-.6309E-04	-.5311E-04	-.5370E-04	-.5511E-04	-.5687E-04	-.5863E-04	-.6027E-04	-.6180E-04	-.4135E-04	-.4273E-04
-.4556E-04	-.4886E-04	-.5207E-04	-.5598E-04	-.2605E-04	-.2929E-04	-.3435E-04	-.3961E-04	-.4375E-04	-.7403E-05
-.1522E-04	-.2539E-04	-.3555E-04							

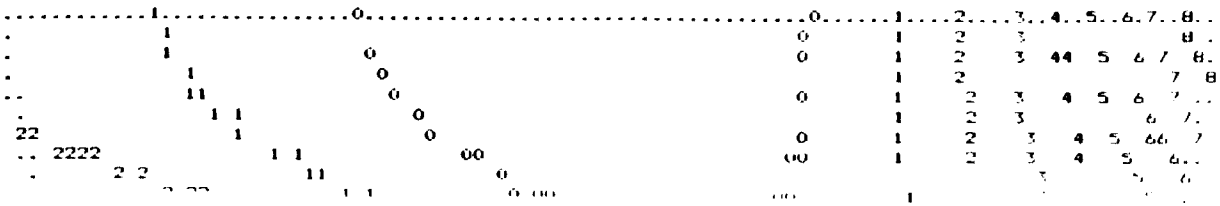

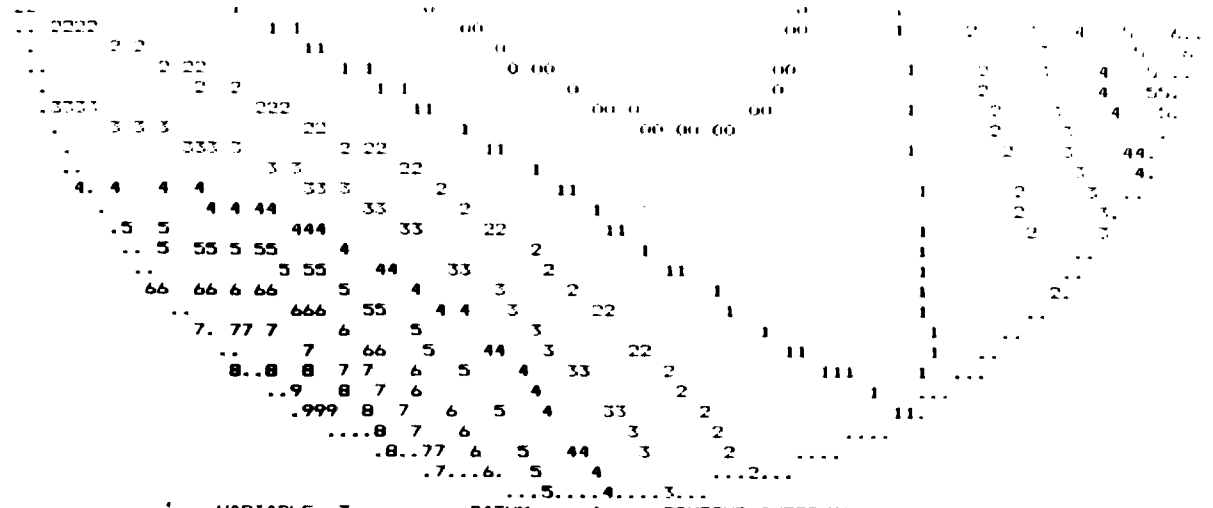

VARIABLE 3 DATUM = .0 CONTOUR INTERVAL = .702E-05

Z DEFLECTIONS

VARIABLE 4

-.5838E-04	-.5720E-04	-.5370E-04	-.4797E-04	-.6051E-04	-.5916E-04	-.5518E-04	-.4872E-04	-.4134E-04	.6295E-04
-.6158E-04	-.5752E-04	-.5082E-04	-.4161E-04	-.2622E-04	-.6563E-04	-.6427E-04	-.6020E-04	-.5342E-04	-.4391E-04
-.3153E-04	-.1295E-04	-.6841E-04	-.6711E-04	-.6319E-04	-.5664E-04	-.4742E-04	-.3536E-04	-.2009E-04	-.3814E-05
-.7110E-04	-.6989E-04	-.6629E-04	-.6031E-04	-.5200E-04	-.4145E-04	-.2897E-04	-.1575E-04	-.1123E-04	-.7343E-04
-.7237E-04	-.6921E-04	-.6402E-04	-.5694E-04	-.4821E-04	-.3835E-04	-.2829E-04	-.2167E-04	-.7509E-04	-.7420E-04
-.7157E-04	-.6728E-04	-.6149E-04	-.5451E-04	-.4680E-04	-.3898E-04	-.3217E-04	-.7574E-04	-.7504E-04	.7296E-04
-.6959E-04	-.6507E-04	-.5967E-04	-.5372E-04	-.4763E-04	-.4176E-04	-.7503E-04	-.7452E-04	-.7301E-04	-.7055E-04
-.6725E-04	-.6327E-04	-.5886E-04	-.5425E-04	-.4996E-04	-.7263E-04	-.7232E-04	-.7139E-04	-.6985E-04	-.6774E-04
-.6511E-04	-.6211E-04	-.5886E-04	-.5637E-04	-.6825E-04	-.6817E-04	-.6787E-04	-.6730E-04	-.6639E-04	-.6511E-04
-.6348E-04	-.6156E-04	-.6069E-04	-.6163E-04	-.6182E-04	-.6228E-04	-.6279E-04	-.6317E-04	-.6329E-04	-.6310E-04
-.6261E-04	-.5249E-04	-.5309E-04	-.5454E-04	-.5634E-04	-.5812E-04	-.5977E-04	-.6129E-04	-.4041E-04	-.4184E-04
-.4474E-04	-.4812E-04	-.5139E-04	-.5534E-04	-.2474E-04	-.2807E-04	-.3325E-04	-.3862E-04	-.4285E-04	-.5691E-05
-.1368E-04	-.2406E-04	-.3446E-04							

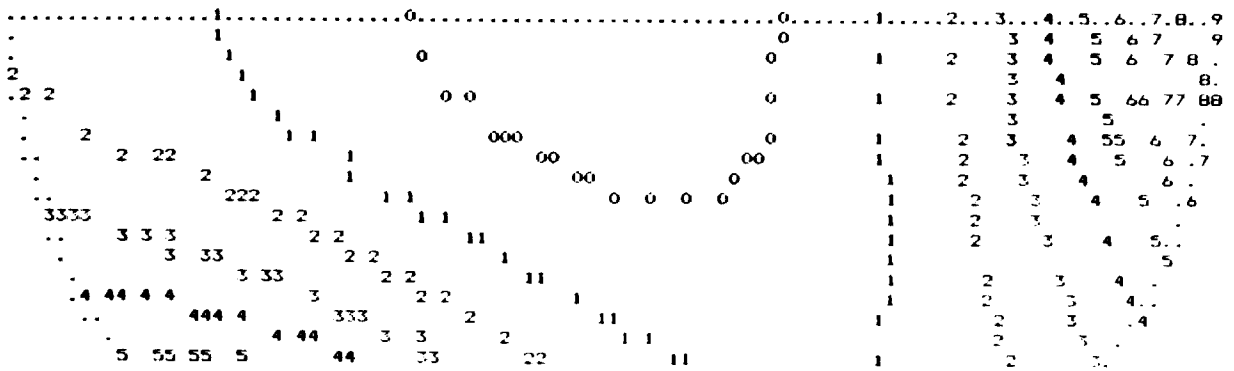

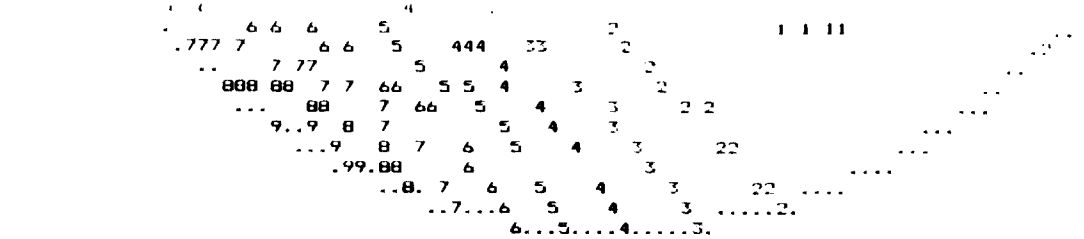

VARIABLE 4 DATUM = .0 CONTOUR INTERVAL = .719E-05

NORMAL DEFLECTIONS

VARIABLE 5

-.6010E-04	-.5891E-04	-.5536E-04	-.4957E-04	-.6201E-04	-.6067E-04	-.5668E-04	-.5023E-04	-.4285E-04	-.6424E-04
-.6287E-04	-.5881E-04	-.5211E-04	-.4290E-04	-.2751E-04	-.6671E-04	-.6535E-04	-.6128E-04	-.5450E-04	-.4499E-04
-.3261E-04	-.1403E-04	-.6927E-04	-.6797E-04	-.6405E-04	-.5750E-04	-.4828E-04	-.3622E-04	-.2095E-04	-.4674E-05
-.7174E-04	-.7054E-04	-.6694E-04	-.6096E-04	-.5265E-04	-.4210E-04	-.2961E-04	-.1639E-04	-.1188E-04	-.7386E-04
-.7280E-04	-.6964E-04	-.6445E-04	-.5737E-04	-.4864E-04	-.3878E-04	-.2872E-04	-.2210E-04	-.7531E-04	-.7442E-04
-.7179E-04	-.6749E-04	-.6171E-04	-.5473E-04	-.4701E-04	-.3919E-04	-.3238E-04	-.7574E-04	-.7504E-04	-.7296E-04
-.6959E-04	-.6507E-04	-.5967E-04	-.5372E-04	-.4763E-04	-.4176E-04	-.7482E-04	-.7431E-04	-.7279E-04	-.7033E-04
-.6703E-04	-.6306E-04	-.5864E-04	-.5403E-04	-.4974E-04	-.7220E-04	-.7189E-04	-.7096E-04	-.6942E-04	-.6731E-04
-.6468E-04	-.6168E-04	-.5843E-04	-.5594E-04	-.6761E-04	-.6752E-04	-.6723E-04	-.6666E-04	-.6574E-04	-.6446E-04
-.6284E-04	-.6092E-04	-.6004E-04	-.6077E-04	-.6096E-04	-.6142E-04	-.6193E-04	-.6231E-04	-.6243E-04	-.6224E-04
-.6175E-04	-.5141E-04	-.5202E-04	-.5346E-04	-.5526E-04	-.5705E-04	-.5870E-04	-.6022E-04	-.3912E-04	-.4055E-04
-.4345E-04	-.4683E-04	-.5010E-04	-.5405E-04	-.2324E-04	-.2656E-04	-.3175E-04	-.3712E-04	-.4134E-04	.3971E-05
-.1197E-04	-.2240E-04	-.3286E-04							

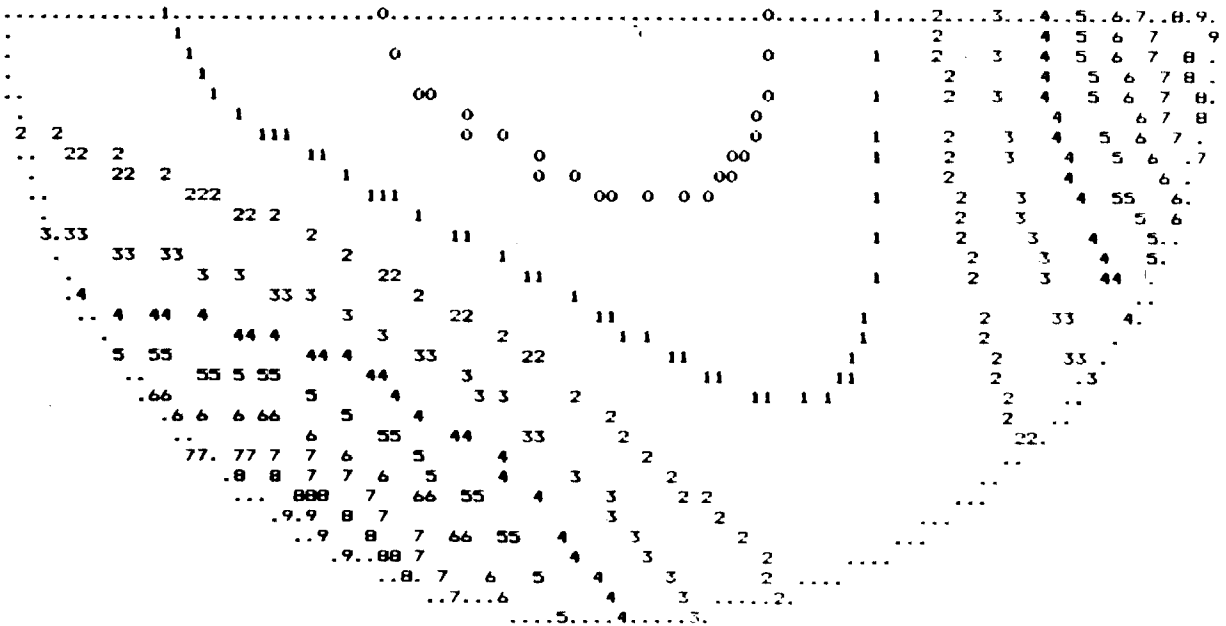

VARIABLE 5 DATUM = .0 CONTOUR INTERVAL = .718E-05

WITH TILT

VARIABLE 6

-.2358E-04	-.2239E-04	-.1884E-04	-.1505E-04	-.1651E-04	-.1577E-04	-.1358E-04	-.1012E-04	.6331E-05	.1092E-04
-.1019E-04	-.7917E-05	-.4216E-05	.8058E-06	.9009E-05	.6838E-05	-.6078E-05	-.2807E-05	.1997E-07	.5700E-05
.1229E-04	.2249E-04	-.4016E-05	-.3308E-05	-.1185E-05	.2364E-05	.7397E-05	.1407E-04	.2275E-04	.2104E-04
-.2295E-05	-.1690E-05	.1159E-06	.3101E-05	.7221E-05	.1238E-04	.1828E-04	.2372E-04	.2464E-04	.1417E-04
-.9571E-06	.4029E-06	.2598E-05	.5495E-05	.8832E-05	.1211E-04	.1439E-04	.1442E-04	.1069E-04	.7013E-06
.5679E-07	.1356E-05	.2949E-05	.4542E-05	.5674E-05	.5711E-05	.4137E-05	.9057E-06	.8036E-06	.5191E-06
-.1393E-06	.1824E-06	.1996E-06	-.4347E-06	-.2131E-05	-.5245E-05	-.5781E-06	-.6665E-06	.9497E-06	.1484E-05
-.2375E-05	.3790E-05	-.5957E-05	-.9173E-05	-.1322E-04	.2394E-06	-.4916E-07	.9167E-06	.2271E-05	.4445E-05
-.7210E-05	-.1079E-04	-.1533E-04	-.1942E-04	.1838E-05	.1328E-05	-.1742E-06	-.2597E-05	.5075E-05	-.9903E-05
-.1494E-04	-.2081E-04	-.2353E-04	.4485E-05	.3696E-05	.1444E-05	-.2062E-05	-.6629E-05	-.1214E-04	-.1854E-04
-.2523E-04	.8458E-05	.7250E-05	.4010E-05	-.7799E-06	.6759E-05	-.1380E-04	.2370E-04	.1416E-04	.1214E-04
.7440E-05	.1068E-05	-.6398E-05	-.1753E-04	.2226E-04	.1874E-04	.1136E-04	.2993E-05	-.4815E-05	.2955E-04
.2455E-04	.1412E-04	.3655E-05							

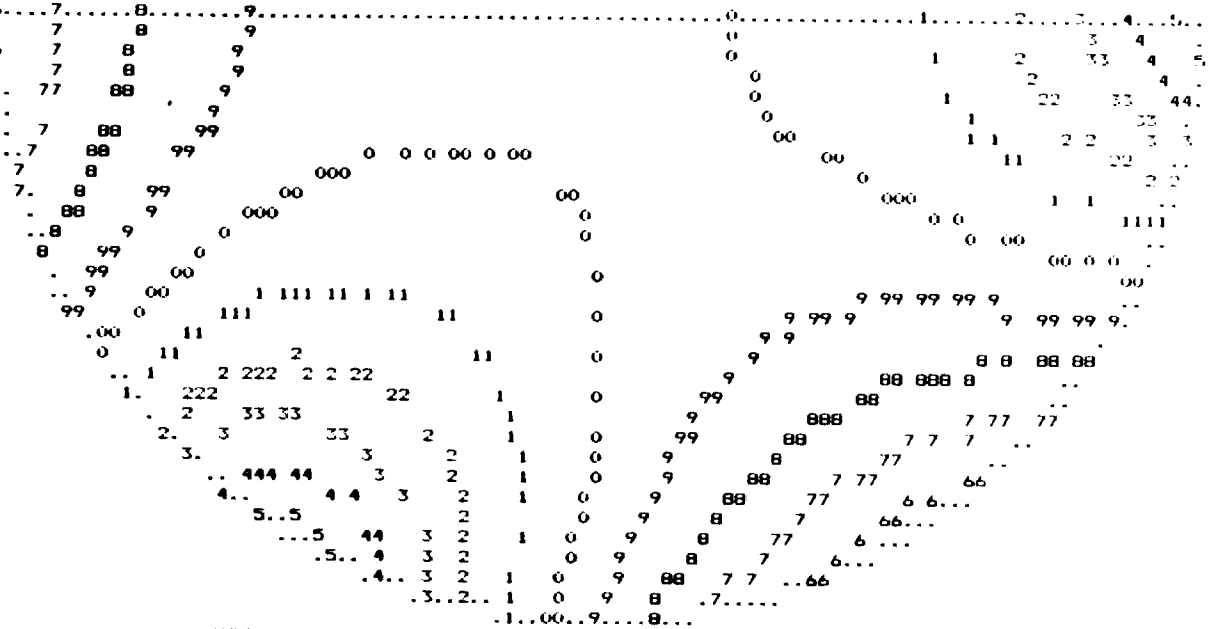

VARIABLE 6 DATUM = .0 CONTOUR INTERVAL = .578E-05

WITH FOCUS SHIFT

C0 = .7483601E-04 C2 = .8739757E-07 C3 = -.9888266E-07 SURFACE RMS DEVIATION = .9674514E-05

1 **INPUT DATA FOR NASA RING SUPPORT**

```
 NELEMS,NODES,NLOADS,NSUPTS,LMODE,MSOL
    0     0     0    24     1     1
OSTRUCTURE ORIENTATION ANGLES IN DEGREES - TX AND TY
        0.          0.

 MATL     E          PR         WT
    1  .101E+08  .170E+00  .800E-01
 RADCURVE= .16E+031D=      .000D=    39.37DEPTH=     4.00
OTTOP= .300TBOTT= .200TRIB= .132TEDGE= .200

          NODE PT.     X COORD    Y COORD    Z COORD          TEMPERATURE

    1  .000E+00 -.197E+02 -.278E+01  .000E+00
    2  .000E+00 -.197E+02 -.784E+00  .000E+00
    3  .000E+00 -.197E+02  .122E+01  .000E+00
  358  .000E+00  .197E+02 -.278E+01  .000E+00
  359  .000E+00  .197E+02 -.784E+00  .000E+00
  360  .000E+00  .197E+02  .122E+01  .000E+00
       SUPPRESSED DEGREES OF FREEDOM

    9   18   27   36   81  135  198  270  351  432  513  594
  521  675  756  837  909  972 1026 1071 1080 1089 1098 1107
OTOTAL WEIGHT OF STRUCTURE
     .48801E+02
THE C.G. OF THE MIRROR IS AT Z=     -1.145
 THE RALEIGH FREQUENCY IS  .638E+03 HERTZ
1            OUTPUT DATA
                    TRANSLATIONS

  NODE       ALONG      ALONG      ALONG
  POINT      X-AXIS     Y-AXIS     Z-AXIS

    1         .00E+00   -.33E-05   -.63E-06
    2         .00E+00    .12E-05   -.47E-06
    3         .00E+00    .60E-05    .00E+00
  172         .00E+00   -.68E-10   -.37E-04
  173         .00E+00   -.41E-10   -.37E-04
  174         .00E+00    .00E+00   -.37E-04
  358         .00E+00    .33E-05   -.63E-06
  359         .00E+00   -.12E-05   -.47E-06
  360         .00E+00   -.60E-05    .00E+00
0ELEMENT NO.       SIGMA XX          SIGMA YY          SIGM                A XY

    3   15   18    1        -.302E+01   -.245E+00   .212E+00
   15   18    6    1        -.270E+00   -.301E+01   .205E+00
   18    6    5    1        -.305E+01   -.277E+00   .192E+00
  147  174  177    1        -.321E+01   -.324E+01   .183E-01
  174  177  150    1        -.321E+01   -.321E+01   .140E-01
  177  150  147    1        -.323E+01   -.321E+01   .967E-02
  150  147  174    1        -.320E+01   -.323E+01   .141E-01
  145  175  175    2        -.570E+01   -.570E+01   .170E-01
  175  175  180    2        -.570E+01   -.570E+01   .170E-01
```

198	171	168	1	-.259E+00	-.305E+01	-.171E-01
171	168	195	1	-.301E+01	-.268E+00	.200E+00
166	193	196	2	.891E+00	.246E+01	-.566E-01
193	196	169	2	.177E+01	.774E+00	.475E-01
196	169	166	2	.712E+00	.175E+01	.193E+00
169	166	193	2	.246E+01	.865E+00	-.244E+00
174	201	204	1	-.322E+01	-.320E+01	.140E-01
201	204	177	1	-.321E+01	-.322E+01	-.964E-02
204	177	174	1	-.321E+01	-.321E+01	.139E-01
177	174	201	1	-.320E+01	-.321E+01	-.182E-01
172	199	202	2	.565E+01	.569E+01	-.415E-02
199	202	175	2	.564E+01	.564E+01	.258E-01
202	175	172	2	.569E+01	.564E+01	-.389E-02
175	172	199	2	.570E+01	.570E+01	-.178E-01
177	204	207	1	-.311E+01	-.319E+01	.378E-01
204	207	180	1	-.322E+01	-.311E+01	-.336E-01
207	180	177	1	-.310E+01	-.322E+01	.460E-01
180	177	204	1	-.319E+01	-.310E+01	-.501E-01
175	202	205	2	.549E+01	.561E+01	-.342E-01
202	205	178	2	.545E+01	.546E+01	.560E-01
205	178	175	2	.551E+01	.546E+01	.956E-02
178	175	202	2	.562E+01	.554E+01	-.314E-01
195	222	225	1	-.268E+00	-.301E+01	.203E+00
222	225	198	1	-.304E+01	-.272E+00	-.190E+00
225	198	195	1	-.233E+00	-.305E+01	.266E-01
198	195	222	1	-.301E+01	-.244E+00	-.211E+00
193	220	223	2	.865E+00	.246E+01	-.246E+00
220	223	196	2	.172E+01	.740E+00	.256E+00
223	196	193	2	.784E+00	.176E+01	.109E+00
196	193	220	2	.246E+01	.891E+00	-.580E-01
345	360	363	1	-.304E+01	-.249E+00	.202E+00
360	363	348	1	-.260E+00	-.306E+01	-.188E-01
363	348	345	1	-.302E+01	-.269E+00	.203E+00
348	345	360	1	-.245E+00	-.302E+01	-.214E+00
343	358	361	2	.178E+01	.779E+00	.469E-01
358	361	346	2	.717E+00	.176E+01	.194E+00
361	346	343	2	.246E+01	.870E+00	-.246E+00
346	343	358	2	.896E+00	.247E+01	-.558E-01

1 EQUILIBRIUM CHECK

0 SUM FORCES X SUM FORCES Y SUM FORCES Z

.99901E-05 .22486E-04 .45073E-03

VARIABLE 3

.0000E+00	.0000E+00	.0000E+00	.0000E+00	-.7771E-05	-.7248E-05	-.5695E-05	-.3154E-05	.0000E+00	-.1480E-04
-.1423E-04	-.1256E-04	-.9833E-05	-.6166E-05	.0000E+00	-.2115E-04	-.2055E-04	-.1876E-04	-.1586E-04	-.1193E-04
-.7067E-05	.0000E+00	-.2662E-04	-.2600E-04	-.2413E-04	-.2108E-04	-.1696E-04	-.1189E-04	-.6047E-05	.0000E+00
-.3106E-04	-.3041E-04	-.2848E-04	-.2534E-04	-.2107E-04	-.1582E-04	-.9786E-05	-.3161E-05	.0000E+00	-.3433E-04
-.3366E-04	-.3169E-04	-.2848E-04	-.2411E-04	-.1873E-04	-.1253E-04	-.5682E-05	.0000E+00	-.3632E-04	-.3565E-04
-.3366E-04	-.3040E-04	-.2597E-04	-.2052E-04	-.1421E-04	-.7232E-05	.0000E+00	-.3700E-04	-.3632E-04	-.3432E-04
-.3105E-04	-.2660E-04	-.2112E-04	-.1477E-04	-.7756E-05	.0000E+00	-.3632E-04	-.3565E-04	-.3366E-04	-.3040E-04
-.2597E-04	-.2052E-04	-.1421E-04	-.7232E-05	.0000E+00	-.3433E-04	-.3366E-04	-.3169E-04	-.2848E-04	-.2411E-04
-.1873E-04	-.1253E-04	-.5682E-05	.0000E+00	-.3106E-04	-.3041E-04	-.2848E-04	-.2534E-04	-.2107E-04	-.1582E-04
-.9786E-05	-.3161E-05	.0000E+00	-.2662E-04	-.2600E-04	-.2413E-04	-.2108E-04	-.1696E-04	-.1189E-04	-.6047E-05
.0000E+00	-.2115E-04	-.2055E-04	-.1876E-04	-.1586E-04	-.1193E-04	-.7067E-05	.0000E+00	-.1480E-04	-.1423E-04
-.1256E-04	-.9833E-05	-.6166E-05	.0000E+00	-.7771E-05	-.7248E-05	-.5695E-05	-.3154E-05	.0000E+00	.0000E+00
.0000E+00	.0000E+00	.0000E+00							

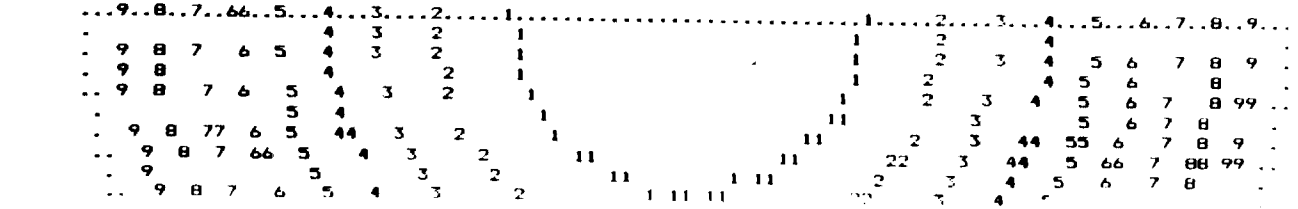

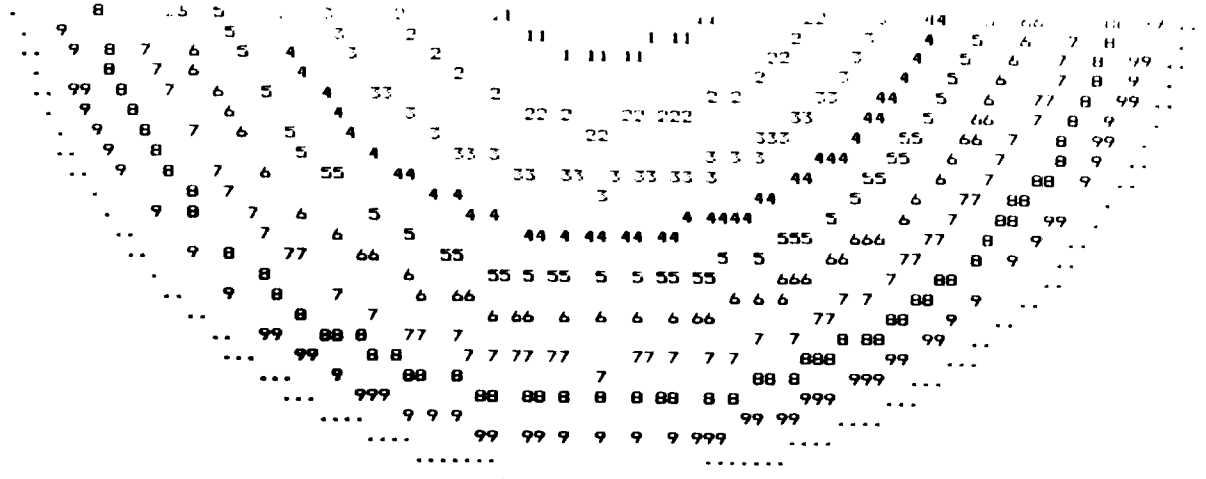

VARIABLE 3 DATUM = .0 CONTOUR INTERVAL = .370E-05

Z DEFLECTIONS

VARIABLE 4

.7364E-06	.7352E-06	.7319E-06	.7270E-06	-.7172E-05	-.6639E-05	-.5061E-05	-.2479E-05	.7156E-06	-.1434E-04
-.1376E-04	-.1205E-04	-.9281E-05	-.5553E-05	.7168E-06	-.2081E-04	-.2020E-04	-.1838E-04	-.1542E-04	-.1142E-04
-.6467E-05	.7182E-06	-.2641E-04	-.2576E-04	-.2386E-04	-.2075E-04	-.1654E-04	-.1138E-04	-.5428E-05	.7187E-06
-.3094E-04	-.3027E-04	-.2830E-04	-.2509E-04	-.2074E-04	-.1538E-04	-.9232E-05	-.2487E-05	.7268E-06	-.3427E-04
-.3359E-04	-.3158E-04	-.2830E-04	-.2384E-04	-.1835E-04	-.1202E-04	-.5048E-05	.7316E-06	-.3631E-04	-.3562E-04
-.3359E-04	-.3026E-04	-.2574E-04	-.2017E-04	-.1373E-04	-.6624E-05	.7348E-06	-.3700E-04	-.3631E-04	-.3426E-04
-.3092E-04	-.2638E-04	-.2079E-04	-.1431E-04	-.7156E-05	.7360E-06	-.3631E-04	-.3562E-04	-.3359E-04	-.3026E-04
-.2574E-04	-.2017E-04	-.1373E-04	-.6624E-05	.7348E-06	-.3427E-04	-.3359E-04	-.3158E-04	-.2830E-04	-.2384E-04
-.1835E-04	-.1202E-04	-.5048E-05	.7316E-06	-.3094E-04	-.3027E-04	-.2831E-04	-.2509E-04	-.2074E-04	-.1538E-04
-.9232E-05	-.2487E-05	.7268E-06	-.2641E-04	-.2576E-04	-.2386E-04	-.2075E-04	-.1654E-04	-.1138E-04	-.5428E-05
.7187E-06	-.2081E-04	-.2020E-04	-.1838E-04	-.1542E-04	-.1142E-04	-.6467E-05	.7182E-06	-.1434E-04	-.1376E-04
-.1205E-04	-.9281E-05	-.5553E-05	.7168E-06	-.7172E-05	-.6639E-05	-.5061E-05	-.2479E-05	.7156E-06	.7364E-06
.7352E-06	.7319E-06	.7270E-06							

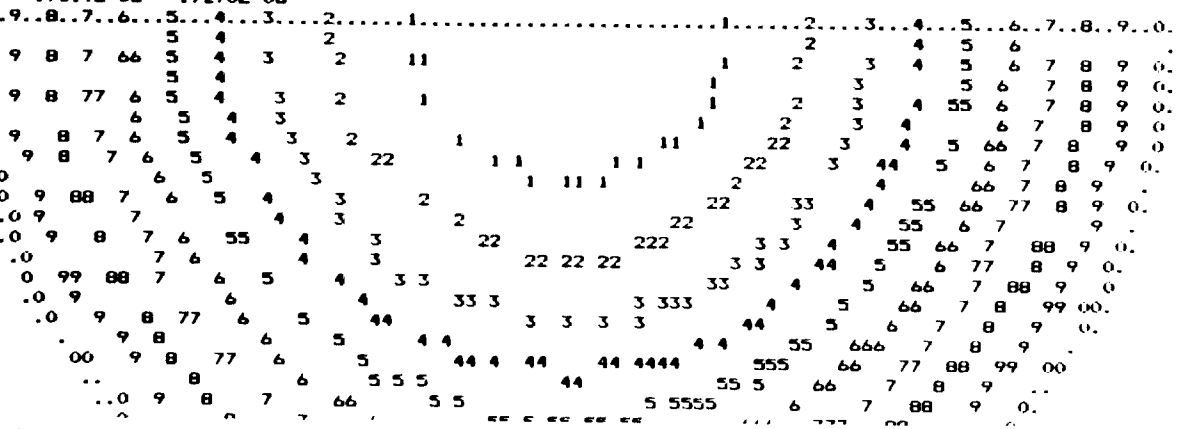

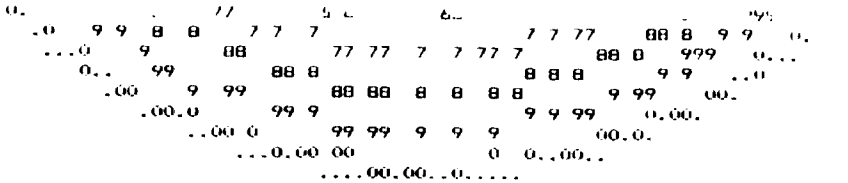

VARIABLE 4 DATUM = .0 CONTOUR INTERVAL = .377E-05

NORMAL DEFLECTIONS

VARIABLE 5

.7390E-06	.7377E-06	.7344E-06	.7294E-06	-.7169E-05	-.6637E-05	-.5058E-05	-.2477E-05	.7179E-06	.1433E-04
-.1376E-04	-.1205E-04	-.9279E-05	-.5551E-05	.7188E-06	-.2081E-04	-.2020E-04	-.1838E-04	-.1542E-04	-.1142E-04
-.6466E-05	.7198E-06	-.2640E-04	-.2576E-04	-.2386E-04	-.2075E-04	-.1654E-04	-.1138E-04	-.5426E-05	.7200E-06
-.3093E-04	-.3027E-04	-.2830E-04	-.2509E-04	-.2073E-04	-.1538E-04	-.9231E-05	-.2486E-05	.7277E-06	-.3427E-04
-.3359E-04	-.3158E-04	-.2829E-04	-.2384E-04	-.1835E-04	-.1202E-04	-.5047E-05	.7323E-06	-.3631E-04	-.3562E-04
-.3359E-04	-.3026E-04	-.2574E-04	-.2017E-04	-.1373E-04	-.6624E-05	.7352E-06	-.3700E-04	-.3631E-04	-.3426E-04
-.3092E-04	-.2638E-04	-.2079E-04	-.1431E-04	-.7156E-05	.7360E-06	-.3631E-04	-.3562E-04	-.3359E-04	-.3026E-04
-.2574E-04	-.2017E-04	-.1373E-04	-.6624E-05	.7345E-06	-.3427E-04	-.3359E-04	-.3158E-04	-.2830E-04	-.2384E-04
-.1835E-04	-.1202E-04	-.5049E-05	.7309E-06	-.3094E-04	-.3027E-04	-.2831E-04	-.2509E-04	-.2074E-04	-.1539E-04
-.9233E-05	-.2488E-05	.7258E-06	-.2641E-04	-.2576E-04	-.2386E-04	-.2075E-04	-.1655E-04	-.1138E-04	-.5429E-05
.7174E-06	-.2082E-04	-.2020E-04	-.1838E-04	-.1542E-04	-.1142E-04	-.6469E-05	.7166E-06	-.1434E-04	-.1376E-04
-.1205E-04	-.9283E-05	-.5555E-05	.7149E-06	-.7174E-05	-.6642E-05	-.5063E-05	-.2481E-05	.7133E-06	.7338E-06
.7326E-06	.7293E-06	.7246E-06							

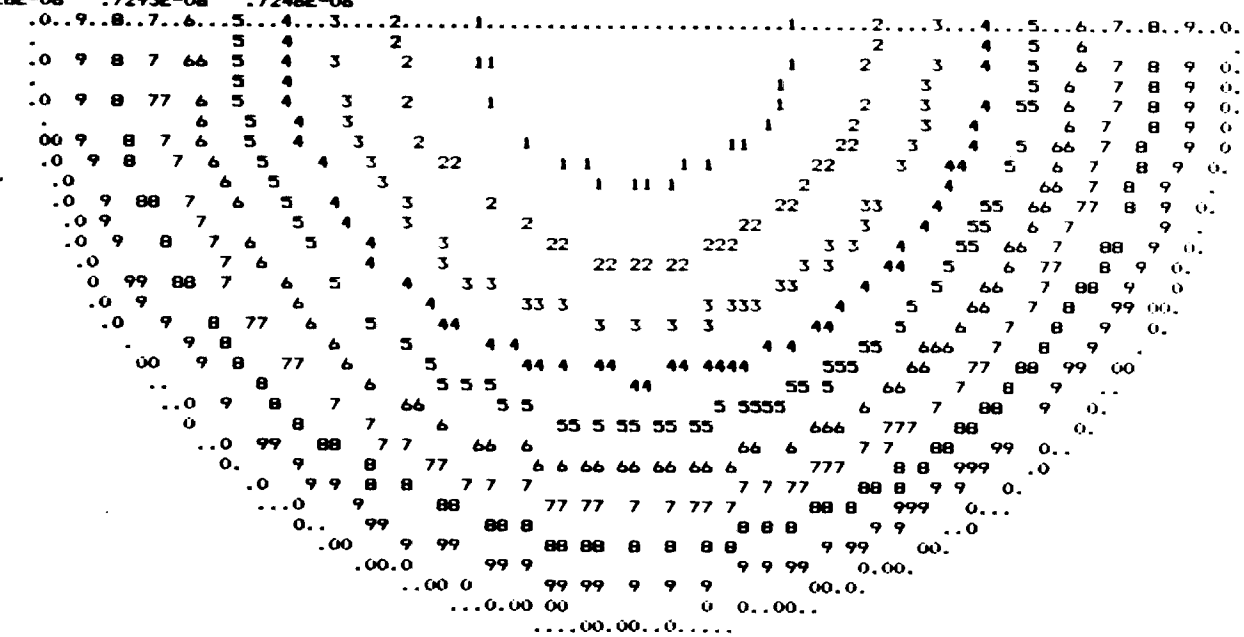

VARIABLE 5 DATUM = .0 CONTOUR INTERVAL = .377E-05

WITH TILT

VARIABLE 6

VARIABLE 6

```
-.9153E-06  -.9165E-06  -.9197E-06  -.9248E-06  -.2135E-07   .7560E-07  -.2576E-06   .6100E-06   .9364E-06   .4830E-06
 .4527E-06   .3796E-06   .2164E-06  -.1674E-06  -.9355E-06   .4201E-06   .4462E-06   .5077E-06   .5297E-06   .4775E-06
 .9557E-07  -.9344E-06   .1096E-06   .1644E-06   .3084E-06   .4808E-06   .5805E-06   .4654E-06  -.3871E-07   .9743E-06
-.5138E-06  -.2379E-06  -.3015E-07   .2490E-06   .4974E-06   .5675E-06   .2640E-06  -.6189E-06  -.9265E-06   .7177E-06
-.6234E-06  -.3725E-06  -.2101E-07   .3296E-06   .5351E-06   .4094E-06  -.2465E-06  -.9220E-06   .9930E-06   .8094E-06
-.6182E-06  -.2245E-06   .1865E-06   .4776E-06   .4566E-06  -.6237E-07  -.9191E-06   .1097E-05   .9914E-06   .7471E-06
-.2995E-06   .1316E-06   .4460E-06   .4651E-06  -.8342E-08  -.9182E-06  -.9937E-06   .8951E-06   .6190E-06   .3295E-06
 .1850E-06   .4729E-06   .4559E-06  -.6301E-07  -.9198E-06   .7153E-06  -.6249E-06  -.3739E-06  -.2244E-07  -.3802E-06
 .5337E-06   .4081E-06  -.2478E-06  -.9233E-06  -.3158E-06  -.2400E-06  -.3227E-07   .2468E-06   .4953E-06   .5665E-06
 .2620E-06  -.6209E-06  -.9285E-06   .1069E-06   .1616E-06   .3056E-06   .4781E-06   .5779E-06   .4627E-06   .4134E-07
 .9368E-06   .4168E-06   .4429E-06   .5404E-06   .5260E-06   .4202E-06   .9228E-07  -.9377E-06   .4785E-06   .4783E-06
 .3756E-06   .2124E-06  -.1674E-06  -.9394E-06  -.2596E-07  -.8021E-07  -.2622E-06  -.6146E-06   .9409E-06   .9305E-06
-.9217E-06  -.9249E-06  -.9297E-06
```

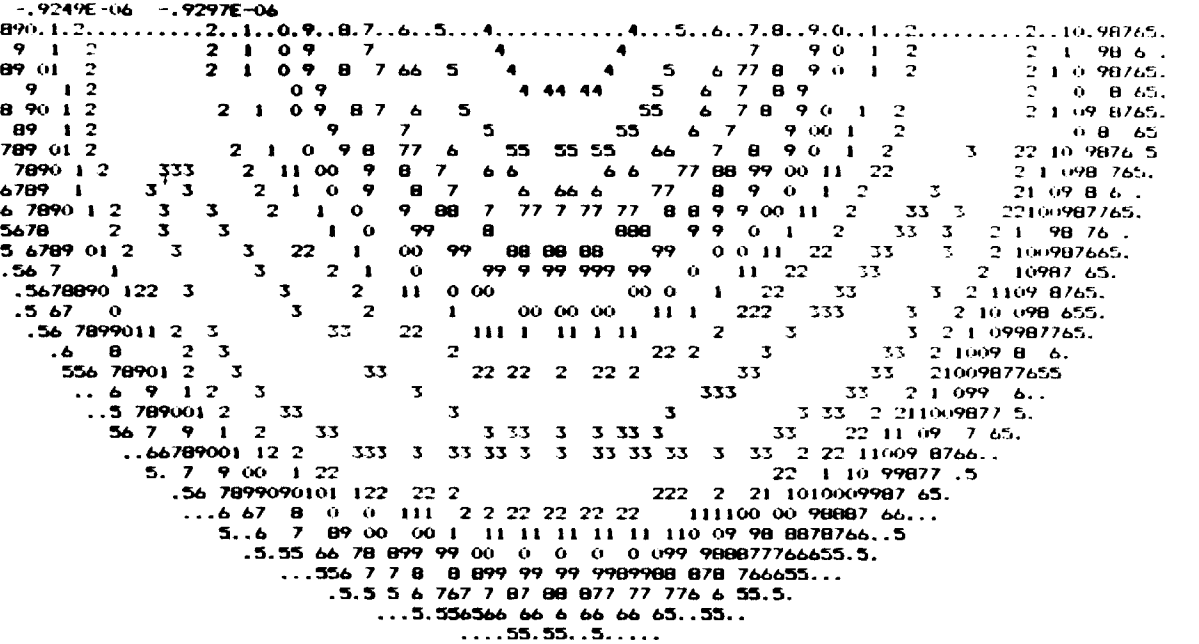

```
VARIABLE  6          DATUM =  .0     CONTOUR INTERVAL =    .167E-06
                                                                    WITH FOCUS SHIFT
I CO =    .3590258E-04     C2 =   -.1328761E-09     C3 =   -.9692109E-07     SURFACE RMS DEVIATION =    .4700565E-06
```